

**Self-assembled monolayer based on
1,3-dimercaptopropan-2-ol: preparation,
characterization and applications in
electrochemical chemosensors**

Von der Fakultät für Umwelt und Naturwissenschaften
der Brandenburgischen Technischen Universität Cottbus-Senftenberg
zur Erlangung des akademischen Grades eines

Dr. rer. nat.

genehmigte Dissertation

vorgelegt von

M. Sc.

Arwa Laroussi

aus *Tunis, Tunesien*

Gutachter: Herr Prof. Dr. Jörg Acker

Gutachter: Herr Prof. Dr. Mourad Mhamdi

Tag der mündlichen Prüfung: 07.02.2022

CO-TUTELLE DOCTORAL THESIS

between

Technical University of Brandenburg
(BTU)

&

University of Tunis El-Manar
(UTM)

Faculty of Environment and Natural Sciences

Faculty of Sciences of Tunis

Presented in order to obtain a doctoral degree in chemistry

by

Ms. Arwa LAROUSI

**Self-assembled monolayer based on 1,3-dimercaptopropan-2-ol:
preparation, characterization and applications in electrochemical
chemosensors**

Defended on 07.02.2022, in front of the jury composed of:

Peter Schierack	<i>Professor at Technical University of Brandenburg Cottbus-Senftenberg</i>	President
Mourad Mhamdi	<i>Professor at the Higher Institute of Medical Technology of Tunis</i>	Reviewer
Jörg Acker	<i>Professor at Technical University of Brandenburg Cottbus-Senftenberg</i>	Reviewer
Noureddine Raouafi	<i>Professor at the Faculty of Sciences of Tunis</i>	Supervisor
Vladimir M. Mirsky	<i>Professor at Technical University of Brandenburg Cottbus-Senftenberg</i>	Supervisor
Anne Kammel	<i>Senior researcher at Technical University of Brandenburg Cottbus-Senftenberg</i>	Evaluator

Table of Contents

ABSTRACTS	1
------------------	----------

GENERAL INTRODUCTION	5
-----------------------------	----------

CHAPTER 1: LITERATURE REVIEW

1 INTRODUCTION	8
-----------------------	----------

2 SELF-ASSEMBLED MONOLAYERS	8
------------------------------------	----------

1.1	8
------------	----------

HISTORIC

1.2	9
------------	----------

DEFINITION

1.3	11
------------	-----------

SELF-ASSEMBLED MONOLAYERS OF ORGANOSULFUR COMPOUNDS ON GOLD

1.1.1	11
--------------	-----------

THE GOLD-SULFUR AFFINITY

1.1.2	11
--------------	-----------

THE PROCESS OF SELF-ASSEMBLY

1.1.3	13
--------------	-----------

LIMITATIONS OF THE SAMs CONCEPT

1.1.4	14
--------------	-----------

ORGANOSULFUR ADSORBATES

1.1.5	15
--------------	-----------

SELF-ASSEMBLED MONOLAYER BASED ON DISULFIDE

1.1.6	16
-------	----

SELF-ASSEMBLED MONOLAYER BASED ON THIOCTIC ACID

3	FUNCTIONALIZATION AND APPLICATION OF QUINONE-BASED SAMs	18
----------	--	-----------

1.4	18
-----	----

QUINONES: BIOLOGICAL PROTOTYPE

1.5	19
-----	----

CHEMICAL REACTIVITY OF QUINONES

1.1.7	20
-------	----

QUINONES: OXIDO-REDUCTIVE PROPERTIES

1.1.8	20
-------	----

QUINONES: ELECTROPHILIC PROPERTIES

1.6	21
-----	----

QUINONE-BASED SAMs

1.7	22
-----	----

QUINONE-BASED SAMs FOR THE ELABORATION OF SENSORS

1.1.9	23
-------	----

CHEMICAL / ELECTROCHEMICAL SENSOR: DEFINITIONS

1.1.10	24
--------	----

ELECTROCHEMICAL SENSORS BASED ON QUINONE-MODIFIED SAMs

1.1.11	26
--------	----

HYDROGEN PEROXIDE ELECTROCHEMICAL(BIO)SENSORS BASED ON SAMs

4	CONCLUSION	28
----------	-------------------	-----------

CHAPTER 2: SYNTHESIS AND CHARACTERIZATION OF THE ANCHOR SITE: 1,3-DIMERCAPTOPROPAN-2-OL

5	INTRODUCTION	34
----------	---------------------	-----------

6	DIMERCAPTOPROPAN-2-OL: SYNTHESIS/CHARACTERIZATION	36
----------	--	-----------

1.8		36
		SYNTHESIS
1.9		37
		SPECTROSCOPIC IDENTIFICATION
7	<u>SELF-ASSEMBLED MONOLAYERS OF 1,3-DIMERCAPTOPROPAN-2-OL ONTO GOLD SURFACE</u>	38
1.10		38
		PREPARATION
1.11		39
		CHARACTERIZATION
1.1.12		39
		CONTACT ANGLE CHARACTERIZATION
1.1.13		40
		XPS CHARACTERIZATION
1.1.14		40
		ELECTROCHEMICAL CHARACTERIZATION
1.1.14.1		40
		<i>ELECTROCHEMICAL CELL</i>
1.1.14.2		41
		<i>ELECTROCHEMICAL BEHAVIOR OF THE SAM-MODIFIED GOLD ELECTRODE</i>
8	<u>ELECTROCHEMICAL AND SPECTROSCOPIC INVESTIGATIONS ON THE IMMOBILIZATION STRUCTURE OF 1,3-DIMERCAPTOPROPAN-2-OL ON THE GOLD SURFACE</u>	43
1.12		43
		QUANTUM MECHANICAL CALCULATIONS
1.13		45
		ELECTROCHEMICAL CHARACTERIZATION
1.1.15		45
		CYCLIC VOLTAMMETRIC CHARACTERIZATION
1.1.15.1		45

	<i>IN POTASSIUM FERRO/FERRICYANIDE SOLUTION</i>	
1.1.15.2		50
	<i>IN PHOSPHATE BUFFERED SALINE SOLUTION</i>	
1.1.16		51
	ELECTROCHEMICAL IMPEDANCE SPECTROSCOPIC CHARACTERIZATION	
1.14		52
	X-RAY PHOTOELECTRON SPECTROSCOPIC CHARACTERIZATION	
9	<u>COMPARATIVE STABILITY OF SAM1 WITH MONOTHIOLS</u>	54
1.15		54
	CAPACITANCE COMPARISON USING EIS	
1.16		55
	STABILITY MONITORING USING CAPACITIVE KINETICS ANALYSIS	
1.17		58
	STABILITY MONITORING USING STEP-POTENTIAL CHRONOAMPEROMETRY	
10	<u>CONCLUSION</u>	59
 <u>CHAPTER 3: ELECTROCHEMICAL AND SPECTROSCOPIC CHARACTERIZATION OF BQ-TERMINATED SAM BASED ON DiSH ON GOLD AND ITS APPLICATION IN NADH SENSING</u> 		
11	<u>INTRODUCTION</u>	63
12	<u>PREPARATION OF BQ-TERMINATED SAMs</u>	63
13	<u>ELECTROCHEMICAL CHARACTERIZATION OF SAM3</u>	64
1.18		64
	DETERMINATION OF ELECTROCHEMICAL PARAMETERS	
1.19		65
	ESTIMATION OF ESTERIFICATION EFFICIENCY θ	
1.20		67

14	XPS CHARACTERIZATION OF SAM3	68
15	ELECTROCHEMICAL BEHAVIOR OF SAM4	70
16	IMMOBILIZATION OF REDOX-ACTIVE LIGAND ON SAM4	72
1.21		72
	IN-SITU IMMOBILIZATION	
1.22		74
	EX-SITU IMMOBILIZATION	
17	APPLICATION OF SAM4 FOR ELECTROCHEMICAL SENSING OF NADH	75
18	CONCLUSION	77

CHAPTER 4: APPLICATION OF SAM4 IN ELECTROCATALYTIC HYDROGEN PEROXIDE SENSING

19	INTRODUCTION	79
20	CYCLIC VOLTAMMETRIC ANALYSIS	80
1.23		80
	CASE OF WIDE POTENTIAL RANGE	
1.24		82
	CASE OF THE CATHODIC RANGE	
1.25		82
	CASE OF THE ANODIC RANGE USING DIFFERENT GOLD SURFACES	
21	CHRONOAMPEROMETRIC ANALYSIS	85
22	SELECTIVITY AND PERFORMANCE	86

23	CONCLUSION	89
	GENERAL CONCLUSION	92
	ANNEXES	94
	ANNEX A: LISTS OF ABBREVIATIONS	94
	ANNEX B: EXPERIMENTAL SECTION	98
	ANNEX C: LIST OF PUBLICATIONS	103

Zusammenfassung

Die vorliegende Arbeit hatte die Entwicklung eines neuen biochemischen Sensors basierend auf einer auf einer Goldoberfläche verankerten funktionellen Grenzflächen-Architektur mit genau definierten strukturellen Nano-Motiven zum Ziel.

Dafür wurde das neue Ankermolekül 1,3-Dimercaptopropan-2-ol synthetisiert. Aufgrund seiner symmetrischen Struktur mit 2 Thiol-Gruppen bildet es auf der Goldoberfläche eine sehr stabile selbstanordnende Monoschicht (self-assembled monolayer SAM) aus. Die Monoschichten aus 1,3-Dimercaptopropan-2-ol wurden mit zyklischer Voltammetrie, Impedanzspektrometrie, Röntgenfotoelektronenspektroskopie (XPS), Kinetik der Kapazität und Kontaktwinkelmessungen untersucht. Die Struktur der SAM wird von den Adsorptionsbedingungen bestimmt. Bei kurzer Inkubationszeit der Gold-Elektrode und hohen Dithiol-Konzentrationen bindet überwiegend nur eine Thiol-Gruppe an die Oberfläche, während bei langen Inkubationszeiten und niedrigen Dithiol-Konzentrationen überwiegend beide Thiolgruppen binden. Die vergleichende Untersuchung der Desorption beider Beschichtungen der SAM zeigt, dass sich die Stabilität der SAM erhöht, wenn die Moleküle zum größten Teil über beide Thiol-Gruppen gebunden sind.

Auf dieser Monoschicht wurde elektrochemisch aktives p-Benzochinon immobilisiert. Das 1,3-Dimercaptopropan-2-ol diente als Ankermolekül, 3-Mercaptopropionsäure fungierte als Abstandhalter (spacer) und 1,4-Benzochinon als Kopfgruppe. Die Oberflächenkonzentration des p-Benzochinons, ermittelt mit zyklischer Voltammetrie, betrug $2.5 \pm 0.2 \times 10^{-10} \text{ mol} \cdot \text{cm}^{-2}$. Das entspricht einer Funktionalisierung von $65 \pm 5\%$ SAM-Molekülen. Mit Hilfe des elektroaktiven Chinons können Chemisorptionsprozesse in Echtzeit verfolgt werden. Die so aufgebaute Schicht kann für die elektrisch adressierbare Immobilisierung von Biomolekülen oder die Entwicklung elektrokatalytischer Sensoren eingesetzt werden.

Die SAM mit endständigem Benzochinon wurde als Sensor zur quantitativen Detektion von Wasserstoffperoxid eingesetzt. Die Sensorcharakterisierung erfolgte mit zyklischer Voltammetrie im Potenzial-Bereich von -0.6 V bis $+0.9 \text{ V}$ als auch jeweils nur im anodischen oder kathodischen Bereich. Die Ergebnisse weisen auf eine oxidative elektrochemische Zersetzung des Wasserstoffperoxids bei einem Potenzial von ca. $+0.4 \text{ V}$ mit Sauerstoffbildung hin, während bei kathodischen Potenzialen eine Reduktion des gebildeten Sauerstoffs als auch des

Wasserstoffperoxids stattfindet. Die Verminderung des Oxidationspotenzials für Wasserstoffperoxid an der Benzochinon-beschichteten Goldelektrode im Vergleich mit dem identischen Schichtaufbau ohne Benzochinon deutet auf einen elektrokatalytischen Effekt dieses Moleküls bei der oxidativen Zersetzung von Wasserstoffperoxid.

Die analytische Bewertung der Sensor-Leistungsfähigkeit erfolgte im voltammetrischen als auch im amperometrischen Modus. Im Konzentrationsbereich von 0.1 mM bis 2.5 mM Wasserstoffperoxid verläuft die Sensor-Antwort linear, die untere Nachweisgrenze liegt bei ca. 4 μ M Wasserstoffperoxid. Der amperometrische Chemosensor zeigt in Gegenwart typischer Stör-Substanzen wie Ascorbinsäure, Harnsäure oder Glukose eine gute Selektivität. Die hohe Empfindlichkeit legt nahe, dieses System nicht nur als Wasserstoffperoxid-Sensor einzusetzen, sondern auch als Transduktor für Biosensoren mit immobilisierten Oxidoreduktasen, wie z.B. als Glukose-Biosensor mit Glukoseoxidase.

Schlagworte: selbstorganisierende Monoschicht, 1,3-Dimercaptopropan-2-ol, Benzochinon, elektrochemisch aktive Schicht, elektrokatalytische Oxidation, Wasserstoffperoxid.

Résumé

L'objectif de ce travail était de développer un nouveau capteur biochimique basé sur une architecture interfaciale fonctionnelle sur une surface en or avec des nano-motifs structuraux bien définis.

Pour cette raison, un nouveau site d'ancrage nommé 1,3-dimercaptopropan-2-ol a été synthétisé. En raison de sa structure symétrique ainsi que de sa possession de deux groupes thiol, il permet la préparation d'une monocouche auto-assemblée (SAM) bien stable sur la surface de l'or. Les monocouches formées à partir du composé 1,3-dimercaptopropan-2-ol ont été étudiées par voltampérométrie cyclique, spectroscopie d'impédance, spectroscopie photoélectronique aux rayons X, mesures de capacité cinétique et d'angle de contact. La structure de la SAM dépend des conditions d'adsorption. Une courte période d'incubation de l'électrode d'or à une concentration élevée de ce di-thiol entraîne l'immobilisation prédominante de l'adsorbat à la surface de l'or par un groupe thiol, tandis qu'une longue incubation à faible concentration entraîne l'immobilisation prédominante des deux groupes thiol. Une étude comparative de la désorption et du remplacement des SAMs indique une augmentation de la stabilité lorsque les molécules de la SAM lient la surface de l'or par deux liaisons principalement.

Cette monocouche a été utilisée pour immobiliser la fraction électrochimiquement active *p*-benzoquinone. L'auto-assemblage moléculaire a été réalisé en utilisant le composé 1,3-dimercaptopropan-2-ol comme site d'ancrage, l'acide 3-mercaptopropionique comme espaceur et la benzoquinone comme groupe de tête. La concentration surfacique de la benzoquinone obtenue par voltampérométrie cyclique est de $2.5 \pm 0.2 \times 10^{-10} \text{ mol}\cdot\text{cm}^{-2}$, ce qui correspond à la fonctionnalisation de $65 \pm 5 \%$ des molécules de la SAM. La présence de la quinone électroactive permet de surveiller en temps réel le processus de la chimisorption. La monocouche formée peut être appliquée dans l'immobilisation des biomolécules par adressage électrique ou dans le développement de capteurs électrocatalytiques.

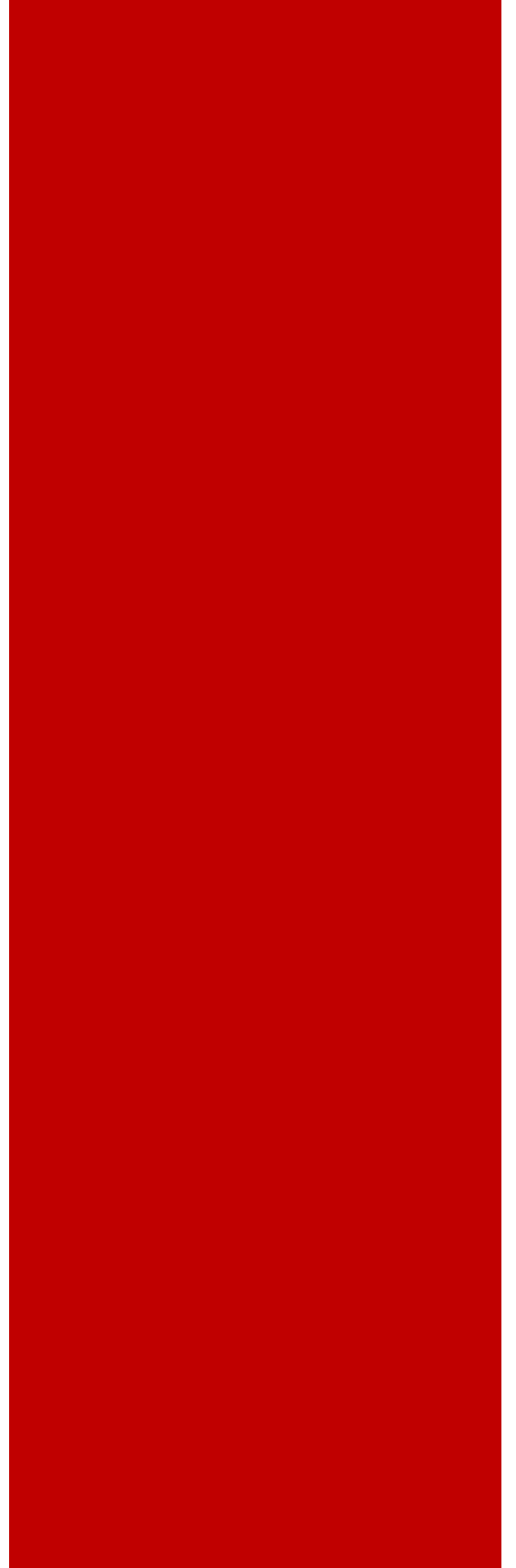
La monocouche auto-assemblée à terminaison benzoquinone a été appliquée pour la détection quantitative du peroxyde d'hydrogène. La caractérisation du capteur a été effectuée par voltampérométrie cyclique dans la plage de potentiel allant de -0.6 V à +0.9 V ainsi que dans la plage anodique ou cathodique uniquement. Les résultats indiquent une décomposition

électrochimique oxydative du peroxyde d'hydrogène à un potentiel de $\sim +0.4$ V conduisant à la formation d'oxygène tandis qu'aux potentiels cathodiques, une réduction de l'oxygène formé ainsi que du peroxyde d'hydrogène se produit. Une diminution du potentiel d'oxydation du peroxyde d'hydrogène sur l'électrode en or revêtue de benzoquinone-SAM par rapport à celui mesuré sur les électrodes revêtues de la même monocouche auto-assemblée sans benzoquinone, indique un effet électrocatalytique de cette fraction sur la décomposition oxydative du peroxyde d'hydrogène.

L'évaluation analytique des performances du capteur a été effectuée en mode voltampérométrique ainsi qu'ampérométrique. Le capteur a présenté une réponse linéaire sur la plage de concentration de 0.1 mM à 2.5 mM avec une limite de détection de ~ 4 μ M. Le chimio-capteur ampérométrique présente une bonne sélectivité en présence d'interférences typiques telles que l'acide ascorbique, l'acide urique ou le glucose. La haute sensibilité nous permet d'envisager des applications de ce système non seulement comme capteurs de peroxyde d'hydrogène mais aussi comme transducteur pour les biocapteurs basés sur les oxydoréductases, par exemple un biocapteur pour le glucose basé sur le glucose-oxydase.

Mots clés: monocouche auto-assemblée, 1,3-dimercaptopropan-2-ol, Benzoquinone, couche électrochimiquement active, oxydation électrocatalytique, peroxyde d'hydrogène.

General Introduction



Currently, the scientific community, whether chemists, physicists or biologists, is facing a major challenge in order to control, in a precise and local way, the properties and reactivity of the molecular species involved in various processes (biological, catalytic, etc.). In this perspective, the assembly of chemical species, into three-dimensional (3D) molecular structures on a conductive surface, is proving to be a very promising tool allowing, moreover, the control of their spatial organization and the monitoring of their interaction with the environment [1] where they are found, even at the nanometric scale.

Since its advent in the 1970s, investigations on modified electrodes has been the basis of numerous electroanalytical applications. Thanks to the phenomena of molecular self-assembly it has become possible to graft monolayers and also multilayers of three-dimensional molecular structures onto an electrode surface. The self-assembly process consists of spontaneous adsorption followed by self-organization of molecular units on the surface of a support. We then speak of self-assembled monolayers or SAMs, which can confer new physicochemical properties to the support, specific to their nature, such as wettability, hydrophobicity, conductance, etc. This technique has positively influenced several fields of scientific research thanks to numerous advantages. Indeed, a rush was observed for the preparation and study of SAMs on different supports and with various adsorbates. This method represents, at the fundamental level, a suitable system for the study and understanding of electron transfer phenomena within molecular wires [2,3] and allows the study of the electrochemical behavior of the insoluble compounds or compounds present at the trace state. Experimentally, this phenomenon finds its importance in the development and implementation of electro-assisted catalytic processes that allow more efficient control of the chemical reactivity of certain species. The immobilization of chiral and electroactive molecules has led to progress in the field of non-linear optics and molecular electronics (development of transistors, sensors, switches, etc.) [4]. Several biomimetic systems have also been developed according to this approach with the immobilization of biomolecules such as enzymes, proteins, antibodies, microorganisms and DNA for numerous applications (improvement of their reactivity and efficiency by facilitating the molecular recognition of their targets in a complex medium, design of highly selective electrochemical sensors and biosensors) [5,6].

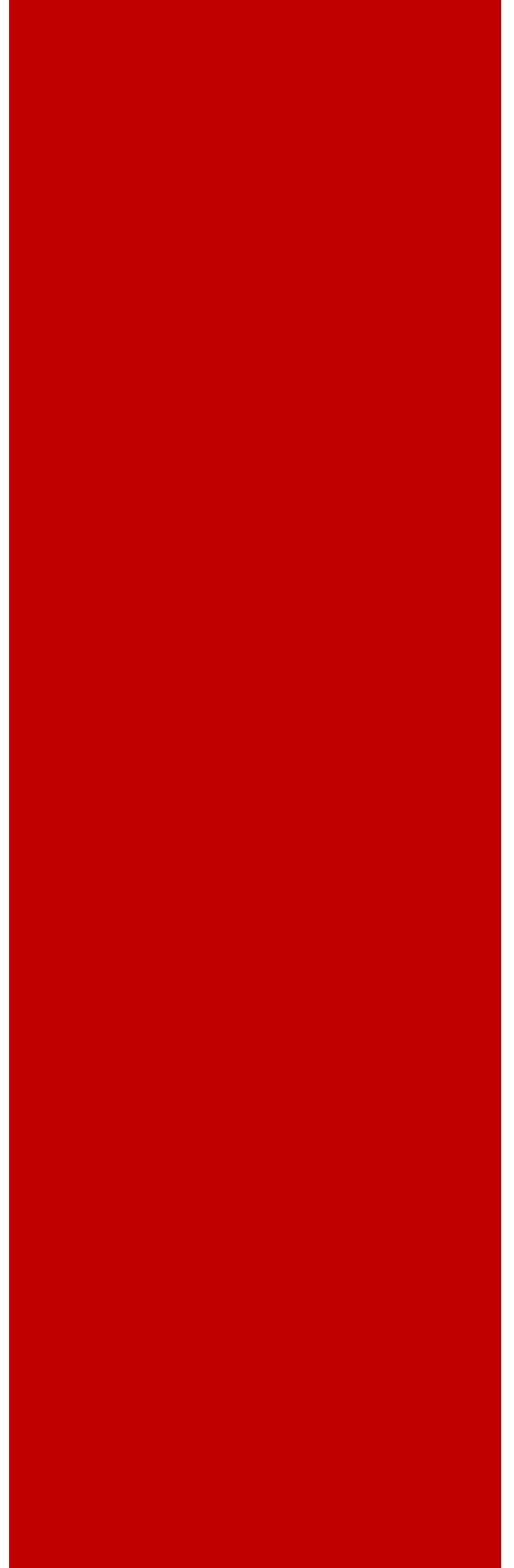
Self-assembly is based on a good interaction between the molecule to be immobilized (adsorbate) and the surface of the electrode (substrate), thus allowing strong bonding in space and time. The choice of the substrate-adsorbate system is therefore decisive. In recent years, a wide range of adsorbates with a specific anchoring site for a material have been investigated. The high affinity of sulfur for gold has made chemisorption of sulfur derivatives the most popular technique in the preparation of self-assembled monolayers on gold surfaces [7].

The work presented in this manuscript, adopting this gold-sulfur tandem, is a contribution to research in the development of molecular assembly on polycrystalline gold electrodes for the tailoring of electrochemical chemosensors. In order to improve the stability of this monolayer, we opted for a symmetrical dithiolated compounds as a new anchoring site, based on pre-synthesized 1,3-dimercaptopropan-2-ol. The presence of two sulfur atoms will provide a stronger binding to the surface of the metal. Functionalization of SAMs by quinone, an electroactive center, will allow to monitor and characterize in real time the formation of the SAM by electrochemical techniques, namely cyclic voltammetry and impedance spectroscopy. In this perspective, a strong bond between the units is a necessity, thus excluding low-energy Van der Waals-type interactions and coordination bonds. Based on this observation, the covalent bond seems to be the most promising. In particular, it can be generated through the concept of *click* chemistry. We have used this approach to obtain an organized molecular film on a solid surface. The first chapter of this work is a bibliographic review to situate the subject in its global context by providing a general description on self-assembled monolayers. A state-of-the-art on quinones, their biological as well as chemical properties and their applications in electrochemical sensing will be developed. In the second chapter, we will introduce a new anchoring molecule named 1,3-dimercaptopropan-2-ol, used for the first time in the elaboration of SAMs onto gold surface. A detailed investigation on its immobilization structure on gold as well as its stability will be described using spectroscopic and electrochemical investigation tools. The third chapter will aim to design a highly stable electrochemically active film on the gold surface involving the same anchor site described in the second chapter. A detailed investigation on the formation of the layer and its application in chemical sensing tool, as an example its electrocatalytical oxidation of β -nicotinamide adenine dinucleotide (NADH) will be described. As for the last chapter, it will describe the investment of the SAM described in the third chapter for the design of a new electrochemical sensor for hydrogen peroxide.

References

- [1] C.R. Martin, C.A. Foss, Chemically modified electrodes, in: P.T. Kissinger, W.R. Heineman (Eds.), *Laboratory Techniques in Electroanalytical Chemistry*, Marcel Dekker, New York, **1996**, 403–442.
- [2] N. Sutin, B. S. Brunshwig, C. Creutz, S. W. Feldberg, *J. Phys.Chem. B*, **2004**, 108, 12092–12102.
- [3] S. W. Feldberg, N. Sutin, *Chem. Phys.*, **2006**, 324, 216–225.
- [4] J. M. Buriak, *Chem. Commun.*, **1999**, 12, 1051–1060.
- [5] V. M. Mirsky, *TrAC-Trend. Anal. Chem.*, **2002**, 21, 439–450.
- [6] W. Zhao, J.-J. Xu, H.-Y. Chen, *Electroanalysis*, **2006**, 18, 1737–1748.
- [7] A. Ulman, *Chem. Rev.*, **1996**, 96, 1533–1554.

Chapter 1: Literature review



1. Introduction

This bibliographic chapter revolves around three main parts. In the first part, a state of the art on self-assembled monolayers (SAMs) onto gold substrate will be presented. In the second part, a deep discussion on the anchor site, which constitute one of the major factor affecting the properties of the formed monolayer, will be conducted in detail. In the third part, we will give some examples of quinones/hydroquinones (Q/HQ) based SAMs as well as their applications in sensing.

2. Self-assembled monolayers

1.1 Historic

Surface phenomena have been observed for the first time in the 18th century when Franklin has noticed the spontaneous organization of oil molecules on a water surface [1]. During the 19th century, several works have focused on the fundamental study of oil-water interfaces by preparing structures organized in layers, currently known as “Langmuir film” [2-3]. Thus it has been demonstrated the existence of a monolayer of vertically oriented fatty acids. The carboxylate group is in contact with water and the alkyl chain is oriented towards the air. The thickness of the film formed by these molecules corresponds to the length of the hydrocarbon chain. Following Blodgett's work, “Langmuir-Blodgett films” [4] have been described as the transfer of “Langmuir films” onto a solid surface [5]. Multilayers can thus be prepared by repetitive immersion of this modified surface in the same solution.

In 1946, Bigelow *et al.* [6] reported the spontaneous adsorption of a surfactant on a platinum metal surface resulting in a monomolecular layer considered to be the first generation of self-assembled monolayers. The formation of SAMs bound to the gold surface from molecules having a thiol or disulfide terminal function has been reported by Nuzzo and Allara [7]. Many investigations [8-10] based on this type of molecular assemblies were performed and discussed later. We can cite the work of Finklea [11], Porter [12], Sabatani [13], Laibinis [14] and Bain [15-17].

1.2 Definition

The concept of self-assembly corresponds to a spontaneous arrangement and combination of subunits (atoms, molecules, biomolecules, etc.) to form a more complex secondary structure with a certain organization. Self-assemblies are ubiquitous in nature. Biological membranes, cell structures or even viruses are good examples (Figure 1.1).

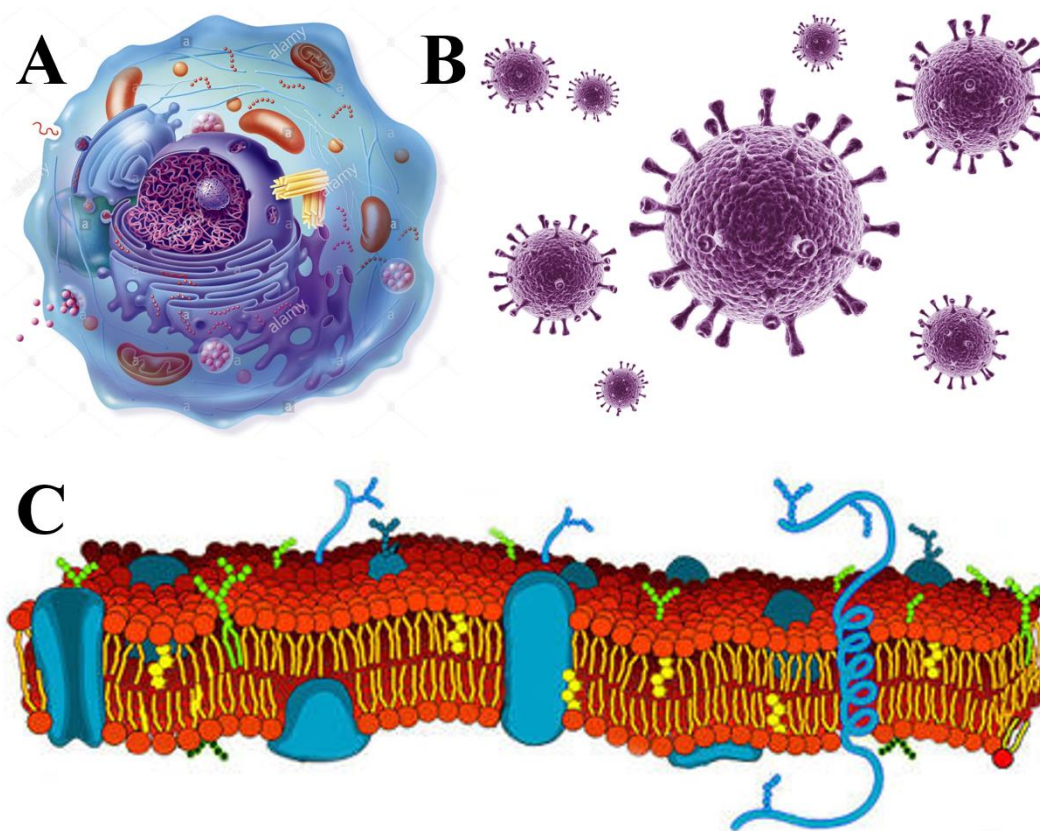


Figure 1.1: Illustration of self-assemblies present in nature: (A) cell structure (B) viruses and (C) cell membrane.

SAMs are much simpler structures formed by spontaneous adsorption of a monomolecular film (called adsorbate) composed of organic molecules from solution or gas phase onto a solid surface (called substrate or support). This functionalization leads to the formation of a monolayer with a nanometric thickness [18] (from 1 to 3 nm) on a substrate with a high degree of organization [7]. The SAM formation process is governed by the nature of the substrate. Thin films on metals are obtained *via* chemisorption. Gold is the ideal substrate because it is non-toxic compared to mercury, harmless compared to platinum, and relatively inert to oxygen as well as a majority of chemicals compared to silver and copper. Au(111) is the most frequently encountered in SAMs on

gold because it has the lowest surface energy and therefore it is the most thermodynamically stable. The adsorbed molecules that constitute the building blocks of the system can be divided into three different parts: the anchor site (head group or linking group), the spacer (the main chain) and the terminal functional group (Figure 1.2).

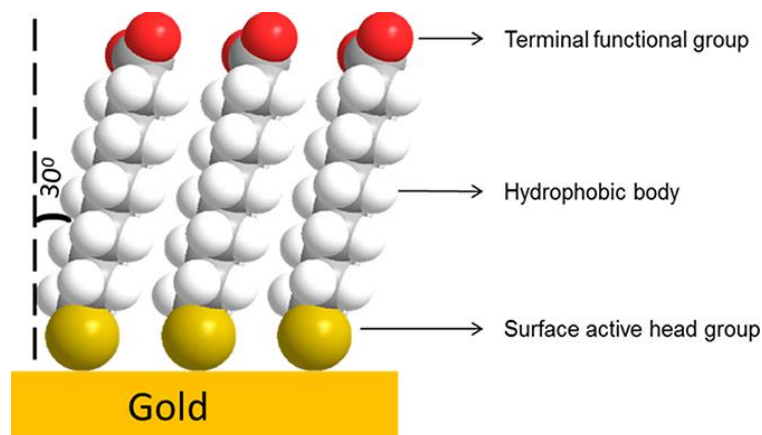


Figure 1.2: Scheme of a self-assembled monolayer from decanethiol molecules adsorbed on Au(111) in a standing up configuration [19].

- The anchor site is at the origin of the self-assembly process as well as its orientation, since it allows the grafting of the molecule on the surface. Its great affinity for the substrate allows its adhesion via Van der Waals interactions between the chains as a first step then *via* a moderately strong bond as a second step allowing the formation of the assembly and ensuring the stability of the structure (thiol, disulfide, dialkylsulfide, dithiol, thioctic acid, etc.).
- The spacer is most often an aliphatic chain of variable length between the functional group and the head group. it contributes to the stability of SAM through Van der Waals and 'hydrophobic' interactions between the adjacent chains. Generally, the longer is the aliphatic chain, the more stable is the assembly [17].
- The terminal functional group corresponds to chemical function (CO_2H , OH , N_3 , NH_2 , Cl , CN , COH , etc.) which conveys its physico-chemical properties to the substrate [20]. It can also serve as a site of attachment for molecules, biomolecules or nanostructures through covalent bonds or weak interactions. Its reactivity is therefore a crucial parameter.

1.3 Self-assembled monolayers of organosulfur compounds on gold

Since their discovery in the early 80s by Nuzzo and Allara [7], self-assembled monolayers of organosulfur compounds on a gold substrate represent the most studied [21] system among SAMs thanks in particular to their relative ease of preparation [18], robustness and stability due to establishment of a relatively strong bond between gold and sulfur [22].

1.1.1 The gold-sulfur affinity

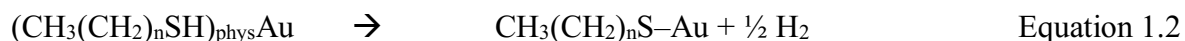
For the formation of SAMs onto gold substrate, planar surfaces, presenting few structural defects, are the most used, either in polycrystalline or monocrystalline state. For instance, gold crystallizes in a cubic network with centered faces where gold atoms are organized at the interface of three possible faces: Au (100), Au(110) and Au(111) [23-25]. The latter is the most used in the development of SAMs [22]. Furthermore, gold does not have stable oxides [26] under ambient conditions and is relatively easy to clean. Mechanical and chemical treatment procedures are essential to remove physisorbed and chemisorbed impurities located on gold surface [27].

Sulfur has a great affinity for gold [28-29] (the binding energy of each thiol group to gold is varies from 170 to 210 kJ·mol⁻¹ [10,30,31]), which is consistent with the soft character of the sulfur/gold couple (anion/cation respectively) according to the Pearson principle [32], unlike acid or amine functions that have a hard character and therefore react weakly with gold [28]. For this reason, direct immobilization of thiolated compounds bearing terminal groups on gold surfaces is possible and can be carried out effectively [33]. Moreover, the small difference in electronegativity ($\Delta\chi = 0.04$) between gold ($\chi = 2.54$) and sulfur ($\chi = 2.58$) measured on Pauling [34] scale gives a covalent character to this non-polar bond between the two atoms.

1.1.2 The process of self-assembly

Sulfur is adsorbed on gold Au(111) preferentially on sites with three atoms separated by a distance of 4.995 Å [35] to yield highly ordered arrays. Grazing incidence X-ray diffraction (GIXD), Low energy electron diffraction (LEED), atomic beam scattering and other spectroscopic techniques have indicated that SAM growth in the absence of a solvent is a complex process involving different steps [36]. The simplest picture of this process (Fig. 1.3. left) implies an initial physisorption step, followed by chemisorption of the molecules, and finally the formation of

crystalline, ordered domains with molecules in a closed-packed configuration [36-38]. The physisorbed state on Au(111), varying from seconds to minutes, allows the obtention of highly recovered surface. It involves Van der Waals interactions and corresponds to a particularly disorganized state (Fig. 1.3. left (i)). After physisorption, thiol molecules chemisorb on the Au(111) substrate across the sulfur headgroup, forming a strong covalent bond, in a process that takes at least some minutes [39]. During the process the thiol molecule loses the mercaptan H atom, transforming itself in a thiolate. These two adsorption steps are summarized as follows:



Where reactions described by equations 1.1 and 1.2 correspond to thiol physisorption and chemisorption, respectively. The nature and mechanism of the chemisorption has not been clearly elucidated till now. It has been proposed that this reaction occurs via oxidative adsorption of the alkanethiol RS–H bond to the metallic gold substrate accompanied by a release of dihydrogen [22], although it is unknown whether the mechanism involves an ion, a radical, or another species. After adsorption, comes the preferred nucleation of islands containing lying down molecules (the so-called striped phases), which takes place at the surface defects [40]. After nucleation, the islands grow, increasing the surface coverage of thiolate species on the Au surface. This growth is the origin of the initial rise in Fig. 1.3. (right), where the H signal arising from the terminal methyl group is plotted against thiol exposure [41]. The completion of this lying down phase is seen as a first plateau in Fig. 1.3. (right). Increasing the exposure to this lying down phase results in a sudden increase in the H signal, and this corresponds to the nucleation of molecules in the standing up configuration (Fig. 1.3. (right)). Then, the second plateau, which leads to saturation, corresponds to dense phases of upright molecules with a surface coverage. The completion of this process can take several hours, or even days, depending on the hydrocarbon chain length, and the result is the formation of ordered domains of molecules arranged in a closely packed, crystalline configuration.

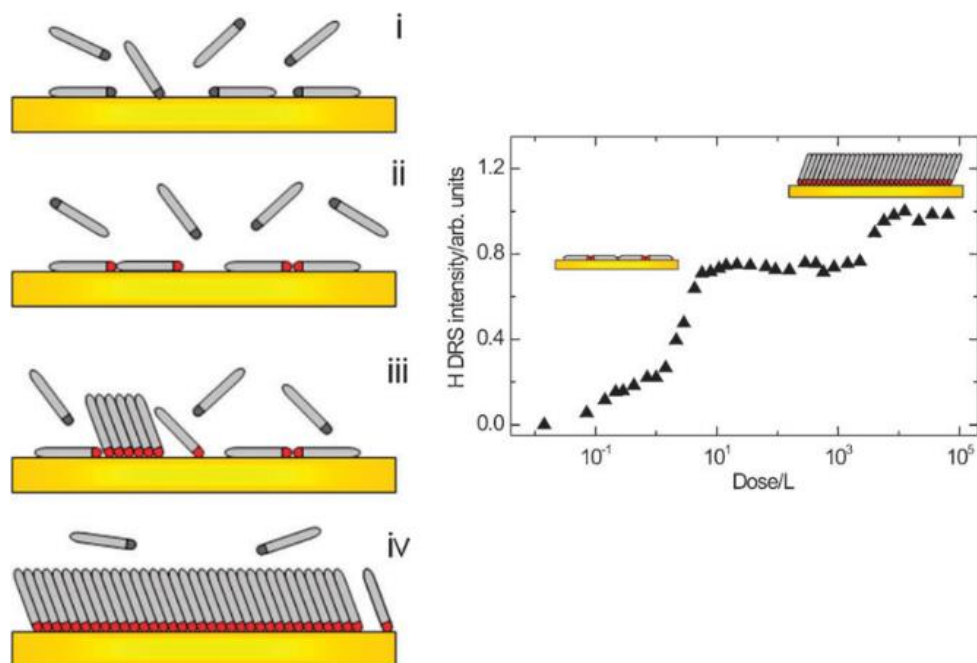


Figure 1.3: Scheme of the different steps taking place during the self-assembly of alkanethiol on Au (111): (i) physisorption, (ii) lying down phase formation, (iii) nucleation of the standing up phase, (iv) formation of a complete SAM (left) [19]. Hydrogen DRS (direct recoil spectroscopy) intensity from Au (111) versus exposure to hexanethiol in UHV. The schemes show the lying down and standing up phase formation corresponding to the two plateaus (right) [41].

1.1.3 Limitations of the SAMs concept

Although the adsorption of thiol molecules onto gold substrate leads to the formation of oriented and well-packed SAMs, a number of experimental factors including solvent, temperature, concentration of the adsorbate, immersion time, purity of the adsorbate, concentration of oxygen in solution, cleanliness of the substrate, and the structure of the adsorbate can affect the configuration of the resulting SAM as well as the rate of its formation. In practice, most experimental conditions for the preparation of SAMs yield organic interfaces with reproducible and desired functional behaviors. These characteristics are acceptable for some applications of SAMs, but fundamental studies of certain materials properties such as wettability, corrosion, tribology, and charge-transfer processes require an understanding of how to minimize defects in SAMs and maximize order in these systems [18]. Controlling the quality of the SAMs is also a key point in many technological problems [19].

Our discussion is focused on the type of the adsorbate, which represents one of the major factor affecting the SAM properties. In fact, still today, our knowledge about the chemistry of the sulfur–

Au bond in thiol SAMs on Au(111) is incomplete. In the case of alkanethiol- and alkanedithiol-based SAMs there are many factors that affect their crystallinity. The “perfect” self-assembled monolayer is far from reality, and different types of defects exist that seriously limit their applications. As regards the stability against oxidation and thermal desorption of S headgroup compounds adsorbed on gold surfaces—either smooth, well-defined surfaces, or rough and disordered substrates (and even nanocurved surfaces, such as nanoparticles)—this is not just an academic problem, but also an important issue with practical implications. The search for strategies to increase the oxidation resistance of SAMs becomes crucial for their use in ambient conditions. It is thus important to investigate the possibility of increasing SAMs stability against oxidation by a correct choice of the adsorbate or more precisely the anchor site.

1.1.4 Organosulfur adsorbates

Various organosulfur derivatives have been used as adsorbate [22] to form self-assembled monolayers on flat surfaces or gold nanoparticles (see Figure 1.4). Regardless alkanethiols, which were intensively characterized, dialkyl disulfides [7], alkanedithiols [42], dialkyl sulfides [43], thiophene [44] and its derivatives, xanthates [45] and dithiocarbamate [46] were also investigated and immobilized on gold. These systems have been used to study several fundamental aspects such as thermal stability [19], adsorption/desorption kinetics [47], electrochemical desorption and displacement of SAMs by exchange [18], structural study of the surface [22], determination of electronic properties and characterization of the charge transfer phenomenon within molecular films [48].

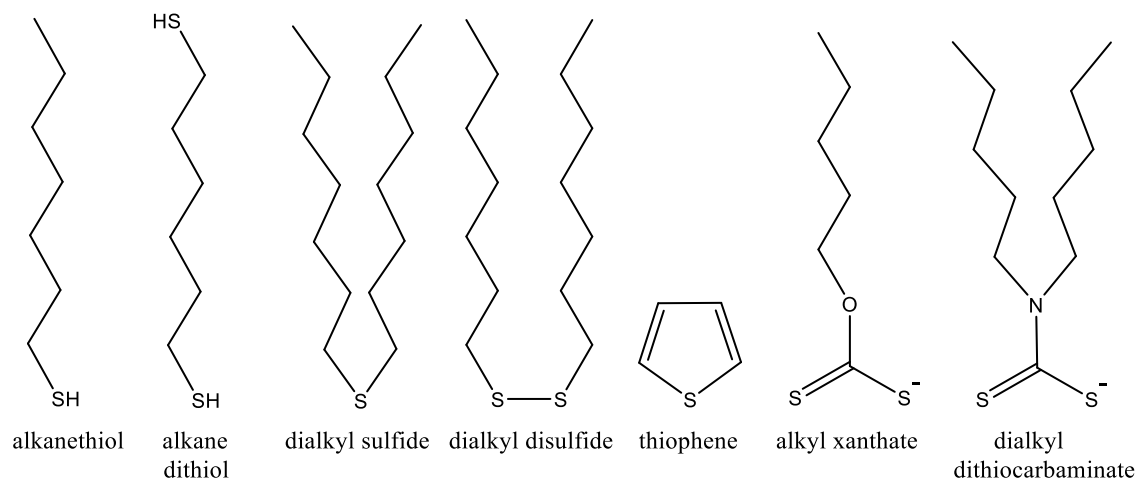


Figure 1.4: Some examples of organosulfur compounds that form self-assembled monolayers.

Electrochemical analysis of thiol stability and electrically driven thiol desorption were performed using different thiol molecules [49-51]. These studies showed that the reductive desorption of thiols with long hydrophobic chains or/and with two thiols occurs at higher cathodic potentials than that of the thiols with short hydrophobic chains or/and with a single thiol group [52]. A determination of the thickness of thiol monolayers by means of optical ellipsometry was used to evaluate thermal stability of SAMs [17]. It was shown that the long-chain thiols are also thermally more stable than the short ones. Such influence of the aliphatic chain on the SAM stability was obtained also by theoretical analysis [53]. No desorption was detected for monolayers made of linear alkylthiol with 15 or more methylene groups [50]. However, so thick monolayers form a high barrier for electron tunneling [30] and therefore cannot be used for electrochemical applications requiring effective charge transfer through the SAMs.

In the case of dialkyl sulfides, SAM formation process is different from that described in section 1.1.2 (The process of self-assembly). Spectroscopic data indicate that a dative bond [54] between sulfur and gold results in the monolayer characterized by a low degree of organization [55] which can be improved at higher temperatures (60 °C) [56]. The cleavage of the C-S bond has not been demonstrated experimentally [57-59]. According to Schlenoff et al. [60], if this type of cleavage occurs during the sulfide adsorption process, it would be very minimal. Although dialkyl sulfides allow the formation of bifunctionalized monolayers with precise control of the distance between the two groups carried by the two alkyl chains of the dialkyl sulfide, this type of SAMs are not very stable [18]. A possible solution to overcome this limitation is the use of anchor molecules possessing more than one thiol moieties bond to the gold substrate.

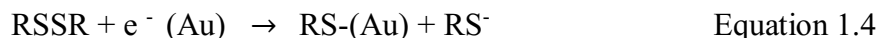
1.1.5 Self-assembled monolayer based on disulfide

The use of SAMs containing disulfide as chemical anchor site was to form SAMs which are strongly bounded to the gold substrate, and, therefore, attractive for applications, e.g., in coating technology. Some research groups have elaborated the formation of thiol-based SAMs obtained from a corresponding disulfides reduction reaction. Thus, Anne and Demaille [61,62] developed SAMs of thiolated oligonucleotides labelled with ferrocene on gold after disulfide reduction using the reducing agent, TCEP (tris(2-carboxyethyl)phosphine). The same team functionalized the surface of a gold microelectrode with a monolayer of ferrocene-poly(ethylene glycol) from the corresponding disulfide [63]. Chemisorption of disulfides on gold involves the cleavage of the S-

S bond and the formation of the S-Au bond similar to that obtained for thiols according to the following equation: [64]



An alternative mechanism involving electronic transfer was proposed [65] for disulfide adsorption on gold. They associate it with a cathodic process according to:



In terms of energy, Schlenoff *et al.* [60] evaluated, based on electrochemical data, a gain of -100.4 kJ/mol for the adsorption of dialkyl disulfides on gold, i.e. -50.2 kJ/mol per RS^- , a gain greater than for thiols. In addition, it was pointed out that the chemisorption of dimethyl disulfides is much faster than that of methanethiol. One can attribute this to the fact that chemisorption of the disulfides does not require breaking of the SH bond [47].

However, it was observed that the physisorption process of disulfides is longer compared to that of thiols. Jung *et al.* [66] reported that SAMs obtained from disulfides form 40% more slowly than that obtained from thiols, referenced to the number of thiolate groups. This may be understandable in view of the fact that the rate-limiting step appeared to be the displacement of solvent molecules. Chemisorption of disulfides requires the simultaneous availability of two sites, which is less probable than the one site required for a thiol molecule. In the same context, Bain *et al.* [15] reported that if mixtures of disulfides and thiols are grown from solution, adsorption of the thiol was strongly preferred.

1.1.6 Self-assembled monolayer based on thioctic acid

Possessing two sulfur atoms in the 1,2-position in a five-membered ring structure, thioctic acid (alpha lipoic acid) is a special case of disulfide. It has been used as an adsorbate for the formation of very stable SAMs on gold. Indeed, each adsorbate molecule is immobilized on the surface by two Au-S bonds, thus enhancing the stability of the layer. Several scientific works have described the use of SAMs of thioctic acid and its derivatives in analytical and biological applications. For example, Madoz *et al.* [67] formed a SAM from thioctic acid on a polycrystalline gold surface after 24 hours incubation in 1 mM solution prepared in ethanol/water mixture. Thioctic acid was used as anchor site to develop, after 5 successive steps, a mixed monolayer of hydroxyl group and a protein recognition site in order to immobilize proteins onto specific sites. This SAM was found to be very stable and gave fast and reproducible electrochemical responses. Under the same

operating conditions of concentration and immersion time, a mixed SAM of thioctic acid and butanethiol was developed to generate antigen/antibody SAMs *via* amide linkages with immobilized thioctic acid for the recognition of the corresponding targets [68]. DNA was also coupled to thioctic acid *via* a peptide bond, the resulting molecule is then used to form a network of DNA-modified gold nanoparticles with good yield (~79%) (Figure 1.5.A) [69].

In the field of development of new organic materials, fluorescent macromolecules coupled with thioctic acid have been immobilized onto gold (Figure.1.5.B) [70]. Fullerenes modified by two thioctic acid groups [71] were also synthesized (Figure.1.5.C) and immobilized on a gold surface after 24 h incubation in 1 mM solution. Electrochemical response confirmed the higher stability of this monolayer compared to that obtained from monothiols. The reduction peak relative to the desorption of thioctic appears at more cathodic potentials than in the case of undecanethiol under the same conditions. A ferrocene functionalized by two thioctic acid molecules *via* an amide link (Figure.1.5.D) was synthesized by Beer *et al.* [72]. The formed monolayer served as a probe for the selective electrochemical detection of anions in both organic and aqueous solution.

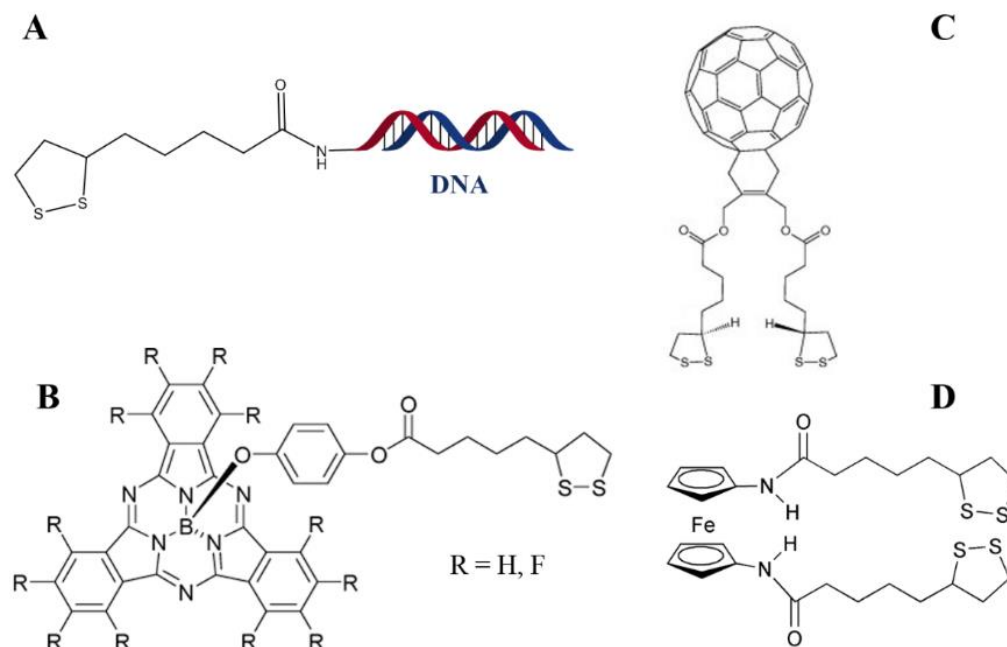


Figure 1.5: Some examples molecules Functionalized thioctic acid used to form SAMs on gold [69-72].

The effect of solvent on the organization of thioctic acid monolayer (1 M for 24 hours) was studied by Li *et al.* [73]. They found that the best solvent for a well-ordered SAM based-thioctic acid is

tetrachloromethane followed by ethanol and acetonitrile. The investigation was based on the reduction of the capacitive current after the formation of the monolayer and its blocking effect against ferricyanide $[\text{Fe}(\text{CN})_6]^{3-}$.

From a fundamental point of view, there are few in-depth studies on the mechanism and formation kinetics of monolayer based-thioctic acid. The evolution of the formation of this type of SAM has been reported by Dong *et al.* [74]. The investigation was based on the reductive desorption of thioctic acid monolayers in a basic medium. The intensity of the reduction peak increases with incubation time (1 min to 2 weeks in a 1 mM solution in ethanol). No details on adsorption kinetics are discussed.

3. Functionalization and application of quinone-based SAMs

SAMs can be considered as the interface between “two worlds”: metals and organic and/or biological materials [19]. Besides their ease of preparation, SAMs are able to link materials with totally different physical and chemical properties in which quinones represent one of the mostly used organic systems.

1.4 Quinones: biological prototype

Quinones represent a class of quinoid compounds that are widely distributed in nature. Until now, more than 1,200 quinones have been described [75]. Since they are formed by an ortho or a para substituted dione conjugated either to an aromatic nucleus (such as benzoquinones) or to a condensed polycyclic aromatic system (such as naphthoquinones, anthraquinones, anthracynones), quinones are characterized by a common basic structural pattern (see Figure 1.6). They correspond to a well-studied class of compounds due, not only to their wide occurrence in nature, but also to their involvement in a number of essential biological processes. For example: Coenzyme Q is a powerful antioxidant and membrane stabilizer, it is implicated in the prevention of cellular damage resulting from normal metabolic processes [76], and the protection against several chronic diseases, including Parkinson’s and cardiovascular diseases [77]. Vitamin K is involved in many biological processes, including blood coagulation [78], prevention of cardiovascular disease [79], as well as prevention and treatment of osteoporosis [80]. In plants, plastoquinones play the role of electron transporter in photosynthesis [81]. Moreover, many

quinones have antioxidant (vitamin E [82]), anti-inflammatory (vitamin E [82-84], thymoquinone [85] and anthraquinone-2,6-disulfonic acid [86]), antibiotic (phaeosphenone [87]), antimicrobial (anthraquinone [88]), and anticancer (thymoquinone [89], Tanshinone IIA [90], emodin [91] and doxorubicin [92]) activities.

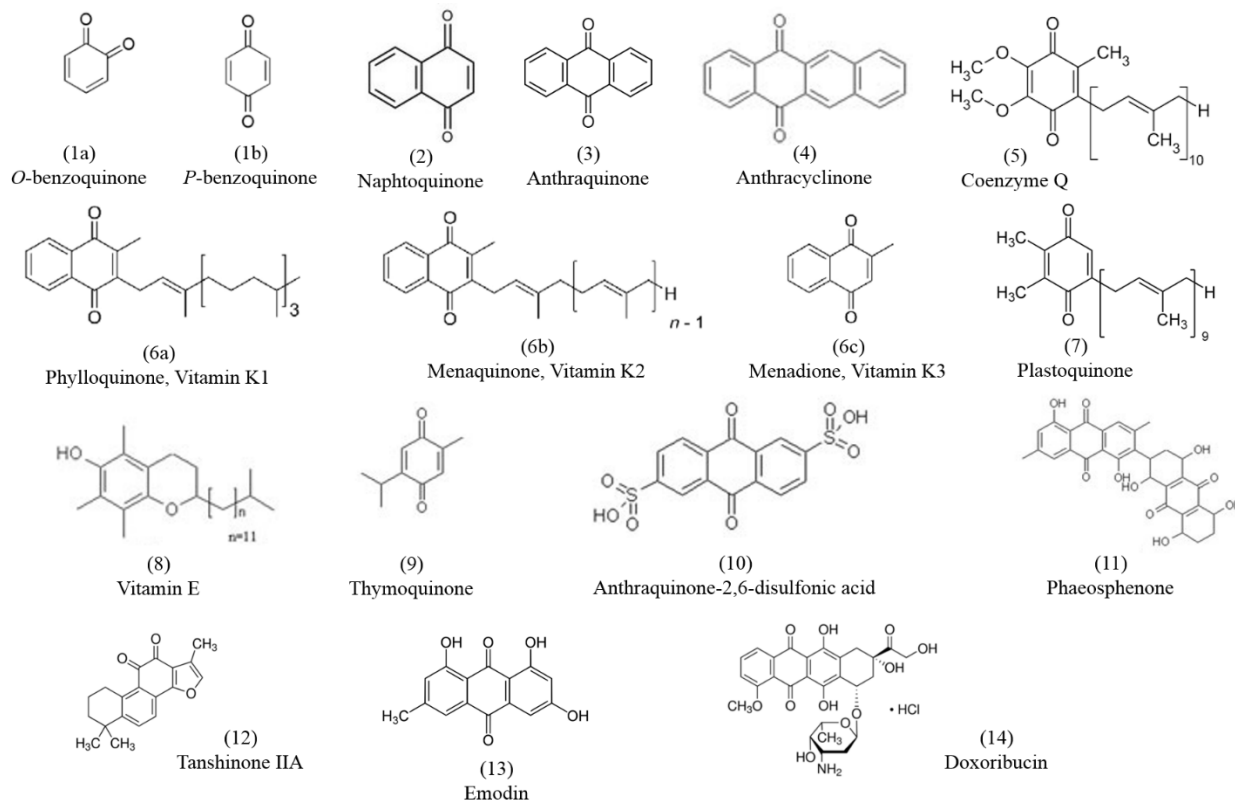


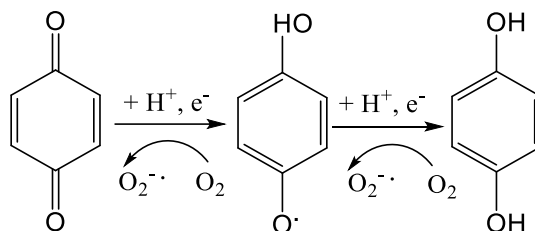
Figure 1.6: Chemical structures of quinones numbered in the same order as mentioned in the text above.

1.5 Chemical reactivity of quinones

The knowledge of the inherent chemical reactivity of quinones is relevant to understand their physiological and toxicological properties. Quinones have two properties that are essential for understanding their biological effects. First, quinones can undergo reversible oxido-reduction reactions and, second, many of them can undergo nucleophilic attack due to their electrophilic character. In the section below an overview of the oxido-reductive and electrophilic properties of quinones are presented [93].

1.1.7 Quinones: oxido-reductive properties

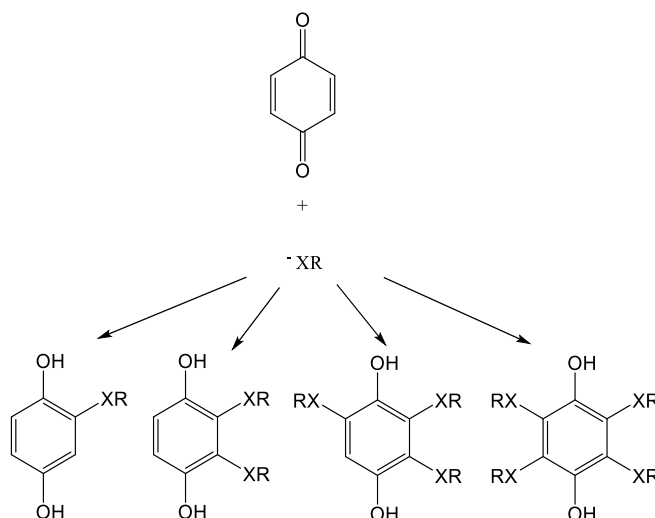
The mechanism of quinone cytotoxicity is attributed mainly to their ease of reduction and therefore to their ability to act as oxidizing or dehydrogenating agents. These biological active compounds can undergo one or two electron reduction by cellular reductases leading to the corresponding semiquinones or hydroquinones, respectively as shown in the scheme below [93]. Redox properties of quinones depend essentially on their chemical potential.



Schema 1: Illustration, using benzoquinone as an example, of one and two electron reduction yielding semiquinone and hydroquinone, respectively [93].

1.1.8 Quinones: electrophilic properties

Electrophilic character of quinones coming either from detoxification or enhanced toxicity [93] allows them to undergo nucleophilic attack through electron-rich nucleophilic species such as amine, hydroxyl and thiol by means of Michael addition [94] (see Scheme 2). P. S. Magee [95] has shown that such nucleophiles may be found in the bound state as reactive side-groups of lysine, serine and cysteine. However, the first nucleophilic group involved in the nucleophilic addition with quinones was thiol group of glutathione (GSH) [93]. In comparison with other nucleophiles, the thiol moiety possesses high, rapid and facile reactivity in this reaction in which the nucleophilic sulfur acts as glue toward quinone's α,β -unsaturated carbonyl moiety forming thus the covalent C-S bond [96-98].



Schema 2: Illustration, using benzoquinone as an example, of the nucleophilic addition with formation of mono-, di-, tri-, and tetra-substitution [93].

Being involved in biological processes, quinones were applied in the development of new bio-interfaces imitating native biological interfaces. A typical bio-interface includes a substrate and a biological coating, quinones are often incorporated into substrates as active components *via* physico-chemical interactions. Considering the high potential of quinones to bind thiol groups, we will give in the following a particular interest to absorbates having as terminal group a quinone or its derivatives onto gold and we will describe their functionalization methods as well as their applications in the detection field.

1.6 Quinone-based SAMs

Self-assembled monolayers based on thiol/dithiol interactions on gold, are widely used in many applications in the field of surface science [47]. In addition, electroactive SAMs provide excellent platforms for studying electron transfer kinetics. In the work of H.-G. Hong and W. Park, a series of thiol-functionalized hydroquinones with different alkyl spacers were used to prepare SAMs on gold electrodes [99]. A process of transfer of two-protons two-electrons has been demonstrated electrochemically while examining the effect of the length of the alkyl chain as well as pH dependence corresponding to this transfer. The influence of the spacer between quinone centers and the gold metal on the electron transfer was deeply investigated by S. A. Trammell *et al.* [100,101].

Naphthoquinone (NQ) derivatives including vitamins K (2-methylnaphthoquinone : 2-MeNQ) are known to be of great physiological significance [102-104] due to their ability to transport both

electrons and protons across biological membranes. The functioning of these compounds in lipophilic systems such as biological membranes, could be mimicked by using two-dimensional SAMs of alkanethiolates [105]. Razumas group reported the synthesis, self-assembling as well as electrochemical properties of 2-methyl-1,4-naphthoquinone derivatives containing different groups in the alkyl chain [106]. The stability of the monolayer and the complete reduction of the 2-MeNQ group was demonstrated by FT-SERS spectroscopy and cyclic voltammetry. Results have shown that the presence of the ester group in the spacer influences the self-assembly properties of the compounds due to the interaction between the dipoles of the ester.

Later, the same group reported a similar study of SAM containing 2-MeNQ as a head group and an alkyl chain as a spacer in order to compare its electrochemical and spectroscopic behavior with its analogs having the ester function [107]. It was demonstrated that monolayers prepared from a high concentration coating solution (1 mM) are disordered and contain a number of *gauche* defects while those obtained from diluted coating solution (0,05 μM) are more ordered and have a vertical orientation. Spectroscopic analyzes of mixed SAMs prepared with short chain length of heptanethiol revealed, the absence of stacking interaction between the 2-MeNQ groups and the involvement of the carbonyl group of naphthoquinones in the hydrogen bond ($\text{C}=\text{O}\dots\text{H}-\text{O}-\text{H}$) at the interface. The use of long chains of dodecanethiol caused a complete loss of the electrochemical activity of the 2-MeNQ group. However, this activity can be restored by replacing the hydrophobic group CH_3 of the diluent with the hydrophilic group CO_2H . This last result shows the importance of the nature of the terminal group of the diluent on the electrochemical properties of the redox functional groups located inside the monolayer. Tunneling microscopy has also been used to study the electron transfer coupled to protons on the functionalized quinone at the interface of gold.

1.7 Quinone-based SAMs for the elaboration of sensors

As discussed previously, quinones have the potential to react with thiol, amine and hydroxyl groups. Due to their electrophilic properties, SAM-terminated-quinone has been widely reported for the design and construction of chemical sensors. In the next part, we will present some examples of these interfaces as well as their applications in sensing and mainly electrochemical sensing.

1.1.9 Chemical / Electrochemical sensor: definitions

A chemical sensor is defined by a small device resulting from a chemical interaction or process between the analyte and the sensor device, which is able to transform chemical or biochemical information of a quantitative or qualitative type into an analytically useful signal [108].

An electrochemical sensor consists of two major components: a chemical or biological recognition element; and a physical transducer (e. g. electrode) which converts the analytical signal of the sensing event into electrical signal [109] as shown in Figure 1.7. Electrochemical sensors are classified into four categories according to the electrical signal generated from the output data of the detected analyte defined by measurable current (amperometric sensor), measurable potential (potentiometric sensor), measurable conductivity change of medium (conductimetric sensor) or measurable change of the conductivity of the electrode surface (impedimetric sensor) [108]. Electrochemical sensors have several advantages such as high sensitivity and selectivity to analyse in the presence of interfering species, rapid response time of electrode materials, and reversibility of the designed sensors [110]. These parameters determine the type of interactions between the sensing element of the substrate and the analytes [111]. Strong interactions are typically associated with higher sensitivity and selectivity, whereas perfect reversibility requires weak interactions [109]. The critical parameters of electrochemical sensors are sensitivity, detection limit, dynamic range, selectivity, linearity, response time, and stability [112].

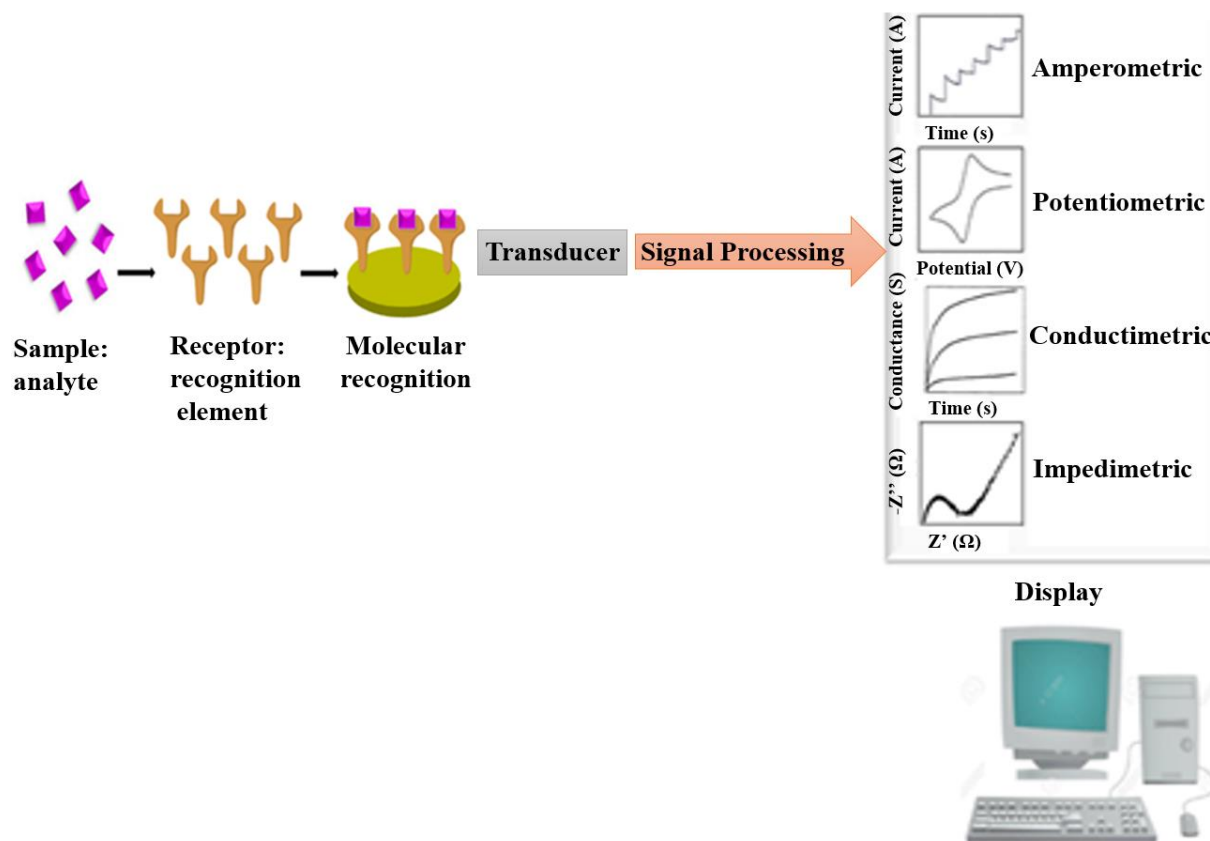


Figure 1.7: Schematic illustration of an electrochemical sensor system showing the three primary elements, the sample (or analyte), the transduction platform, and the signal processing step.

1.1.10 Electrochemical sensors based on quinone-modified SAMs

Quinones/hydroquinones (Q/HQ) are active redox systems with a high reactivity allowing their use in the field of chemical detection. Indeed, the molecular orbital spectrum of 1,4-benzoquinone shows an uneven electron density distribution, which explains its broad spectrum of activity [113]. As a result, several types of interfacial reactions have been studied on SAMs modified by quinones. These include Diels-Alder addition reactions [114,115], or with amines [116], or with aminoxy groups [117] and thiols [118], which can be monitored electrochemically.

For instance, Li *et al.* [119] reported an investigation of an electrochemically switched heterocyclization reaction of L-cysteine on hydroquinone-terminated SAMs. The reaction process was controlled by X-ray photoelectron spectroscopy and electrochemical surface-enhanced Raman spectroscopy. Applying a moderate anodic potential, the hydroquinone is converted to quinone

which reacts with the thiol of L-cysteine to give a cyclization product (Figure 1.8). Such reaction was discussed earlier by Crescenzi *et al.* [120].

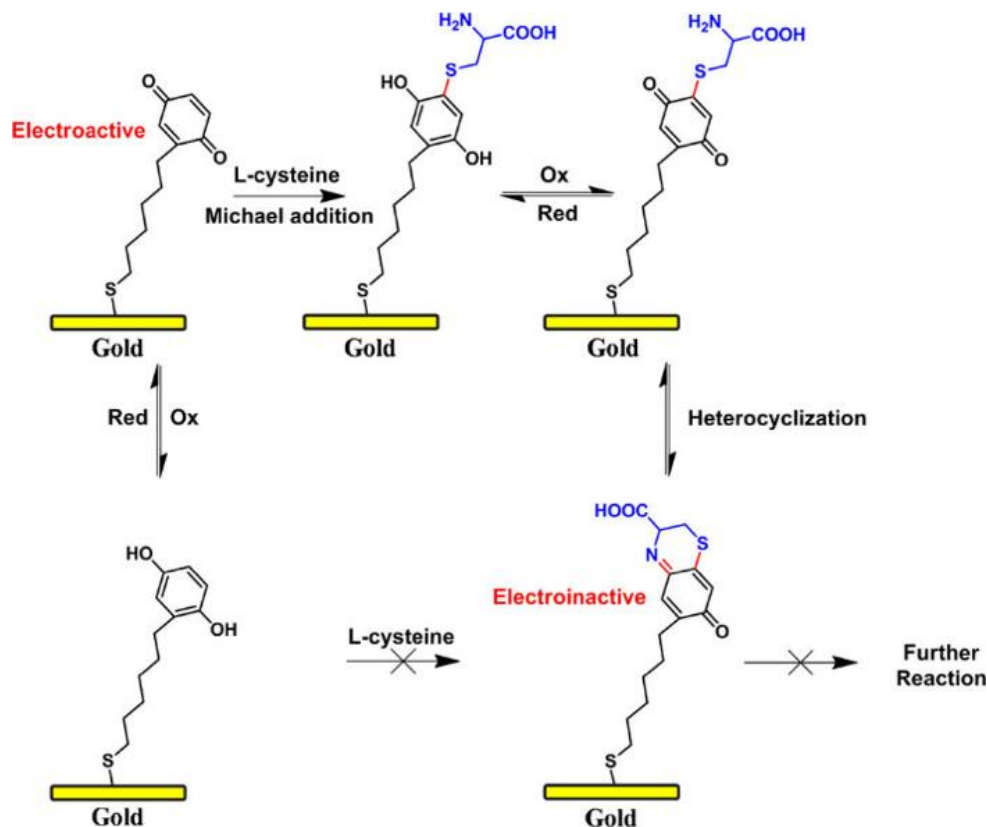


Figure 1.8: Illustration of the reaction between the benzoquinone immobilized on gold surface and L-cysteine [119].

An electroactive sensor based on HQ-terminated dodecanethiol was reported by Shamsipur *et al.* [121] for the detection of glutathione in solution (Figure 1.9). Electrochemical behavior of the sensor involves interfacial Michael-addition reaction [113] between quinone moiety and glutathione. The reaction was controlled by cyclic voltammetry, electrochemical impedance and infrared spectroscopy. Electrochemical and kinetic parameters have been evaluated and discussed.

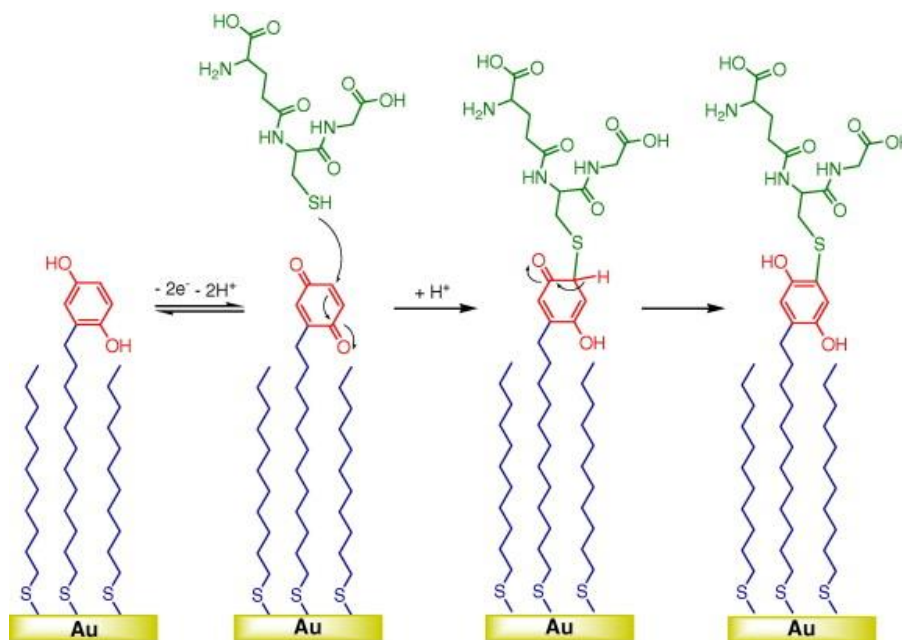


Figure 1.9: Schematic representation of the immobilization of glutathione onto modified gold surface through interfacial Michael-addition reaction between glutathione and the generated quinone under electrochemically activated surface [119].

In another interesting work [122], Hammami *et al.* developed an electrochemical sensor for dopamine using a gold electrode functionalized with a self-assembled monolayer of ω -mercaptopropyl naphthoquinone. The presence of dopamine in aqueous media produces an increase of the reduction current peak at -0.30 V vs. AgCl/Ag which corresponds to the reduction of naphthoquinone to hydronaphthoquinone. Differential pulse voltammetry was applied to confirm the selectivity of the sensor. Results obtained from urine samples were satisfactory, proving the sensitivity of the system toward dopamine.

1.1.11 Hydrogen peroxide electrochemical (bio)sensors based on SAMs

Hydrogen peroxide is a byproduct of several highly selective oxidases, and also an essential mediator in food, biology, medicine, industry and environmental analysis [123]. The development of reliable, sensitive and accurate methods for hydrogen peroxide determination is becoming of practical importance. Various techniques have been used for this determination, such as titrimetry [124], spectroscopy [125], fluorescence [126-127], high performance liquid chromatography [128], but these techniques suffer from interferences, long analysis time and use of expensive reagents. Among these techniques, electrochemical techniques have received a considerable interest since H_2O_2 itself is electrochemically active [129]. For example, Eftekhari [130] developed

a film of manganese hexacyanoferrate immobilized onto aluminium electrode surface. The stability of the electroactive film was controlled using cyclic voltammetry. The modified electrode was applied for H₂O₂ sensing. Results show a linear response in concentration range of 6.0×10^{-7} – 7.4×10^{-3} M with a low limit of detection. Application of the film for H₂O₂ detection in real samples confirmed its good selectivity. In another work, Yan *et al.* [131] reported the synthesis of a non-enzymatic sensor for hydrogen peroxide based on Cu₂O granular nanowires. The sensor was prepared on the basis of a gold electrode modified with Cu₂O nanowires and Nafion. Both cyclic voltammetry and chronoamperometry were applied for the detection of H₂O₂. A high sensitivity, a wide linear range, and a low detection limit were obtained.

Because of their convenience, high sensitivity and selectivity, electrochemical biosensors have received considerable interest [132]. In such sensors, the enzymes are immobilized onto different solid surfaces and used to generate signals corresponding to specific analytes in solution. Indeed, incorporation of enzyme into suitable films modified on electrodes constitute an effective way to avoid enzyme leaching and improve the direct electron transfer of redox enzymes [132]. As an example, Şenel *et al.* [133] reported the development as well as the application of an amperometric biosensor for the determination of H₂O₂ in aqueous medium. The biosensor is based on catalase immobilized on copolymer film of poly(glycidyl methacrylate-co-vinylferrocene), (poly(GMA-co-VFc)), modified glassy carbon electrode via amine group (Figure 1.10). Amperometric response was measured as a function of concentration of H₂O₂, at fixed potential of +0.35 V vs. AgCl/Ag. The biosensor showed a fast response of less than 7 s with linear range 0.5-14 mM. The sensitivity of the biosensor for H₂O₂ was 34 nA/mM·cm².

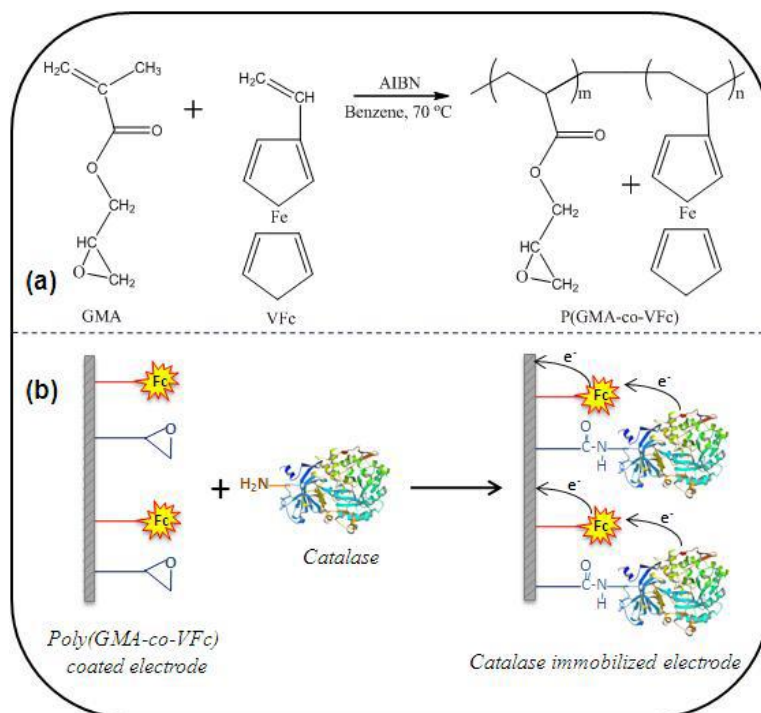


Figure 1.10: (a) Preparation of poly (GMA-co-VFc) and (b) immobilization of catalase via amine group onto Poly (GMA-co-VFc) film electrode [133].

As a last example, an amperometric and impedimetric biosensor for H₂O₂ detection based on horseradish peroxidase (HRP) has been developed by Periasamy *et al.* [134]. HRP was covalently immobilized at ruthenium oxide nanoparticles-modified glassy carbon electrode surface using chitosan–glutaraldehyde as cross-linking agent. Both electrochemical impedance spectroscopy and amperometry showed good sensitivity toward hydrogen peroxide. The developed biosensor gave acceptable H₂O₂ recovery in the contact lens cleaning solution.

4. Conclusion

In this chapter, we have presented a description of self-assembled monolayers. First and after defining SAMs and a brief review of the work devoted to them, we have described their main characteristics and the different methods used to their preparation. Then we devoted a part of this chapter to review the various bibliographical data concerning quinone-based redox SAMs, their functionalization modes as well as their applications. A reminder concerning electrochemical sensors and an illustration of some examples of these systems based on quinone-terminated SAMs have been elucidated.

References

- [1] B. Franklin, W. Brownrigg, Mr. Farish, *Philos. Trans. R. Soc., London*, **1774**, 64, 445–460.
- [2] I. Langmuir, *J. Am. Chem. Soc.*, **1917**, 39, 1848–1906.
- [3] I. Langmuir, *Trans. Faraday Soc.*, **1920**, 15, 62–74.
- [4] K. B. Blodgett, *J. Am. Chem. Soc.*, **1935**, 57, 1007–1022.
- [5] K. B. Blodgett, I. Langmuir, *Phys. Rev.*, **1937**, 51, 964–982.
- [6] W. C. Bigelow, D. L. Pikett, W. A. Zisman, *J. Colloid. Interface Sci.*, **1946**, 1, 513–538.
- [7] R. G. Nuzzo, D. L. Allara, *J. Am. Chem. Soc.*, **1983**, 105, 4481–4483.
- [8] D. L. Allara, A. F. Hebard, F. J. Padden, R. G. Nuzzo, D. R. Falcone, *J. Vac. Sci. Technol. A*, **1983**, 1, 376–382.
- [9] R. G. Nuzzo, F. A. Fusco, D. L. Allara, *J. Am. Chem. Soc.*, **1987**, 109, 2358–2368.
- [10] R. G. Nuzzo, B. R. Zegarski, L. H. Dubois, *J. Am. Chem. Soc.*, **1987**, 109, 733–740.
- [11] H. O. Finklea, S. Avery, M. Lynch, T. Furtch, *Langmuir*, **1987**, 3, 409–413.
- [12] M. D. Porter, T. B. Bright, D. L. Allara, C. E. D. Chidsey, *J. Am. Chem. Soc.*, **1987**, 109, 3559–3568.
- [13] E. Sabatani, I. Rubinstein, *J. Phys. Chem.*, **1987**, 91, 6663–6669.
- [14] P. E. Laibinis, J. J. Hickman, M. S. Wrighton, G. M. Whitesides, *Science*, **1989**, 245, 845–847.
- [15] C. D. Bain, H. A. Biebuyck, G. M. Whitesides, *Langmuir*, **1989**, 5, 723–727.
- [16] C. D. Bain, G. M. Whitesides, *Langmuir*, **1989**, 5, 1370–1378.
- [17] C. D. Bain, E. B. Troughton, Y. T. Tao, J. Evall, G. M. Whitesides, R. G. Nuzzo, *J. Am. Chem. Soc.*, **1989**, 111, 321–335.
- [18] J. C. Love, L. A. Estroff, J. K. Kriebel, R. G. Nuzzo, G. M. Whitesides, *Chem. Rev.*, **2005**, 105, 1103–1169.
- [19] C. Vericat, M. E. Vela, G. Benitez, P. Carro, R. C. Salvarezza, *Chem. Soc. Rev.*, **2010**, 39, 1805–1834.
- [20] R. K. Smith, P. A. Lewis, P. S. Weiss, *Prog. Surf. Sci.*, **2004**, 75, 1–68.
- [21] D. Mandler, I. Turyan, *Electroanalysis*, **1996**, 8, 207–213.
- [22] A. Ulman, *Chem. Rev.*, **1996**, 96, 1533–1554.
- [23] K. Arihara, T. Ariga, N. Takashima, K. Arihara, T. Okajima, F. Kitamura, K. Tokuda, T. Ohsaka, *Phys. Chem. Chem. Phys.*, **2003**, 5, 3758–3761.
- [24] A. Hamelin, *J. Electroanal. Chem.*, **1996**, 407, 1–11.
- [25] H. Angerstein-Kozłowska, B. E. Conway, A. Hamelin, L. Stoicoviciu, *Electrochim. Acta*, **1986**, 31, 1051–1061.
- [26] H. Shi, C. Stampfl, *Phys. Rev. B*, **2007**, 76, 075327.
- [27] L. M. Fischer, M. Tenje, A. R. Heiskanen, N. Masuda, J. Castillo, A. Bentien, J. Émneus, M. H. Jakobsen, A. Boisen, *Microelectron. Eng.*, **2009**, 86, 1282–1285.
- [28] F. Davis, S. P. J. Higson, *Biosens. Bioelectron.*, **2005**, 21, 1–20.
- [29] M. Cohen-Atiya, D. Mandler, *J. Electroanal. Chem.*, **2003**, 550–551, 267–276.
- [30] H. O. Finklea, *Encyclopedia of Analytical Chemistry*, Online © 2006 John Wiley & Sons, Ltd, **2006**.
- [31] J. L. Trevor, K. R. Lykke, M. J. Pellin, L. Hanley, *Langmuir*, **1998**, 14, 1664–1673.
- [32] R. G. Pearson, *Inorganica Chim. Acta*, **1995**, 240, 93–98.
- [33] D. Mandler, S. Kraus-Ophir, *J. Solid State Electr.*, **2011**, 15, 1535–1558.
- [34] L. Pauling, *J. Am. Chem. Soc.*, **1932**, 54, 3570–3582.

- [35] G. E. Poirier, *Chem. Rev.*, **1997**, 97, 1117–1127.
- [36] F. Schreiber, A. Eberhardt, T. Y. B. Leung, P. Schwartz, S. M. Wetterer, D. J. Lavrich, L. Berman, P. Fenter, P. Eisenberger, G. Scoles, *Phys. Rev. B*, **1998**, 57, 12476–12481.
- [37] S. Xu, S. J. N. Cruchon-Dupeyrat, J. C. Garno, G.-Y. Liu, G. Kane Jennings, T.-H. Yong, P. E. Laibinis, *J. Chem. Phys.*, **1998**, 108, 5002–5012.
- [38] G. E. Poirier, E. D. Pylant, *Science*, **1996**, 272, 1145–1148.
- [39] X. Torrelles, C. Vericat, M. E. Vela, M. H. Fonticelli, M. A. Daza Millone, R. Felici, T.-L. Lee, J. Zagenhagen, G. Muñoz, J. A. Martín-Gago, R. C. Salvarezza, *J. Phys. Chem. B*, **2006**, 110, 5586–5594.
- [40] M. Kara, H. Sasabe, W. Knoll, *Thin Solid Films*, **1996**, 273, 66–69.
- [41] L. M. Rodríguez, J. E. Gayone, E. A. Sánchez, O. Grizzi, B. Blum, R. C. Salvarezza, L. Xi, W. M. Lau, *J. Am. Chem. Soc.*, **2007**, 129, 7807–7813.
- [42] M. A. D. Millone, H. Hamoudi, L. Rodríguez, A. Rubert, G. A. Benítez, M. E. Vela, R. C. Salvarezza, J. E. Gayone, E. A. Sánchez, O. Grizzi, C. Dablemont, V. A. Esaulov, *Langmuir*, **2009**, 25, 12945–12953.
- [43] E. B. Troughton, C. D. Bain, G. M. Whitesides, R. G. Nuzzo, D. L. Allara, M. D. Porter, *Langmuir*, **1988**, 4, 365–385.
- [44] T. T. T. Li, H. Y. Liu, M. J. Weaver, *J. Am. Chem. Soc.*, **1984**, 106, 1233–1239.
- [45] A. Ihs, K. Uvdal, B. Liedberg, *Langmuir*, **1993**, 9, 733–739.
- [46] T. Arndt, H. Schupp, W. Schrepp, *Thin Solid Films*, **1989**, 178, 319–326.
- [47] F. Schreiber, *Prog. Surf. Sci.*, **2000**, 65, 151–257.
- [48] B. D. Gates, Q. Xu, M. Stewart, D. Ryan, C. G. Willson, G. M. Whitesides, *Chem. Rev.* **2005**, 105, 1171–1196.
- [49] M. Riepl, V. M. Mirsky, O. S. Wolfbeis, *Microchim. Acta*, **1999**, 131, 29–34.
- [50] M. Riepl, V. M. Mirsky, I. Novotny, V. Tvarozek, V. Rehacek, O. S. Wolfbeis, *Anal. Chim. Acta*, **1999**, 392, 77–84.
- [51] C. A. Widrig, C. Chung, M. D. Porter, *J. Electroanal. Chem. Interf. Electrochem.*, **1991**, 310, 335–359.
- [52] A. Kolodziej, F. Fernandez-Trillo, P. Rodriguez, *J. Electroanal. Chem.*, **2018**, 819, 51–57.
- [53] R. C. Salvarezza, P. Carro, *J. Electroanal. Chem.*, **2018**, 819, 234–239.
- [54] H. Takiguchi, K. Sato, T. Ishida, K. Abe, K. Yase, K. Tamada, *Langmuir*, **2000**, 16, 1703–1710.
- [55] J. Noh, F. Nakamura, J. Kim, H. Lee, M. Hara, *Mol. Cryst. Liq. Cryst.*, **2002**, 377, 165–169.
- [56] H. Schönherr, G. J. Vancso, B.-H. Huisman, F. C. J. M. van Veggel, D. N. Reinhoudt, *Langmuir*, **1999**, 15, 5541–5546.
- [57] H. Lee, Z. He, C. L. Hussey, D. L. Mattern, *Chem. Mater.*, **1998**, 10, 4148–4153.
- [58] M. C. Leavy, S. Bhattacharyya, W. E. Cleland, Jr., C. L. Hussey, *Langmuir*, **1999**, 15, 6582–6586.
- [59] M. W. J. Beulen, B.-H. Huisman, P. A. van der Heijden, F. C. J. M. van Veggel, M. G. Simons, E. M. E. F. Biemond, P. J. de Lange, D. N. Reinhoudt, *Langmuir*, **1996**, 12, 6170–6172.
- [60] J. B. Schlenoff, M. Li, H. Ly, *J. Am. Chem. Soc.*, **1995**, 117, 12528–12536.
- [61] K. Wang, C. Goyer, A. Anne, C. Demaille, *J. Phys. Chem. B*, **2007**, 111, 6051–6058.
- [62] A. Anne, C. Demaille, *J. Am. Chem. Soc.*, **2008**, 130, 9812–9823.
- [63] A. Anne, E. Cambriel, A. Chovin, C. Demaille, C. Goyer, *ACS Nano*, **2009**, 3, 2927–2940.
- [64] W. Paik, S. Eu, K. Lee, S. Chon, M. Kim, *Langmuir*, **2000**, 16, 10198–10205.
- [65] S. Eu, W.-K. Paik, *Mol. Cryst. Liq. Cryst.*, **1999**, 337, 49–52.

- [66] C. Jung, O. Dannenberger, Y. Xu, M. Buck, M. Grunze, *Langmuir*, **1998**, 14, 1103–1107.
- [67] J. Madoz, B. A. Kuznetsov, F. J. Medrano, J. L. Garcia, V. M. Fernandez, *J. Am. Chem. Soc.*, **1997**, 119, 1043–1051.
- [68] Y. Dong, C. Shannon, *Anal. Chem.*, **2000**, 72, 2371–2376.
- [69] J. Sharma, R. Chhabra, C. S. Andersen, K. V. Gothelf, H. Yan, Y. Liu, *J. Am. Chem. Soc.*, **2008**, 130, 7820–7821.
- [70] D. González-Rodríguez, M. V. Martínez-Díaz, J. Abel, A. Perl, J. Huskens, L. Echegoyen, T. Torres, *Org. Lett.*, **2010**, 12, 2970–2973.
- [71] A. S. Viana, S. Leupold, C. Eberle, T. Shokati, F.-P. Montforts, L. M. Abrantes, *Surf. Sci.*, **2007**, 601, 5062–5068.
- [72] P. D. Beer, J. J. Davis, D. A. Drillsma-Milgrom, F. Szemes, *Chem. Commun.*, **2002**, 16, 1716–1717.
- [73] Z. Li, T. Niu, Z. Zhang, G. Feng, S. Bi, S. Thin Solid Films, **2011**, 519, 4225–4233.
- [74] Y. Dong, S. Abaci, C. Shannon, M. J. Bozack, *Langmuir*, **2003**, 19, 8922–8926.
- [75] P. M. Dey, J. B. Harborne, *Methods in plant biochemistry*, J. B. Harborne (ed) Plant phenolics, Academic Press, London, **1989**, 1, 452–791.
- [76] R. Nageswara Rao, M. V. N. Kumar Talluri, D. D. Shinde, *J. Pharmaceut. Biomed.*, **2008**, 47, 230–237.
- [77] C. Cleren, L. Yang, B. Lorenzo, N. Y. Calingasan, A. Schomer, A. Sireci, E. J. Wille, M. F. Beal, *J Neurochem.*, **2008**, 104, 1613–1621.
- [78] M. K. Azharuddin, D. S. J. O'Reilly, A. Gray, T. Talwar, *Clin Chem*, **2007**, 53, 1706–1713.
- [79] R. Wallin, L. Schurgers, N. Wajih, *Thromb. Res.*, **2008**, 122, 411–417.
- [80] P. Weber, *Nutrition*, **2001**, 17, 880–887.
- [81] R. C. Prince, P. Leslie Dutton, J. Malcolm Bruce, *FEBS Lett.*, **1983**, 160, 273–276.
- [82] S. Rahman, K. Bhatia, A. Q. Khan, M. Kaur, F. Ahmad, H. Rashid, M. Athar, F. Islama, S. Raisuddin, *Chem.-Biol. Interact.*, **2008**, 172, 195–205.
- [83] Q. Zhu, M. A. Emanuele, N. LaPaglia, E. J. Kovacs, N. V. Emanuele, *Endocr.*, **2007**, 32, 59–68.
- [84] M. R. Rizzo, A. M. Abbatecola, M. Barbieri, M. T. Vietri, M. Cioffi, R. Grella, A. M. Molinari, R. Forsey, J. Powell, G. Paolisso, *J. Am. Coll. Nutr.*, **2008**, 27, 505–511.
- [85] M. Mansour, S. Tornhamre, *J. Enzym. Inhib. Med. Ch.*, **2004**, 19, 431–436.
- [86] L. Savarino, A. Fioravanti, G. Leo, R. Aloisi, M. Mian, *Clin. Orthop. Relat. R.*, **2007**, 461, 231–237.
- [87] C. Zhang, J. G. Ondeyka, D. L. Zink, A. Basilio, F. Vicente, J. Collado, G. Platas, G. Bills, J. Huber, K. Dorso, M. Motyl, K. Byrne, S. B. Singh, *J. Nat. Prod.*, **2008**, 71, 1304–1307.
- [88] B. N. Lenta, B. Weniger, C. Antheaume, D. T. NOUNGOU, S. Ngouela, J. C. N. Assob, C. Vonthron-Sénécheau, P. A. Fokou, K. P. Devkota, E. Tsamo, N. Sewald, *Phytochemistry*, **2007**, 68, 1595–1599.
- [89] P. S. Koka, D. Mondal, M. Schultz, A. B. Abdel-Mageed, K. C. Agrawal, *Exp. Biol. Med.*, **2010**, 235, 751–760.
- [90] C.-C. Su, G.-W. Chen, J.-C. Kang, M.-H. Chan, *Planta Med.*, **2008**, 74, 1357–1362.
- [91] Y. Lu, J. Zhang, J. Qian, *Cancer Biother. Radio.*, **2008**, 23, 222–228.
- [92] L. Álvarez-Cedrón, M. L. Sayalero, J. M. Lanao, *J. Chromatogr. B Biomed. Appl.*, **1999**, 721, 271–278.
- [93] N. El-Najjar, H. Gali-Muhtasib, R. A. Ketola, P. Vuorela, A. Urtti, H. Vuorela, *Phytochem. Rev.*, **2011**, 10, 353–370.

- [94] E. J. Land, C. A. Ramsden, P. A. Riley, *Method. Enzymol.*, **2004**, 378, 88–109.
- [95] P. S. Magee, *Quant. Struct. Act. Relat.*, **2000**, 19, 22–28.
- [96] M. M. Villalba, V. J. Litchfield, R. B. Smith, A. M. Franklin, C. Livingstone, J. Davis, J. *Biochem. Biophys. Methods*, **2007**, 70, 797–802.
- [97] R. B. Smith, C. Canton, N. S. Lawrence, C. Livingstone, J. Davis, *New J. Chem.*, **2006**, 30, 1718–1724.
- [98] A. R. Katritzky, D. Fedoseyenko, P. P. Mohapatra, P. J. Steel, *Synthesis*, **2008**, 5, 777–787.
- [99] H.-G. Hong, W. Park, *Langmuir*, **2001**, 17, 2485–2492.
- [100] S. A. Trammell, D. S. Seferos, M. Moore, D. A. Lowy, G. C. Bazan, J. G. Kushmerick, N. Lebedev, *Langmuir*, **2007**, 23, 942–948.
- [101] S. A. Trammell, M. Moore, T. L. Schull, N. Lebedev, *J. Electroanal. Chem.*, **2009**, 628, 125–133.
- [102] J. Q. Chambers, S. Patai (Eds), *The Chemistry of Quinonoid Compounds*, Wiley, New York, **1974**, Chapter 14, 737.
- [103] R. A. Morton (Ed.), *Biochemistry of Quinones*, Academic Press, New York, **1965**.
- [104] K. Öllinger, *Cellular Toxicity of Quinones: Redox- and addition chemistry*, Linköping University, Linköping, **1992**.
- [105] N. Sandhyarani, T. Pradeep, *Int. Rev. Phys. Chem.*, **2003**, 22, 221–262.
- [106] M. Kažemėkaitė, A. Bulovas, Z. Talaikytė, V. Railaitė, G. Niaura, E. Butkus, V. Razumas, *Tetrahedron Lett.*, **2008**, 49, 6212–6216.
- [107] A. Bulovas, N. Dirvianskytė, Z. Talaikytė, G. Niaura, S. Valentukonytė, E. Butkus, V. Razumas, *J. Electroanal. Chem.*, **2006**, 591, 175–188.
- [108] J. R. Stetter, W. R. Penrose, S. Yao, *J. Electrochem. Soc.*, **2003**, 150, 11–16.
- [109] M. Govindhan, B.-R. Adhikari, A. Chen, *RSC Adv.*, **2014**, 4, 63741–63760.
- [110] F. S. Omar, N. Duraisamy, K. Ramesh, S. Ramesh, *Biosens. Bioelectron.*, **2016**, 79, 763–775.
- [111] A. Hierlemann, R. Gutierrez-Osuna, *Chem. Rev.*, **2008**, 108, 563–613.
- [112] M. Bonizzoni, E. V. Anslyn, *J. Am. Chem. Soc.*, **2009**, 131, 14597–14598.
- [113] L. R. De Astudillo, L. Rivera, R. Brito-Gómez, R. J. Tremont, *J. Electroanal. Chem.*, **2010**, 640, 56–60.
- [114] M. N. Yousaf, M. Mrksich, *J. Am. Chem. Soc.* **1999**, 121, 4286–4287.
- [115] W.-S. Yeo, M. N. Yousaf, M. Mrksich, *J. Am. Chem. Soc.* **2003**, 125, 14994–14995.
- [116] E. Katz, T. Lötzbeyer, D. D. Schlereth, W. Schuhmann, H.-L. Schmidt, *J. Electroanal. Chem.*, **1994**, 373, 189–200.
- [117] E. W. L. Chan, M. N. Yousaf, *J. Am. Chem. Soc.*, **2006**, 128, 15542–15546.
- [118] K. T. (n.d.) Finley, *The Chemistry of Quinonoid Compounds*, **1974**, 2, 877–1144.
- [119] J. Li, C.-L. Sun, L. Tan, Y.-L. Xie, H.-L. Zhang, *Langmuir*, **2013**, 29, 5199–5206.
- [120] O. Crescenzi, G. Prota, T. Schultz, L. J. Wolfram, *Tetrahedron*, **1988**, 44, 6447–6450.
- [121] M. Shamsipur, S. H. Kazemi, A. Alizadeh, M. F. Mousavi, M. S. Workentin, *J. Electroanal. Chem.*, **2007**, 610, 218–226.
- [122] A. Hammami, R. Sahli, N. Raouafi, *Microchim. Acta*, **2016**, 183, 1137–1144.
- [123] L. Wang, E. Wang, *Electrochem. Commun.*, **2004**, 6, 225–229.
- [124] E. C. Hurdis, J. Hendrik Romeyn, *Anal. Chem.*, **1954**, 26, 320–325.
- [125] C. Matsubara, N. Kawamoto, K. Takamura, *Analyst*, **1992**, 117, 1781–1784.
- [126] H. Chen, H. Yu, Y. Zhou, L. Wang, *Spectrochim. Acta A*, **2007**, 67, 683–686.
- [127] M. E. Abbas, W. Luo, L. Zhu, J. Zou, H. Tang, *Food Chem.*, **2010**, 120, 327–331.

- [128] M. Tarvin, B. McCord, K. Mount, K. Sherlach, M. L. Miller, *J. Chromatogr. A*, **2010**, 1217, 7564–7572.
- [129] M. S. Lin, H. J. Leu, *Electroanal.*, **2005**, 17, 2068–2073.
- [130] A. Eftekhari, *Talanta*, **2001**, 55, 395–402.
- [131] Z. Yan, J. Zhao, L. Qin, F. Mu, P. Wang, X. Feng, *Microchim. Acta*, **2012**, 180, 145–150.
- [132] M. Shamsipur, M. Asgari, M. F. Mousavi, R. Davarkhah, *Electroanal.*, **2011**, 24, 357–367.
- [133] M. Şenel, E. Çevik, M. Fatih Abasıyanık, *Anal. Bioanal. Electrochem.*, **2011**, 3, 14–25.
- [134] A. P. Periasamy, S. W. Ting, S.-M. Chen, *Int. J. Electrochem. Sci.*, **2011**, 6, 2688–2709.

**Chapter 2: Synthesis and
characterization of the anchor
site: 1,3-dimercaptopropan-2-ol**



5. Introduction

Over the last decades, thiols are widely used as anchor molecules for preparing stable and oriented SAMs onto gold surfaces [1-3]. The advantages of SAMs include the simplicity of preparation, the high reproducibility and the possibility of introducing of different chemical functionalities with a high level of order in the molecular scale. These features have led to a convenient approach for surface functionalization which is often required for the preparation of chemical sensors and biosensors [4,5].

But despite of successful applications of this approach well documented in thousands of scientific publications, this system isn't thermodynamically stable. Let us consider a SAM in the contact with aqueous environment that does not contain the precursor adsorbate. Because of the high value of the difference of chemical potentials of the SAM molecules in the monolayer and in the aqueous phase, such a system cannot be in equilibrium. Therefore, one can expect a slow desorption of the adsorbates and/or replacement of these molecules by other ones (see Figure 2.1) and consequently this weak interface layer cannot provide highly effective sensing for chemical or biochemical products. Such processes were investigated in many papers using different approaches [6,7]. The results show that the long chain thiols are thermally more stable than the short chain ones. Such influence of the aliphatic chain on the SAM stability was also demonstrated by theoretical simulations. [8]. No desorption was detected for monolayers made of linear alkylthiol with 15 or more methylene groups [7]. However, so thick monolayers form a high barrier for electron tunneling [2] and therefore cannot be used for electrochemical applications requiring effective charge transfer through the SAM.

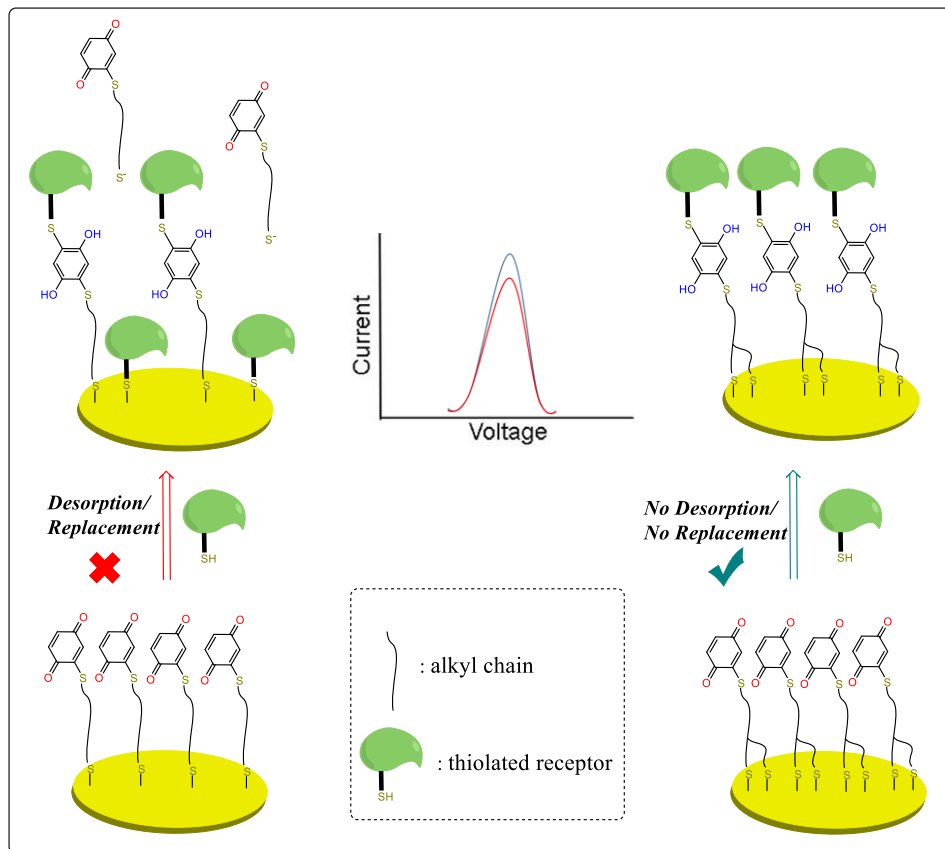


Figure 2.1: Representative scheme of the main goal of the performed work.

A possible solution to overcome this hindrance is the use of anchor molecules possessing more than one thiol moieties, for instance thioctic acid (alpha lipoic acid). This system was applied as pH-sensors [9], as impedimetric sensors for heparin [10], for chiral molecules [11] and for antigen–antibody interaction [12,13]. An electrochemical sensor for detection of lead ions made by gold electrode modified thioctic acid followed by covalent attachment of human angiotensin was also described [14]. Due to higher stability of the SAM based on thioctic acid it was possible to perform many analysis/regeneration cycles with this sensor while the sensor based on mercaptopropionic acid could be applied only once. However, the asymmetry and chirality of thioctic acid may lead to some limitations in its applications. Pure mechanistically, one can expect a formation of defects in SAMs between two adjacent 8-th carbon atoms of thioctic acid molecules adsorbed with a random orientation.

In this chapter, we suggest a new type of anchoring molecule: 1,3-dimercaptopropan-2-ol to grow SAM on gold. Contrary to its isomer 2,3-dimercapto-1-propanol, 1,3-dimercaptopropan-2-ol

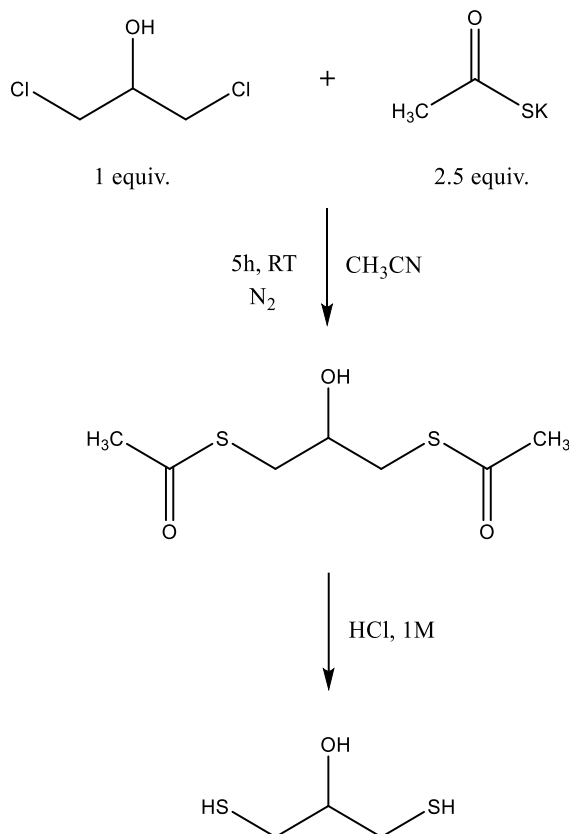
(further referred as DiSH) has a symmetric structure which can provide well-oriented SAMs onto the gold surface. This chapter gives a detailed study on the formation, characterization and immobilization structure of SAMs formed from this compound at different conditions of preparation as well as its stability and electrically driven desorption with comparison to other SAMs, in aqueous media and in the presence of other thiols using cyclic voltammetry, impedance spectroscopy, quantum mechanical calculations, contact angle, X-ray photoelectron spectroscopy, kinetic capacitance and step-potential chronoamperometry.

6. Dimercaptopropan-2-ol: Synthesis/characterization

1.8 Synthesis

DiSH was formed by deprotection of thiol groups of 1,3-dithioacetatepropan-2-ol which contains two thiol groups protected by acetate. This protection makes the compound highly stable; it can be stored for a long time at atmospheric air. To prevent a formation of disulfide byproducts, the removing of the protective group was performed immediately before SAM preparation.

The chemical synthesis of 1,3-dithioacetatepropan-2-ol was performed according to thioacetate-protected poly(ethylene glycol) synthesis described earlier [15] with some modifications in the experimental conditions. In a dropping funnel, 1.0 g of highly concentrated solution of 1,3-dichloro-2-propanol in dry acetonitrile was added dropwise during 15 minutes to the freshly prepared highly concentrated solution of 330 μL potassium thioacetate in dry acetonitrile in a 1:2.5 molar ratio (Schema 2.1). The mixture was stirred under argon atmosphere and incubated with a constant stirring for five hours at room temperature (RT).



Schema 2.1: Representation of the synthesis reaction of 1,3-dimercaptopropan-2-ol.

The white KCl precipitate was filtered off and the solvent was evaporated. Then small amount of water was added, the mixture was shaken, and the organic phase was extracted in dichloromethane. Then, the formed 1,3-dithioacetatepropan-2-ol was isolated and purified by column chromatography on silica gel using cyclohexane/ethyl acetate (7:3, v/v) eluate. First, mono-thioacetatepropan-2-ol product was eluted, then dithioacetatepropan-2-ol. Both products are oily and yellow. Then the solvents were evaporated. The reaction yield for dithioacetatepropan-2-ol was 23 %. The deprotection of the thiol group reported in literature [16] was performed under acidic conditions.

1.9 Spectroscopic identification

1,3-dithioacetatepropan-2-ol identification was performed by nuclear magnetic resonance (NMR) of ¹H and ¹³C and by infrared (IR) spectroscopy. DiSH identification was performed using IR spectroscopy. ¹H NMR, ¹³C NMR and IR spectra as well as the attributed peaks are given in Annex B.

7. Self-assembled monolayers of 1,3-dimercaptopropan-2-ol onto gold surface

1.10 Preparation

Gold wires (99% gold, diameter 0.5 mm, length 1.0 cm) and gold-coated glass slides with dimensions of 20×20×1 mm³ (www.biosuplar.com) further referred as gold slides were used for the preparation of DiSH-based SAMs. Before the preparation of monolayers, a simple cleaning procedure based on conventional solvent rinses was used: acetone, ethanol, isopropanol, distilled water applied in consecutive order to remove loosely adhesive contaminations. The samples were fixed in a mount and washed under a stream of solvent from laboratory wash bottles in a direction tangential to the surface. After treatment in solvents, the remaining water was removed in a stream of dried argon under pressure, directed tangentially to the surface, or placed in a container with distilled water. The next treatment procedure consists on the use of ‘‘Piranha’’ solution composed by 1:3 (v:v) mixture of 30% H₂O₂/concentrated H₂SO₄. The samples were etched and held in a freshly prepared piranha solution for not more than 20s for gold slides, rinsed thoroughly with deionized water then with methanol and dried under a stream of filtered argon at RT. *Caution: piranha solution reacts violently with most organic materials and must be handled with extreme care.*

Gold slides were then incubated in 1:1:48 (v:v:v) mixture of 37% HCl/30% H₂O₂/H₂O for 15 minutes, washed again thoroughly with distilled water and dried. These cleaning steps were investigated and interpreted in details in our publication [B. Snopok, A. Laroussi, C. Cafolla, K. Voitchovsky, T. Snopok, V. Mirsky, Gold surface cleaning by etching polishing: Optimization of polycrystalline film topography and surface functionality for biosensing, Surf. Interfaces, 2021, 22, 100818.] dedicated to perform simple, reliable and fast method for the preparation of well-cleaned gold surface. After cleaning, the samples were modified by DiSH by simple immersion in a freshly prepared solution of 1.0 mM of DiSH in acetonitrile at RT for 12 h. At the end, and before each measurement, the samples were washed thoroughly with methanol to get rid of the physisorbed DiSH then dried for a few seconds under a stream of filtered argon.

1.11 Characterization

We have used the water contact angle (WCA), X-ray photoelectron spectroscopy (XPS) as well as electrochemical measurements in order to highlight the immobilization of DiSH on the gold surface.

1.1.12 Contact angle characterization

Contact angle measurements of water droplet were performed in order to get a qualitative evaluation of the gold surface properties, mainly the wettability of the surface, before and after the incubation process. Figure 2.2 shows the images of the gold slide before and after the addition of DiSH captured using a contact angle analyzer. The angle was calculated using the instrument software and the values shown represent the average of the angles from both sides of the droplet for fifty frames. The low value of the standard deviation confirms the reproducibility of the result. Results show that the formation of the SAM on the gold surface leads to the decrease in the contact angle of water droplet from 83° to 53° . This was expected since the DiSH monolayer possesses OH functional groups thus increasing the hydrophilicity of the surface during the formation of the SAM.

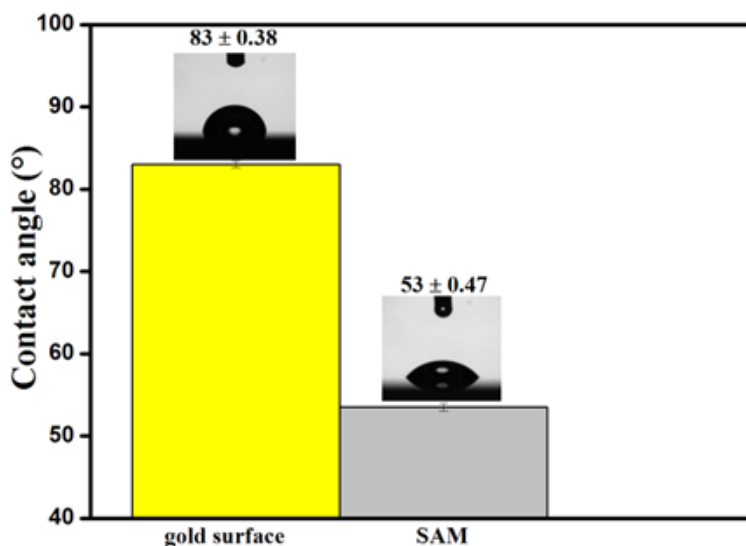


Figure 2.2: Static water contact angle measurements obtained from gold surfaces before and after modification with DiSH-SAM.

1.1.13 XPS characterization

XPS is a surface analysis technique that provides information on the chemical composition of a solid substrate with a thickness of less than a few μm . The XPS spectrum measured after the formation of DiSH monolayer on a gold slide indicates the presence of the chemical elements of the DiSH. The underlying gold gives an intense peak at 83.9 eV. The peak at 284.7 eV corresponds to C1s (carbon in aliphatic chains), [17] the peak at 532.4 eV can be attributed to O1s (oxygen in hydroxyl groups) [18] and the small peak at ~ 161.0 eV can be attributed to sulfur [19] of the DiSH monolayer.

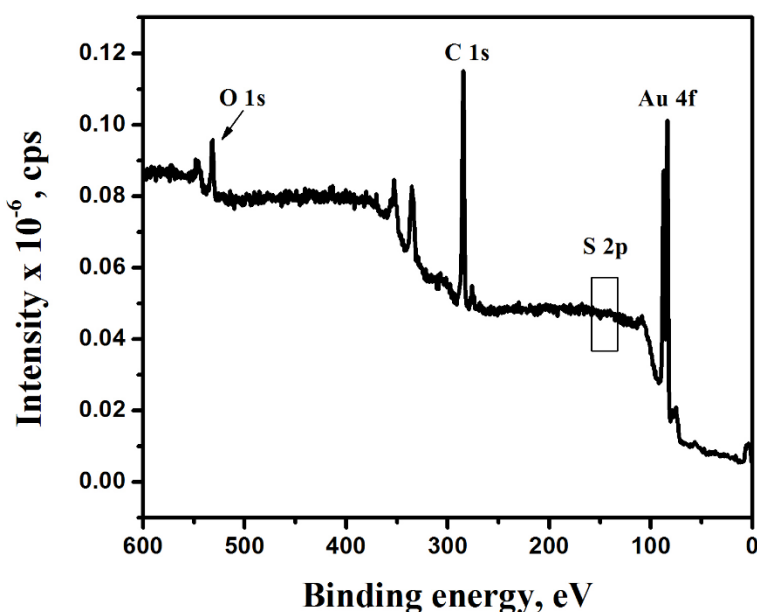


Figure 2.3: XPS spectrum of gold coated slide modified by DiSH-SAM.

1.1.14 Electrochemical characterization

A more detailed investigation of the SAM was performed by electrochemical techniques using cyclic voltammetry (CV) and electrochemical impedance spectroscopy (EIS).

1.1.14.1 Electrochemical cell

The polycrystalline gold wire (diameter 0.5 mm, length 1.0 cm) was used as working electrode. The gold wire was coated by melted glass to get a constant value of the electrode surface area. Platinum wire was served as an auxiliary electrode and AgCl/Ag (sat. KCl) electrode as a reference electrode. As indicated previously, gold wires undergo a cleaning step. Sometimes this step is not

enough to efficiently clean the gold surface. Therefore, we have resorted in many cases to the “restructuring” method which consists on polishing the gold electrode electrochemically in sulfuric acid solution (0.05 M) with a cyclic voltammetric sweep from -0.1 V to 1.5 V at a sweep rate of 50 mV/s. This technique is very effective to check the surface quality [20]. In acidic solution, the CV curves of a typical clean gold surface show oxidation and reduction peaks which correspond to the oxide formation and reduction on gold [21,22]. Another cleaning method consisting on boiling gold wires in a KOH solution (2.5M) under stirring for few hours was also used.

1.1.14.2 Electrochemical behavior of the SAM-modified gold electrode

The use of a redox probe allows to check the behavior of the treated surface. In our case, we carried out the characterization of the SAM using the ferro/ferricyanide couple $[\text{Fe}(\text{CN})_6]^{3-/4-}$ which presents a reversible signal. The CVs measured in presence of the redox probe before and after formation of the DiSH-based SAM on the gold electrode show that the electron transfer is influenced by the presence of the monolayer (Figure 2.4.a). The formed SAM leads to a decrease in the cathodic and anodic peak currents and to an increase in the gap between the potentials of these peaks (curve ii). However, the reaction is still diffusion controlled probably due to the low thickness of the formed layer. Therefore, one can confirm that the self-assembly of the DiSH on the electrode surface forms a semi-impermeable layer to redox entities and partially inhibits the electron transfer to the gold surface.

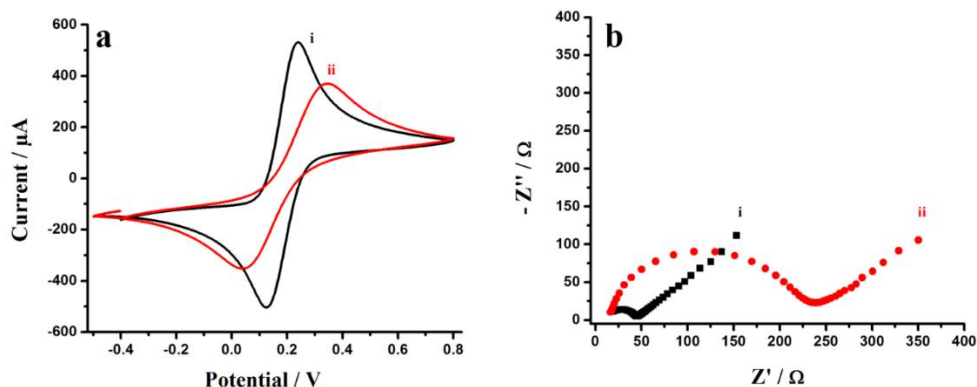


Figure 2.4: (a) Cyclic voltammograms at a scan rate of 200 mV s^{-1} , (b) impedance spectra in Nyquist representation recorded at the frequency range from 0.1 Hz to 100 kHz at a potential of +0.2 V (i) before and (ii) after modification with DiSH in a solution of: 10 mM $[\text{Fe}(\text{CN})_6]^{3-/4-}$, 0.1 M KCl.

To confirm this result, EIS measurements were performed by applying to the working electrode, in contact with a 10 mM solution of $[\text{Fe}(\text{CN})_6]^{3-/4-}$, a potential of 200 mV. EIS spectra, obtained in a frequency range from 100 kHz to 100 mHz, show an increase in the charge transfer resistance as a result of the increase in the loop diameter that intercepts the X axis (Z') confirming the change from a conductive surface, with low resistance to charge transfer, to a less conductive surface after modification by the DiSH-based SAM (Figure 2.4.b). Furthermore, impedance spectra were fitted by simplified Randles equivalent circuit [23-25] which simulates the surface. (Figure 2.5).

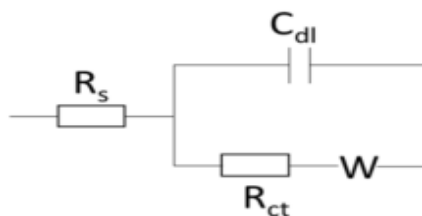


Figure 2.5: Schematic representation of Randles equivalent circuit for modified surface modelization.

In the circuit:

- R_s characterizes the resistance of the electrolyte solution,
- C_{dl} is the capacitance of the double layer,
- R_{CT} is the resistance of the charge transfer,
- Z_w is Warburg impedance which provides information on the diffusion of the species present in the environment.

To determine the charge, transfer resistance of the surface, it is recommended to use an active electrochemical probe and to apply an alternating potential of variable frequency with a small amplitude variation of ± 5 mV. The frequency sweep generally extends from high to low frequencies in a well-defined range by imposing a fixed potential. The ratio of the potential applied to the measured current gives the impedance, $Z(\omega)$, which is a complex function having a real part and another imaginary part. One of the most widely used representations is that of Nyquist that gives the inverse of the imaginary part according to the real part and appears as a semi-circle or two semi-circles. The diameter of the loop allows us to deduce the value of the charge transfer resistance while the origin of the loop corresponds to the resistance of the electrolyte R_s . Table 2.1 shows that R_s is fixed which is predictable because of the constant ionic strength of the solution while R_{CT} increases from 26 Ω to 220 Ω proving a partial blocking of the surface.

Table 2.1: Comparison between the resistance of the electrolyte solution R_S and the charge transfer resistance R_{CT} before and after modification of the gold electrode by DiSH.

Resistance	Bare gold electrode	SAM modified electrode
R_S / Ω	18 ± 1	17 ± 1
R_{CT} / Ω	26 ± 1	220 ± 2

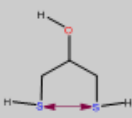
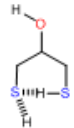
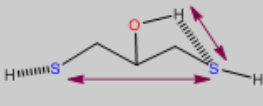
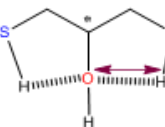
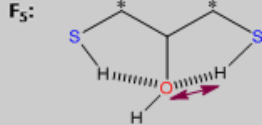
8. Electrochemical and spectroscopic investigations on the immobilization structure of the 1,3-dimercaptopropan-2-ol on the gold surface

1,3-dimercaptopropan-2-ol possesses two thiol groups. Therefore, its immobilization onto gold surface can occur by either one or both thiol groups. It was essential to determine the parameters monitoring the orientation structure of the DiSH in the SAM. Different procedures for the preparation of DiSH-based SAMs were used. One type of DiSH monolayer (further referred as SAM1) was performed by overnight incubation of the gold electrodes (or gold slides) in 1.0 mM of DiSH in acetonitrile at RT. Another type of DiSH SAM (further referred as SAM2) was performed by incubation of the gold electrode in 0.1 M solution of DiSH for 3 h.

1.12 Quantum mechanical calculations

Quantum mechanical calculations (QMCs) were performed using the density functional theory (DFT) [26,27] after optimization [28] of all obtained geometries. QMC of the DiSH-structure have given a number of possible conformations with relatively small difference in their energy (Table 2.2).

Table 2.2: Spatial representation of DiSH conformations using Gaussian software with the corresponding quantum mechanical calculation of relative energy and S-S distance.

DiSH Conformation	Relative Energy / Kcalmol ⁻¹	Distance / Å
F₁: 	5.61	$d_{S-S} = 3.477$
F₂: 	3.46	$d_{S-H} = 2.76$ $d_{S-S} = 3.74$
F₃: 	0.29	$d_{S-H} = 2.72$ $d_{S-S} = 5.046$
F₄: 	0	$d_{O-H} = 2.704$ $d_{S-S} = 5.65$
F₅: 	1.29	$d_{O-H} = 2.566$ $d_{S-S} = 5.64$

The distance between sulfur atoms can be from 3.47 till 5.65 Å. However, the binding energy of each thiol group to gold being $\sim 40 \text{ kcal}\cdot\text{mol}^{-1}$ is much larger, [2,29] therefore one can expect that namely this interaction defines the conformation of DiSH on the gold surface. The distance between adjacent thiol groups cannot be smaller than the distance between gold atoms which is 4.99 Å for the crystal facet with minimal surface energy (111) or 4.07 Å for the 100 facet [30,31]. Therefore, we suggest that the conformation of DiSH at which mainly both thiol groups bond gold atoms should be similar to that indicated in Fig. 2.6, left. In the same time, we cannot exclude that if an adsorption of DiSH is performed for a short time from a very concentrated solution, the majority of the di-thiols bind through only one sulfur atom to the gold surface. (Fig. 2.6, right).



Figure 2.6 Schematic representation of spatial conformation of the two types of binding of DiSH to the gold surface: binding by both thiol groups (left), and binding by only one thiol group (right).

1.13 Electrochemical characterization

Electrochemical characterizations on the orientation structure of DiSH monolayers were monitored using CV and EIS.

1.1.15 Cyclic voltammetric characterization

1.1.15.1 In potassium ferro/ferricyanide solution

The changes in the CVs measured in the presence of potassium ferro/ferricyanide after formation of SAM1 (Figure 2.7.b) and SAM2 (Figure 2.7.c) are very different. The CV measured at bare gold electrode (Figure 2.7.a) show clear oxidation and reduction peaks which indicates an essential diffusion control of the electrochemical reaction. As in the case of SAM1, a formation of SAM2 (Figure 2.7.c) on the electrode surface also leads to the decrease in the cathodic and anodic peaks and to a much smaller increase in the potential gap (Table 2.3). Also, in this case the electrochemical redox reaction of ferro/ferricyanide is essentially diffusion controlled.

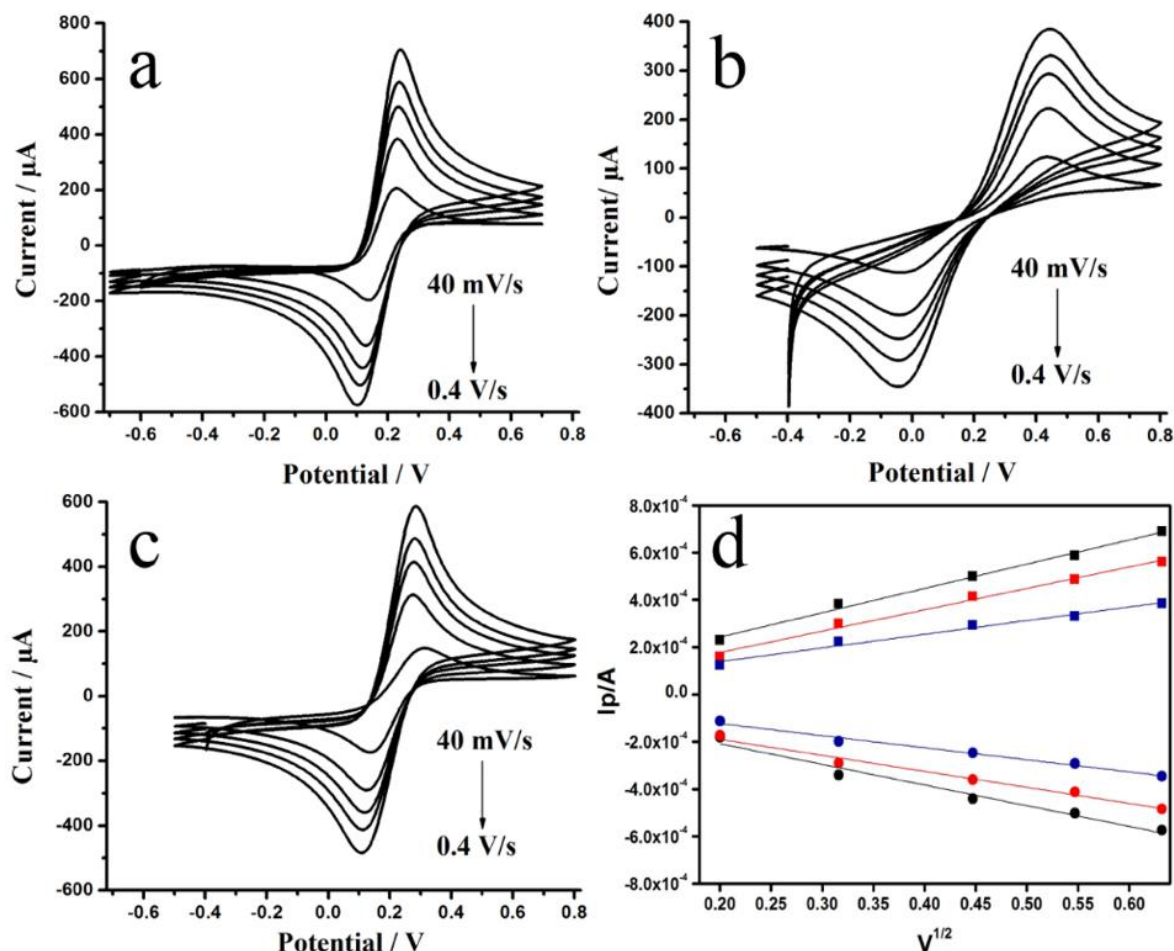


Figure 2.7: Cyclic voltammograms in 10 mM K₄[Fe(CN)₆] 0.1 M KCl at different sweep rates and Randles-Sevcik plots for the reduction (circles) and oxidation (squares) peaks of uncoated gold electrode (a, d black curves), gold electrode modified by SAM1 (b, d bleu curves) and gold electrode modified by SAM2 (c, d red curves).

A detailed analysis of CVs relative to bare gold electrode, gold electrode modified by SAM1 and SAM2 were realized involving several electrochemical parameters:

✓ Calculation of the diffusion coefficient

The Randles-Sevcik equation describes the peak current of reversible electrochemical reaction, i_p , measured as the distance from the baseline to the peak, to the scan rate was used for the determination of the diffusion coefficient D of ferro/ferricyanide ions. It is written as:

$$i_p = (2.69 \times 10^5) \times n^{3/2} A c D^{1/2} v^{1/2} \quad \text{Equation 2.1}$$

Where: i_p is the peak current, (A)

n is the number of electrons transferred in the reaction,

A is the area of the electrode, (m^2)

c is the concentration of the solution used, ($\text{mol}\cdot\text{m}^{-3}$)

D is the diffusion coefficient, ($\text{m}^2\cdot\text{s}^{-1}$)

ν is the scan rate, ($\text{V}\cdot\text{s}^{-1}$).

To determine the value of the diffusion constant D of ferro/ferricyanide ions, the electrochemical active surface area of the uncoated electrode A was postulated to be equal to the geometrical area of this electrode A_0 .

The surface area of the gold wire with a diameter Φ of 0.5 mm and a length L of 1 cm is:

$$A = 2\pi rL + \pi r^2$$

Where r is the radius, $2\pi rL$ is the lateral surface area and πr^2 is the base area.

$$A = 0.1589 \text{ cm}^2 = 0.1589 \times 10^{-4} \text{ m}^2$$

Applying this relation using CVs relative to bare gold electrode at different sweep rate (from 0.04 till 0.4 Vs^{-1}) (Figure 2.7. a) with $c = 10 \text{ mM} = 10 \text{ mol/m}^3$, $n = 1$.

we find: $D_{ox} = 0.580 \times 10^{-9} \text{ m}^2/\text{s}$, $D_{red} = 0.418 \times 10^{-9} \text{ m}^2/\text{s}$.

These values are close to those found in literature, for example $0.588 \times 10^{-9} \text{ m}^2/\text{s}$ [32] or $0.424 \times 10^{-9} \text{ m}^2/\text{s}$ [33]. The slight differences are due either to the use of different analysis methods or to the application of different equations.

✓ Calculation of the electrode area

Quantitative analysis of the electrode area A was performed based on Randles-Sevcik relation (Equation 2.1). As it was mentioned in the paragraph before, the electrochemical active surface area of the uncoated gold electrode A is equal to the geometrical area of this electrode A_0 . The electrode area A values of modified gold electrodes were calculated using CVs relative to SAM1 (Figure 2.7.b) and SAM2 (Figure 2.7.c) measured at different scan rates. The quantitative analysis of these CVs (Table 2.3), performed from Figure 2.7 d, gives a decrease in the electrochemical effective surface area till 57% for SAM1 of that of the uncoated electrode and only a 17% decrease

for SAM2. Assuming that the potential gap between the reduction and oxidation peaks characterizes the kinetics of the electron transfer, one can suggest that in the first case (SAM1) the electron tunneling occurs through a thin organic layer while in the second case (SAM2) the reaction occurs at numerous defects in the monolayer.

✓ Calculation of the kinetic constant

The kinetic constant of the electron transfer k^0 for unmodified and modified gold surfaces were calculated from the dependence of the potential gap on the sweep rate according to the equation of Nicholson and Chain [33] written as:

$$k^0 = 2.18 \left[\frac{D\beta n\nu F}{RT} \right]^{\frac{1}{2}} \exp \left[- \left(\frac{\beta^2 n F}{RT} \right) \times (E_p^a - E_p^c) \right] \quad \text{Equation 2.2}$$

Where: k^0 is the effective constant rate of an uncompleted quasi-reversible electrochemical reaction for the redox couple ($\text{Fe}^{3+}/\text{Fe}^{2+}$) involved in a simple electron-transfer reaction, ($\text{cm}\cdot\text{s}^{-1}$)

D is the diffusion coefficient of ferro/ferricyanide ions obtained from CV experiments,

β is the transfer coefficient for the electrode process,

n is the number of electrons transferred in the reaction, $n = 1$

ν is the scan rate, ($\text{V}\cdot\text{s}^{-1}$)

F is the Faraday constant,

R is the molar gas constant,

T is the temperature,

$E_p^a - E_p^c$ is the peak-to-peak separation of the anodic and cathodic waves.

Systematic dependence of these data (Table 2.3) on the sweep rate and clear contribution of the diffusion limitation indicate that the obtained values can be considered only as a coarse estimation. Themselves, the obtained values indicate that the kinetics of the electron transfer for the SAM2 is very similar to that on the bare gold electrodes, while SAM1 leads to essential decrease of this kinetics. Therefore, we can suggest that a long adsorption time from low concentration (SAM1) leads to the predominating binding by both thiol groups of the DiSH to the gold surface resulting

in the formation of a very thin layer. The electrons can tunnel easily through this layer. In contrast, the DiSH-based SAM formed by a faster adsorption from the highly concentrated solution binds the surface by one thiol group mainly. The OH group can cause steric hindrances in the occupation of the adjacent binding sites, and lead to defects in the monolayer. In order to make sure this hypothesis, the hydrodynamic size of the ferricyanide ion $[\text{Fe}(\text{CN})_6]^{3-}$ was calculated.

Table 2.3: Electrochemical parameters extracted from cyclic voltammograms (Figure 2.7).

Electrodes	CV in $\text{K}_3[\text{Fe}(\text{CN})_6]$ 10 Mm			
	ΔE_p (mV)	$I_{p,a}$ (μA)	A / A_0	k^0 (ms^{-1})
Bare gold	115 ± 2	1040.2 ± 0.1	1	$(3.05 \pm 0.67) \times 10^{-5}$
SAM1	308 ± 7	722.5 ± 0.4	0.569	$(0.52 \pm 0.03) \times 10^{-5}$
SAM2	160 ± 5	774 ± 1	0.827	$(1.93 \pm 0.62) \times 10^{-5}$

ΔE_p is the potential gap.

$I_{p,a}$ is the current of the anodic potential.

✓ Calculation of the hydrodynamic radius of the ferricyanide ion

The radius of $[\text{Fe}(\text{CN})_6]^{3-}$ was calculated from the diffusion coefficient using the following Einstein-Stokes equation:

$$D = \frac{kT}{6\pi\eta r} \quad \text{Equation 2.3}$$

Where: k is the Boltzmann constant,

T is the temperature,

η is the viscosity of the electrolyte,

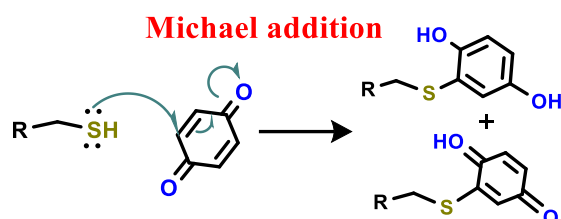
r is the radius of $[\text{Fe}(\text{CN})_6]^{3-}$ ion.

The obtained value $r = 3.76 \text{ \AA}$ is close to the literature data [34]. Notably, the cross-section of this ion (44 \AA^2) is larger than that of the SAM from linear alkylthiols [35] (21.6 \AA^2), therefore the redox activity of ferro-ferricyanide on SAM coated electrodes characterizes molecular defects in the adsorbed layers. The comparison of electrochemical parameters extracted from CVs (Table 2.3) indicates that in the case of SAM2, the number of large defects is higher, and more

ferro/ferricyanide ions can come closer to the metal surface. Similar analysis for different types of linear SAMs was done previously [36].

1.1.15.2 In phosphate buffered saline solution

The suggestion on different predominating orientation of thiols in SAM1 and SAM2 was also examined by binding of 1,4-benzoquinone (BQ) to these monolayers. One can expect such a binding through Michael addition to the free thiol group (schema 2.2) if only one group bonds gold surface, while a binding of both thiol groups to the gold surface leads to the absence of free thiol groups on the SAM surface thus making impossible the reaction with BQ.



Schema 2.2: Schematic representation of Michael addition reaction between thiol group and α,β -unsaturated carbonyl moiety of BQ.

The results are shown in Figure 2.8. No BQ signal was observed for the monolayer adsorbed from low concentrations of DiSH (at the conditions defined for SAM1 preparation) while well pronounced BQ signals were observed for fast SAM deposition from the solutions of high concentrations of DiSH (at the conditions defined for SAM2 preparation).

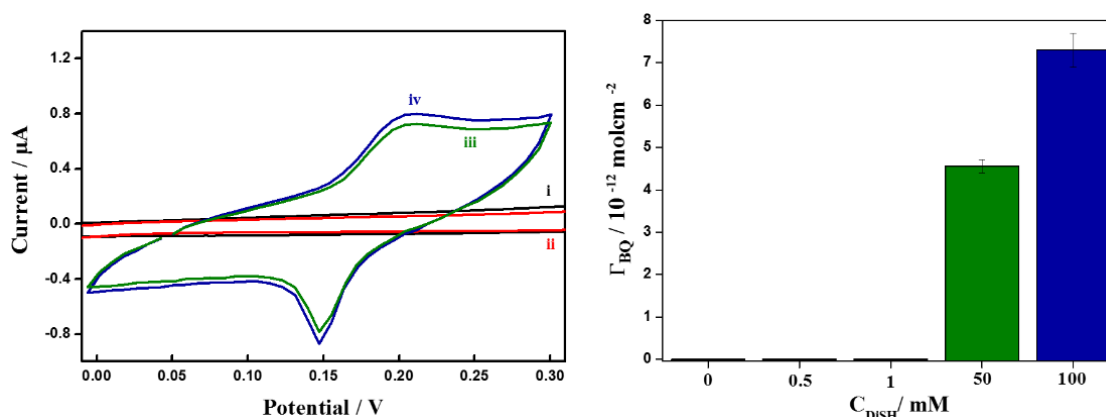


Figure 2.8: Cyclic staircase voltammograms recorded in phosphate buffered saline (PBS) at pH = 7.4 after 40 min incubation in 5mM ethanolic solution of BQ and subsequent washing in pure ethanol of the uncoated gold electrode (i) and of the gold electrodes coated by DiSH from 0.5 and 1 mM solutions for 12 h (ii) or from 50 mM (iii) and 100 mM (iv) solutions for 3h; the surface concentrations of BQ moiety calculated from the oxidation charges are shown in the diagram

1.1.16 Electrochemical impedance spectroscopic characterization

Further characterization of SAM1 and SAM2 was performed by impedance spectroscopy in the absence of redox active compounds (Figure 2.9). The obtained data demonstrated almost pure capacitive behavior in the frequency range 0.1 – 1000 Hz. EIS curves were analyzed and fitted according to the equivalent electrical circuit model (Figure 2.10) serially connecting resistance and capacitance.

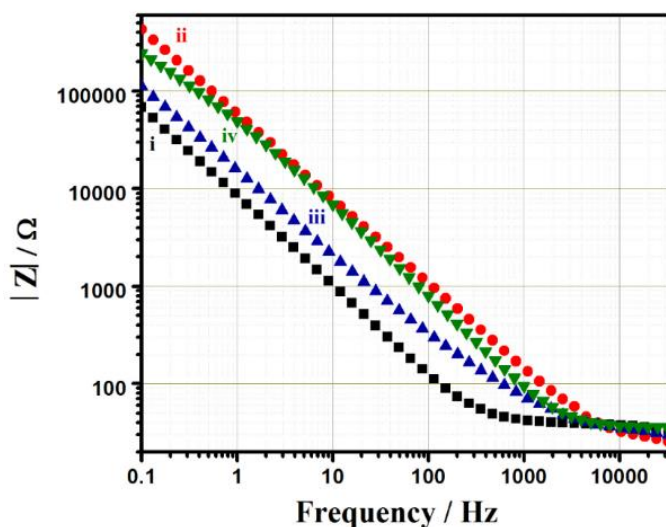


Figure 2.9: Impedance spectra of bare gold electrode (i), SAM1 (ii), SAM2 (iii) and 2-mercaptoethanol SAM (iv) at 0 V vs. AgCl/Ag in 0.1 M KCl.

Indeed, the impedance Z is defined as: $Z(\omega) = R + 1/j\omega C$ where R is the resistance, C is the capacitance and ω is the radial frequency. In the frequency range 0.1 – 1000 Hz, the impedance Z depends on the frequency. It is therefore purely characterized by its imaginary component which leads directly to the measurement of C . The obtained values of the electrical capacitance are shown in Table 2.4.

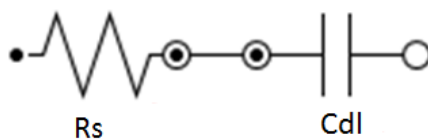


Figure 2.10: Schematic representation of the equivalent circuit used for modified surface modeling.

The impedance spectrum measured at bare gold electrode shows specific electrical capacitance (C_{spc}) of $109 \pm 2 \mu\text{F}\cdot\text{cm}^{-2}$ which is in the range of typical capacitance values of electrical double

layers. The adsorption leads to ~10 times decrease in this capacitance for the case of SAM1 formation but only to ~2.3 times decrease for SAM2 (Table 2.4). The specific capacitance of SAM2 is about four times higher than SAM1. This may be attributed to the defects in the monolayer formed due to steric hindrances of immobilized molecules or due to earlier described desorption of short chain alkylthiols [37].

Table 2.4: Specific capacitance of gold electrode with different coatings.

Electrodes	$C_{spc} / \mu\text{F}\cdot\text{cm}^{-2}$
Bare gold	109 ± 2
SAM1	12 ± 1
SAM2	48 ± 2
2-Mercaptoethanol SAM	22 ± 1

In conclusion, one can suggest, according to the obtained electrochemical results, that the SAM structure depends on the adsorption conditions. A short incubation time of the electrode at high concentration of this di-thiol (SAM2) leads to the predominating binding through one thiol group of the adsorbate to the gold surface, while a long incubation at low concentration (SAM1) leads to the predominating binding by both thiol groups.

1.14 X-ray photoelectron spectroscopic characterization

Gold surface modified by SAM1 was carefully monitored by S(2p) XPS signal in comparison with that modified by SAM2, not only to check the pertinence of the proposed approach, but also to perform a quantitative study on the immobilization structure of DiSH on the gold surface. Indeed, XPS is a powerful tool to explore the chemistry of the sulfur and to quantify the different S-containing moieties present in SAMs. In particular, XPS can give information on both physisorbed and chemisorbed species [38]. Because bulk thiolated-alkyls have S(2p_{3/2}) peaks, at the different position from thiolate on gold (at ~163 eV for free thiol and ~162 eV for the adsorbed one [39]), “unbound” and “bound” sulfurs in DiSH-based SAMs can be distinguished by the S(2p) XPS peak position and the immobilization structure of the formed monolayer can be followed. The XPS (S2p) spectra of SAM1 and SAM2 (Figure 2.11), obtained by deconvolution, show that not

all sulfurs are attached to gold. For SAM1, the highly intensive peaks of 161.7 eV and 162.9 eV were respectively attributed to the spin-orbit split doublet of S(2p_{3/2}) and S(2p_{1/2}) and were assigned to the gold-bound sulfur. The binding energies at 163.7 and 164.9 eV, corresponding to the spin-orbit split doublet of S(2p_{3/2}) and S(2p_{1/2}), were attributed to –SH or –S–S– sulfur atoms [40,41]. The probability of the formation of S–S bonds between thiol groups bond to the gold surface is very low [42], therefore we can ignore a contribution of this bond into 163.7 and 164.9 eV peaks. The results demonstrate that DiSH can bind gold by either one or both thiol groups. The presence of the sulfur atoms which are bonded- and not bonded to the gold with the ratio of ~5 shows that the immobilization of DiSH onto the gold surface via both SH groups is more preferable at the conditions of SAM1 formation. However, when the gold is modified by DiSH at the conditions of SAM2 formation, this ratio gives ~1.8, thus proving that in this case the binding via single SH group is predominating. The weak peaks at 167.4 and 168.6 eV (in Figure 2.11), respectively attributed to the spin-orbit split doublet of S(2p_{3/2}) and S(2p_{1/2}), reflect the presence of sulfur atoms in oxygen environment [43], and can be attributed to contaminants due to not complete removing of the protective acetyl groups, by adsorption from atmospheric air or by oxidation of thiol groups [44,45].

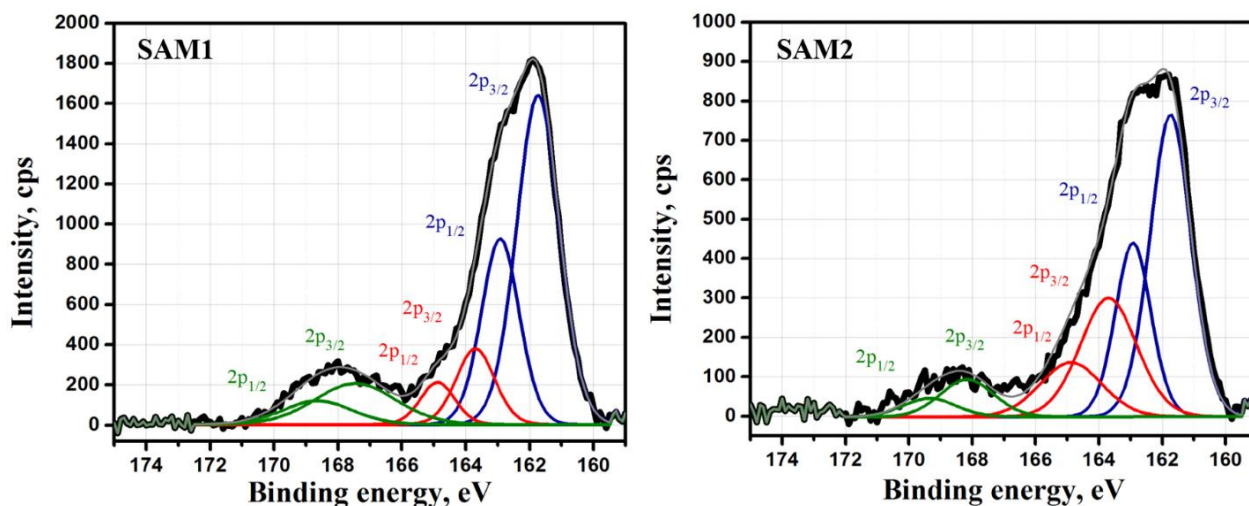


Figure 2.11: High-resolution XPS spectra of gold coated slides modified by SAM1 (A), SAM2 (B) in the sulfur 2p spectral region. Decomposition into single spectral components of a Gauss-Lorentzian shape is shown, the baseline was subtracted.

XPS analysis confirmed that the monolayer formed from DiSH is obtained from a contribution of both basic structures into SAM1 and SAM2. however, the ratio of these structures is very

different in these SAMs. The SAM1 is formed mainly (for about 70%) through two thiol groups of DiSH molecules bonded to gold (Figure 2.12, left) while the SAM2 is formed mainly (also for about 70%) through one thiol group of DiSH molecules bonded to gold (Figure 2.12, right). According to these results, one can confirm that the structure of DiSH-based SAM depends essentially on the SAM-preparation conditions.

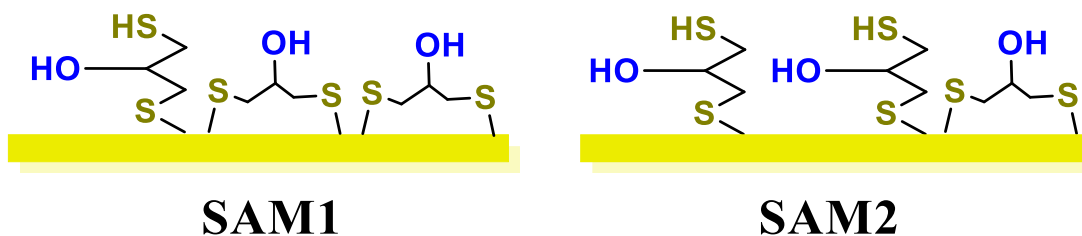


Figure 2.12: Schematic representation of the immobilized DiSH in SAM1 (left) and SAM2 (right).

9. Comparative stability of SAM1 with monothiols

Information on the comparative stability of SAM1 with other alkanethiols were performed using different electrochemical analysis.

1.15 Capacitance comparison using EIS

Specific electrical capacitance (C_{spc}) of SAM1 calculated from EIS after fitting was compared to that of 2-mercaptoethanol-based SAM. Indeed, 2-mercaptoethanol is an anchoring site with almost the same thickness compared to DiSH possessing only one thiol group bounded to gold surface. The formation of 2-mercaptoethanol-SAMs on the electrode surface, obtained by overnight incubation in 1.0 mM aqueous solution, gives ~80% decrease in the capacitance compared to the bare gold electrode. Widrig *et al.* [46] and Lingler *et al.* [47] studied the electrical capacitance of SAMs of different chain lengths. The capacitance of SAM formed by linear alkanethiol of the same geometrical thickness 1-propanethiol is ~2.5 times lower than that of the SAM1. This difference can be essentially attributed to the difference between dielectric and geometrical thickness of dithiols caused by a larger cross-section of the molecule near thiol groups. This suggestion is confirmed by the fact that for SAMs formed by di- and monothiols with a longer chain (thioctic acid and 6-mercaptohexan-1-ol SAMs [48]) this deviation is even higher (~3.4 times). Because of higher solubility in water, the desorption effect of short chain alkylthiols [37]

is expected to be more pronounced for the SAM from 2-mercaptoethanol demonstrating electrical capacitance almost two times higher than that of SAM1 (Table 2.4).

1.16 Stability monitoring using capacitive kinetics analysis

Additional information on the comparative stability of SAMs can be obtained from analysis of capacitance kinetics in the absence of adsorbates in aqueous media. This is a very sensitive technique to monitor desorption of SAMs [37]. The experiments were based on the capacitive monitoring in 0.1 M KCl under intensive stirring. For comparison, the stability of gold electrodes covered by SAM1 and 2-mercaptoethanol-based SAM was studied. A fast increase (~ 0.12 nF/s) of the electrode capacitance was observed for 2-mercaptoethanol-based SAM (Figure 2.13, right). This effect can be explained only by a desorption of 2-mercaptoethanol molecules from the electrode surface. In the case of SAM1 (Figure 2.13, left), no capacitance increase was observed. SAM1, formed mainly by DiSH molecules immobilized through two thiol groups, form a very strong layer that remains on the gold surface. The curve relative to 2-mercaptoethanol-based SAM shows a capacitance decrease of about 4% during the first several seconds after immersion of the dry electrode in the aqueous solution. This effect is probably caused by electrode hydration [37]. In the case of SAM1, the relative curve shows good stability of the SAM in aqueous electrolyte.

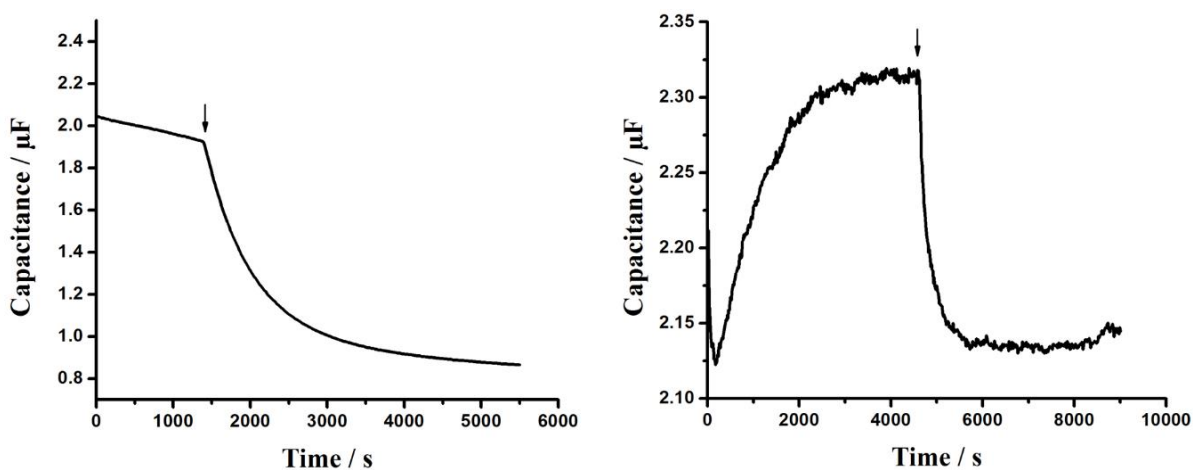


Figure 2.13: Test of stability of adsorbed monolayer: SAM1 (left) and 2-mercaptoethanol-based SAM (right) expressed as capacity changes due to long time incubation in 0.1 M KCl before and after addition of hexanethiol. The arrow indicates an injection of 30 μ L of 1mM of hexanethiol.

In addition, analysis of kinetics of the replacement process of compounds in these monolayers by another thiol from the solution was performed by addition of 1-hexanethiol (1 mM ethanolic solution) to the aqueous medium. Let us assume that both adsorption and replacement processes

can be described by simple formal kinetics and correspondingly by exponential equations. First kinetics of the binding of hexanethiol to the uncoated gold electrode was studied (Figure 2.14, black curve). The capacitance kinetics $C(t)$ can be fitted by one-exponential curve:

$$C(t) = C_0 - \Delta C \left(1 - \exp^{-\frac{t}{\tau}}\right) \quad \text{Equation 2.4}$$

Here C_0 is the initial capacitance and τ is the characteristic time of this process.

For adsorption of hexanethiol onto the uncoated electrode the characteristic time is $\tau = 535 \pm 4$ s (Table 2.5). In the case of addition of the same concentration of hexanethiol to the same gold electrode coated by any SAM, one can expect two processes: (1) filling of the defects leading to the capacitance decrease, (2) change in the capacitance due to replacement of one thiol by another one; if the replacing thiol forms a thicker layer, the capacitance should decrease. We can expect that for the same concentration of hexanethiol, the characteristic time of the process (1) is similar to that for the thiol binding to the uncoated gold electrode, while the process (2) being physically very different can have another characteristic time. In general, the process (2) consisting from two subsequent processes – desorption and filling – may include two characteristic times. An addition of 1 mM hexanethiol to the gold electrode coated by SAM1 leads to ~55% decrease in the electrical capacitance (Figure 2.14, red curve). The reaction kinetics for SAM1 can be represented not only by one but two-exponential function:

$$C(t) = C_0 - \Delta C_1 \left(1 - \exp^{-\frac{t}{\tau_1}}\right) - \Delta C_2 \left(1 - \exp^{-\frac{t}{\tau_2}}\right) \quad \text{Equation 2.5}$$

The fastest characteristic time of this process τ_2 is 550 ± 2 s which is very close to the characteristic time of adsorption of this thiol to the gold surface (Table 2.5). Therefore, we conclude that the decrease of the capacitance due to addition of hexanethiol is caused by filling of defects in the monolayer. The slowest characteristic time τ_1 of this process 2308 ± 60 s is attributed to a slow desorption of SAM1 probably that of DiSH molecules immobilized through only one thiol group to the gold surface (Table 2.5). Different kinetics was observed for addition of the same amount of hexanethiol to the monolayer of 2-mercaptoethanol (Figure 2.14, bleu curve). Also in this case the process can be described by two-exponential function. The characteristic time τ_1 , being the faster (37 ± 8 s), is attributed probably to a partial desorption of 2-meraptoethanol molecules forming the layer. The characteristic time τ_2 , being the slower (276 ± 9 s), is attributed probably to

the replacement of desorbed 2-mercaptoethanol by hexanethiol molecules (Table 2.5). The latter process kinetics is about two times lower compared to that of the uncoated gold and the gold coated by SAM1 due probably to the strong competition between the desorbed 2-mercaptoethanol and hexanethiol molecules. In the case of uncoated gold and gold coated by SAM1, no competition occurs between thiols in the aqueous media which explain the slow kinetics of the process.

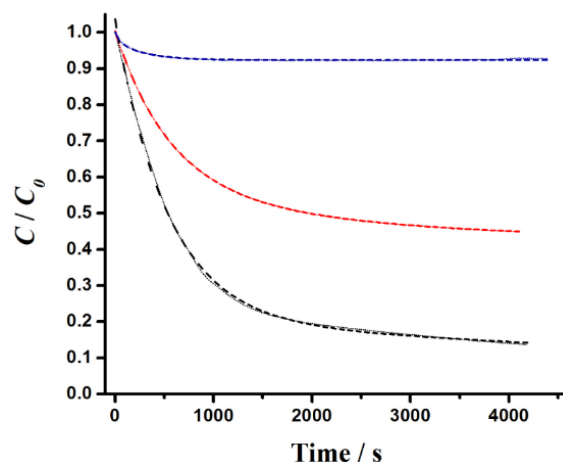


Figure 2.14: Capacitance change of the uncoated gold electrode (black curve) and the gold electrode coated by SAM1 (red curve) and the 2-mercaptoethanol-based SAM (bleu curve) after addition of 1 mM ethanolic solution of 1-hexanethiol into the aqueous medium. The discontinued curves represent the fitting.

Table 2.5: Parameters taken from capacitance kinetic curves (Figure 2.14) of gold electrode with different coatings after fitting by two-exponential kinetics according to the equation 2.5.

Electrodes	Bare gold	SAM1	2-Mercaptoethanol SAM
R^2	0.9990	0.9999	0.9766
C_0	0.84 ± 0.003	1.0 ± 0.004	1.0 ± 0.004
ΔC_1	3862	0.15 ± 0.001	0.02 ± 0.002
ΔC_2	0.84 ± 0.003	0.43 ± 0.002	0.06 ± 0.002
τ_1	2.8	2308 ± 60	37 ± 8
τ_2	535 ± 4	550 ± 2	276 ± 9

1.17 Stability monitoring using step-potential chronoamperometry

It is well-known that SAMs are subject to oxidative and reductive desorption that compromises the integrity of the monolayer. The stability of SAM1 and 2-mercaptoethanol-based SAM was evaluated using step-potential chronoamperometry. The proposed approach provides relevant information on the stability of the SAMs. The protocol relies on the application of thirty (30) successive desorption potentials from 0.95 V till -0.5 V in steps of 0.05 V vs. AgCl/Ag (1 s each). Figure 2.15 shows the polarization curves for the progressive step-potential protocol on the DiSH-modified gold electrode at the conditions defined for SAM1 preparation (left) and 2-mercaptoethanol-modified gold electrode (right). The sharp transient current at each potential step associated to the fast double layer charging is followed by smooth transient current which we assign to the slow desorption of the chemisorbed molecules at the given potential.

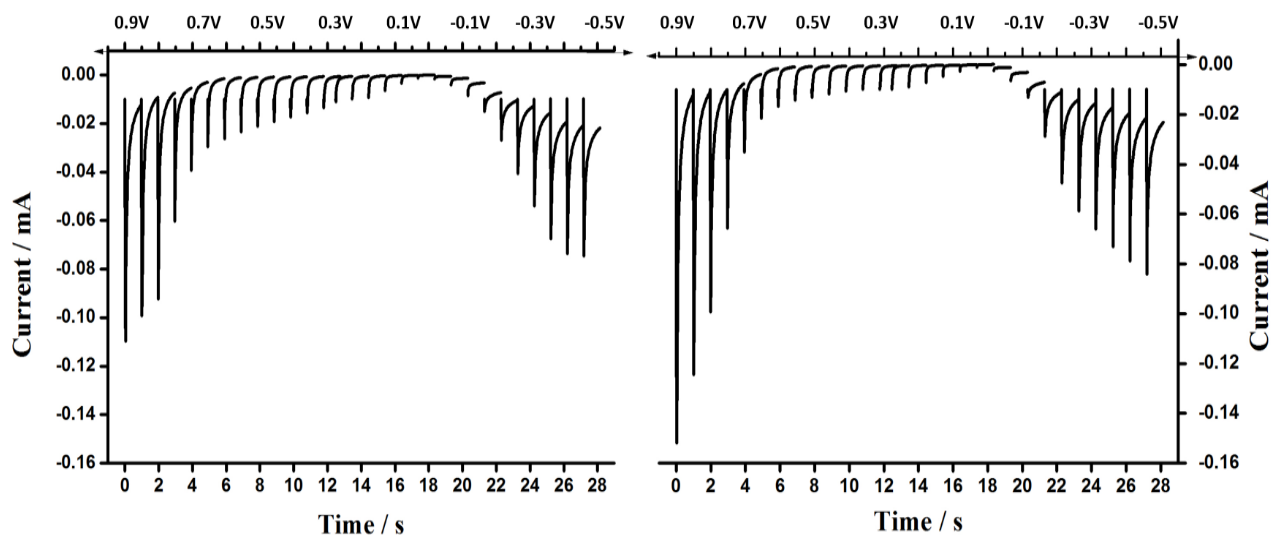


Figure 2.15: Progressive potential-step chronoamperometry recorded for a polycrystalline gold electrode modified with SAM1 (left) and 2-mercaptoethanol-SAM (right) with 1 s step at each applied potential vs AgCl/Ag in PBS pH = 7.4.

Quantitative information on the desorption process of these molecules as a function of the potential was obtained by integrating the charge under each step potential. The resulting values, shown in the Figure 2.16, confirm the low stability of 2-mercaptoethanol-SAM in comparison with SAM1. The desorption of DiSH molecules from SAM1 was potential-dependent and only a partial

desorption of the compounds took place at every single potential. The results indicate the need for a more negative (or positive) potential to trigger the desorption of the remaining strongly adsorbed molecules. In both cases, the charge associated to the desorption process increased at more negative (or positive) potentials.

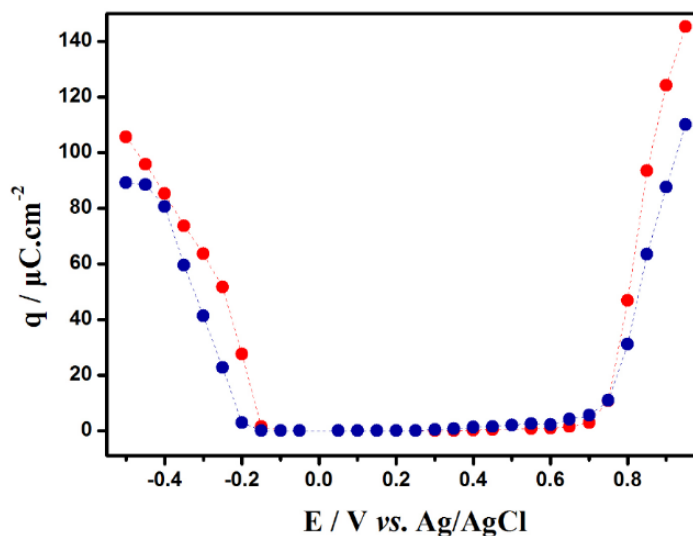


Figure 2.16: Charge of the oxidative and reductive desorption from polycrystalline gold electrodes modified SAM1 (bleu curve) and 2-mercaptoethanol-SAM (red curve) obtained from step-potential chronoamperometries recorded with 1 s step.

The stability of monolayers formed from DiSH (at the conditions defined for SAM1 preparation) and 2-mercaptoethanol was assessed in simulated physiological conditions (PBS at pH = 7.4). The results demonstrate that the surface structure constitute one of the parameters that govern the adsorption/desorption of these molecules from the gold surface. The coordination of the thiols and dithiols significantly affects the stability of the self-assembled monolayer. The understanding of the stability of adsorbed sulfur-containing molecules on gold electrodes at physiological conditions has enormous implications in sensing.

10. Conclusion

In this chapter, we have proposed a new type of anchor molecule, 1,3-dimercaptopropan-2-ol, to be immobilized on the gold surface. Firstly, a detailed investigation on the immobilization structure of the SAM made from this compound was realized using different conditions of preparation. Electrochemical as well as XPS measurements confirmed that the SAM is obtained

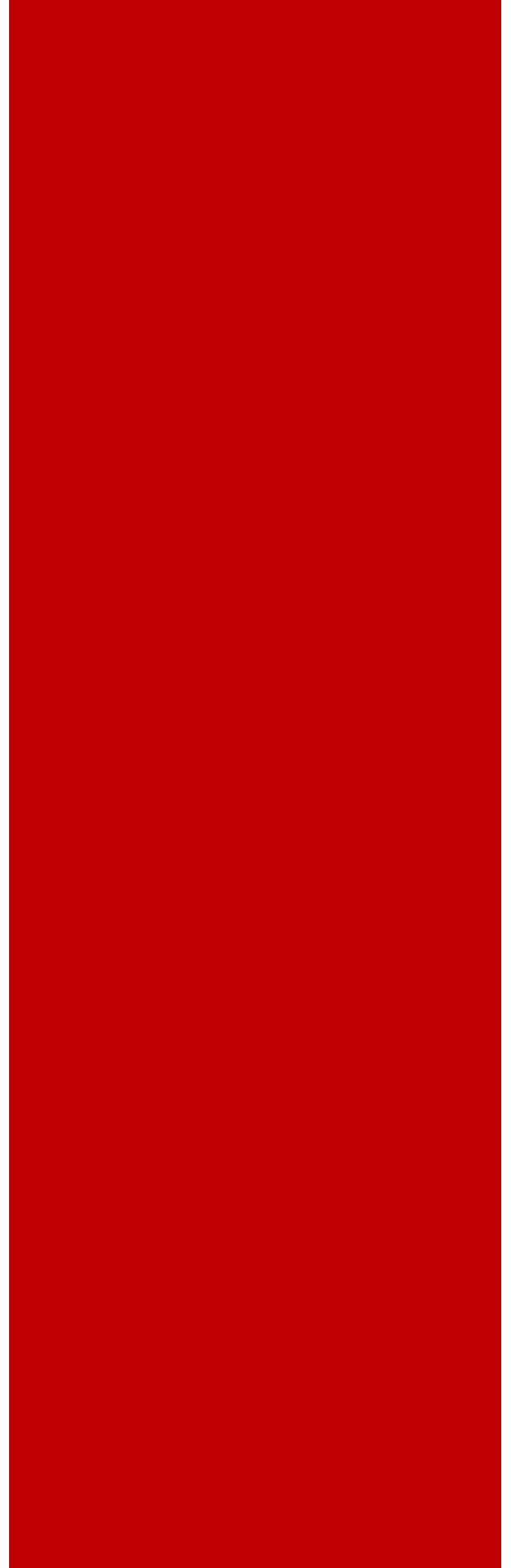
by a contribution of mono and bi-immobilization of DiSH on the gold surface and the ratio of both structures strongly depends on the conditions of preparation. We have also demonstrated, using different approaches, that this compound leads to the formation of thin and stable self-assembled monolayers, this makes it perspective for the development of chemical sensors and other devices requiring electron tunneling through the anchoring layer.

References

- [1] J. C. Love, L. A. Estroff, J. K. Kriebel, R. G. Nuzzo, G. M. Whitesides, *Chem. Rev.*, **2005**, 105, 1103–1170.
- [2] H. O. Finklea, *Encyclopedia of Analytical Chemistry*, Online © 2006 John Wiley & Sons, Ltd, **2006**.
- [3] V. M. Mirsky, *Trends Anal. Chem.*, **2002**, 21, 439–450.
- [4] T. Wink, S. J. van Zuilen, A. Bult, W. P. van Bennekom, *Analyst*, **1997**, 122, 43–50.
- [5] S. Flink, F. C. J. M. van Veggel, D. N. Reinhoudt, *Adv. Mater.*, **2000**, 12, 1315–1328.
- [6] M. Riepl, V. M. Mirsky, O. S. Wolfbeis, *Microchim. Acta*, **1999**, 131, 29–34.
- [7] M. Riepl, V. M. Mirsky, I. Novotny, V. Tvarozek, V. Rehacek, O. S. Wolfbeis, *Anal. Chim. Acta*, **1999**, 392, 77–84.
- [8] R. C. Salvarezza, P. Carro, *J. Electroanal. Chem.*, **2018**, 819, 234–239.
- [9] Q. Cheng, A. Brajter-Toth, *Anal. Chem.*, **1996**, 68, 4180–4185.
- [10] V. P. Y. Gadzekpo, P. Bühlmann, K. P. Xiao, H. Aoki, Y. Umezawa, *Anal. Chim. Acta*, **2000**, 411, 163–173.
- [11] M. I. Prodromidis, T. Hirsch, V. M. Mirsky, O. S. Wolfbeis, *Electroanalysis*, **2003**, 15, 1795–1798.
- [12] C. Berggren, G. Johansson, *Anal. Chem.*, **1997**, 69, 3651–3657.
- [13] W. Argoubi, M. Saadaoui, S. Ben Aoun, N. Raouafi, *Beilstein J. Nanotech.*, **2015**, 6, 1840–1852.
- [14] E. Chow, D. B. Hibbert, J. J. Gooding, *Anal. Chim. Acta*, **2005**, 543, 167–176.
- [15] Y. Liu, M. K. Shipton, J. Ryan, E. D. Kaufman, S. Franzen, D. L. Feldheim, *Anal. Chem.*, **2007**, 79, 2221–2229.
- [16] D. Witt, R. Klajn, P. Barski, B. Grzybowski, *Curr. Org. Chem.*, **2004**, 8, 1763–1797.
- [17] S. Caporali, F. Muniz-Miranda, A. Pedone, M. Muniz-Miranda, *Sensors*, **2019**, 19, 2700.
- [18] B. Sivaranjini, R. Mangaiyarkarasi, V. Ganesh, S. Umadevi, *Sci. Rep.*, **2018**, 8.
- [19] P. Sokolov, V. Demidov, L. Vedeneeva, N. Kasyanenko, *J. Phys. Chem. C*, **2015**, 119, 24358–24363.
- [20] L. M. Fischer, M. Tenje, A. R. Heiskanen, N. Masuda, J. Castillo, A. Bienten, J. Émneus, M. H. Jakobsen, A. Boisen, *Microelectron. Eng.*, **2009**, 86, 1282–1285.
- [21] S. Štrbac, R. R. Adžić, A. Hamelin, *J. Electroanal. Chem.*, **1988**, 249, 291–310.
- [22] H. Angerstein-Kozłowska, B. E. Conway, A. Hamelin, L. Stoicoviciu, *J. Electroanal. Chem.*, **1987**, 228, 429–453.
- [23] E. P. Randviir, C. E. Banks, *Anal. Methods*, **2013**, 5, 1098–1115.
- [24] M. Ates, *Prog. Org. Coat.*, **2011**, 71, 1–10.
- [25] B.-Y. Chang, S.-M. Park, *Annu. Rev. Anal. Chem.*, **2010**, 3, 207–229.
- [26] W. Kohn, A. D. Becke, R. G. Parr, *J. Phys. Chem.*, **1996**, 100, 12974–12980.
- [27] Gaussian 09, Revision D.01, M. J. Frisch, et al., Gaussian, Inc., Wallingford CT, **2009**.
- [28] M. Chebbi, Y. Arfaoui, *J. Mol. Model.*, **2018**, 24, 198.
- [29] J. L. Trevor, K. R. Lykke, M. J. Pellin, L. Hanley, *Langmuir*, **1998**, 14, 1664–1673.
- [30] G. E. Poirier, *Chem. Rev.*, **1997**, 97, 1117–1127.
- [31] W. P. Davey, *Phys. Rev.*, **1925**, 25, 753–761.
- [32] A. J. Arvía, J. C. Bazán, J. S. W. Carrozza, *Electrochim. Acta*, **1968**, 13, 81–90.
- [33] I. Lavagnini, R. Antiochia, F. Magno, *Electroanalysis*, **2004**, 16, 505–506.

- [34] O. Mergel, A. P. H. Gelissen, P. Wünnemann, A. Böker, U. Simon, F. A. Plamper, *J. Phys. Chem. C*, **2014**, 118, 26199–26211.
- [35] F. Schreiber, *Prog. Surf. Sci.*, **2000**, 65, 151–257.
- [36] R. Bilewicz, T. Sawaguchi, R. V. Chamberlain, M. Majda, *Langmuir*, **1995**, 11, 2256–2266.
- [37] V. M. Mirsky, M. Riepl, O. S. Wolfbeis, *Biosens. Bioelectron.*, **1997**, 12, 977–989.
- [38] C. Vericat, M. E. Vela, G. Benitez, P. Carro, R. C. Salvarezza, *Chem. Soc. Rev.*, **2010**, 39, 1805–1834.
- [39] M. W. J. Beulen, J. Bügler, B. Lammerink, F. A. J. Geurts, E. M. E. F. Biemond, K. G. C. van Leerdam, F. C. J. M. van Veggel, J. F. J. Engbersen, D. N. Reinhoudt, *Langmuir*, **1998**, 14, 6424–6429.
- [40] P. Kalimuthu, P. Kalimuthu, S. A. John, *J. Phys. Chem. C*, **2009**, 113, 10176–10184.
- [41] D. G. Castner, K. Hinds, D. W. Grainger, *Langmuir*, **1996**, 12, 5083–5086.
- [42] C. D. Bain, H. A. Biebuyck, G. M. Whitesides, *Langmuir*, **1989**, 5, 723–727.
- [43] C. M. Whelan, M. R. Smyth, C. J. Barnes, N. M. D. Brown, C. A. Anderson, *Appl. Surf. Sci.*, **1998**, 134, 144–158.
- [44] M.-T. Lee, C.-C. Hsueh, M. S. Freund, G. S. Ferguson, *Langmuir*, **1998**, 14, 6419–6423.
- [45] A.-S. Duwez, *J. Electron Spectrosc. Relat. Phenom.*, **2004**, 134, 97–138.
- [46] C. A. Widrig, C. Chung, M. D. Porter, *J. Electroanal. Chem.*, **1991**, 310, 335–359.
- [47] S. Lingler, I. Rubinstein, W. Knoll, A. Offenhäusser, *Langmuir*, **1997**, 13, 7085–7091.
- [48] Q. Cheng, A. Brajter-Toth, *Anal. Chem.*, **1992**, 64, 1998–2000.

Chapter 3: Electrochemical and spectroscopic characterization of BQ-terminated SAM based on DiSH on gold and its application in NADH sensing



11. Introduction

The goal of the third chapter is to develop a highly stable SAM based on DiSH as anchor site and terminated by BQ moieties. The preparation of the SAM is performed in two steps: Steglich esterification in the presence of 3-mercaptopropionic acid, followed by immobilization of BQ by means of Michael addition. Electrochemical as well as spectroscopic measurements were applied for the characterization of the SAM. A detailed analysis on each modification step of the SAM has been done. The presence of BQ moieties as a terminal group of the monolayer provides a sensitive monitoring of the 1,4-addition (Michael addition) of nucleophiles to the α,β -unsaturated carbonyls of BQ groups. In order to make sure this assumption, we have studied the addition of the ferrocenylhexanethiol by simple incubation and by electrically controlled interaction. The obtained highly stable SAM with redox-active terminal group can be applied for different tasks of chemical sensing and biosensing. As an example, an application of this system for electrocatalytical oxidation of β -nicotinamide adenine dinucleotide (NADH) was examined.

12. Preparation of BQ-terminated SAMs

In this part of work, DiSH-based SAMs used for subsequent esterification followed by immobilization of BQ were performed at the same conditions used for the preparation of SAM1 (see chapter 2). First, these samples were rinsed with water and sonicated in $\text{NaBH}_4/\text{CH}_3\text{OH}$ for 1h in an ice bath in order to activate hydroxyl terminal groups of the monolayer. Then, the samples were rinsed with methanol and immersed into the fresh solution of 8.0 mM 3-mercaptopropionic acid (MPA), 8.0 mM of N,N' -dicyclohexylcarbodiimide (DCC) and 2.0 mM of 4-(dimethylamino)pyridine (DMAP) in chloroform for 24 h. During the Steglich esterification reaction, free OH-groups on the surface of the monolayer link covalently to the carboxylic acid groups of the MPA to form SH-terminated SAM (further referred as SAM3). Finally, BQ was immobilized to these terminal thiol moieties, it was performed through Michael addition (often related as one of the “click” reactions) by incubation in ethanolic solution of 5.0 mM for 40 min. The whole procedure for the formation of BQ-terminated SAM (further referred as SAM4) is shown in Figure 3.1.

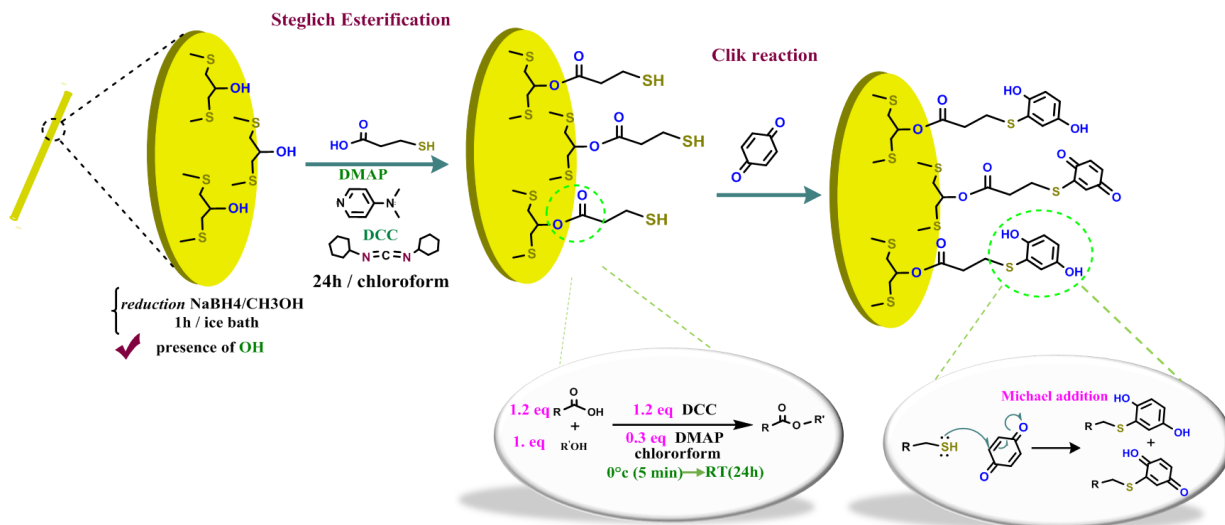


Figure 3.1: Multistep formation of the BQ-terminated monomolecular layer.

13. Electrochemical characterization of SAM3

Electrochemical characterization of SAM3 was performed using CV and EIS in the presence of the redox label $[\text{Fe}(\text{CN})_6]^{3-/4-}$ and in aqueous medium in order to calculate the electrochemical parameters during the addition of the MPA on SAM1 proving thus Steglich esterification.

1.18 Determination of electrochemical parameters

The esterification of the gold surface modified by SAM1 was analyzed firstly by CV in the presence of ferro/ferricyanide. Results show that an esterification of the SAM1 leads to ~ 1.6 times decrease in the cathodic and anodic peak currents and an increase in the gap between potentials of anodic and cathodic peaks (Figure 3.2 a). A quantitative analysis of the electrochemically effective electrode area using Randles-Seviçk equation gives $\sim 50\%$ decrease in the effective electrochemical electrode area compared to the bare gold electrode and $\sim 10\%$ in comparison to the SAM1 (see Table 3.1 and Table 2.3). These changes are in favor of the esterification reaction occurred at the electrode surface. Furthermore, the reaction effects on the electron-transfer between the redox probe and the gold electrode: the kinetic constant of the electron transfer decreases for two or three order of magnitude compared to SAM1 or uncoated gold electrode (see Table 3.1 and Table 2.3). This confirms an expected increase in the thickness of the dielectric layer on the electrode due to the immobilization of the MPA. This assumption was also proved by impedance spectroscopy in the presence of redox probe (Figure 3.2 b). A comparison of impedance

spectra of SAM1 before (Figure 2.4b, curve ii) and after (Figure 3.2b) addition of MPA show a remarkable increase in the semicircle thus indicating a formation of an additional layer on the electrode due to esterification. The values of the reaction resistances are summarized in Table 3.1.

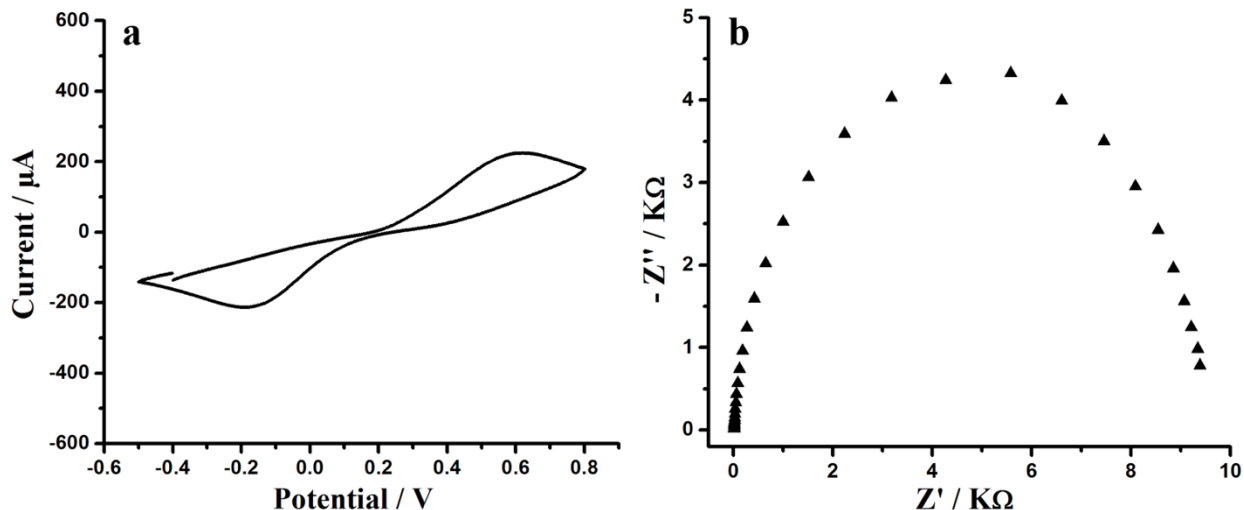


Figure 3.2: a) Cyclic voltammogram at scan rate of 200 mV.s⁻¹ and b) impedance spectrum recorded at the frequency range from 0.1 Hz to 100 kHz at +0.2 V of the gold electrode coated by SAM3. Electrolyte: 10 mM [Fe(CN)₆]^{3-/4-}, 0.1 M KCl.

Table 3.1: Electrochemical parameters extracted from CV and EIS (Figure 3.2).

Electrode of gold coated by SAM3	CV in 10 mM K ₃ [Fe (CN) ₆] + 0.1 M KCl		EIS in 10 mM K ₃ [Fe (CN) ₆] + 0.1 M KCl	
	ΔE_p (mV)	812 ± 11	R_s / Ω	19 ± 3
	$I_{p,a}$ (µA)	437 ± 2		
	A / A_0	0.516	R_{CT} / Ω	9300 ± 10
k^0 (ms ⁻¹)	(3.8 ± 0.40) × 10 ⁻⁸			

ΔE_p is the potential gap.

$I_{p,a}$ is the current of the anodic potential.

1.19 Estimation of esterification efficiency θ

In order to get more informative result on the immobilization structure during esterification, we estimated the value of the esterification efficiency, θ , defined as the part of the electrode surface coated by MPA from capacitive analysis of impedance spectra measured in aqueous medium. Figure 3.3 shows Bode plots of the gold electrode modified by SAM3 (black curves). Fitted Bode

plots (Figure 3.3, red curves) using Randles circuit without Warburg impedance gives the value of electrical capacitance of the organic layer $C_{org} = 8.2 \pm 0.2 \mu\text{F}/\text{cm}^2$. This capacitance is formed by the capacitance of the electrical double layer C_{dl} serially connected with the capacitances of the esterified layer θC_{MPA} and θC_{SAMI} , and by the capacitance of the non-esterified layer $(1-\theta)C_{SAM}$ (Figure 3.4).

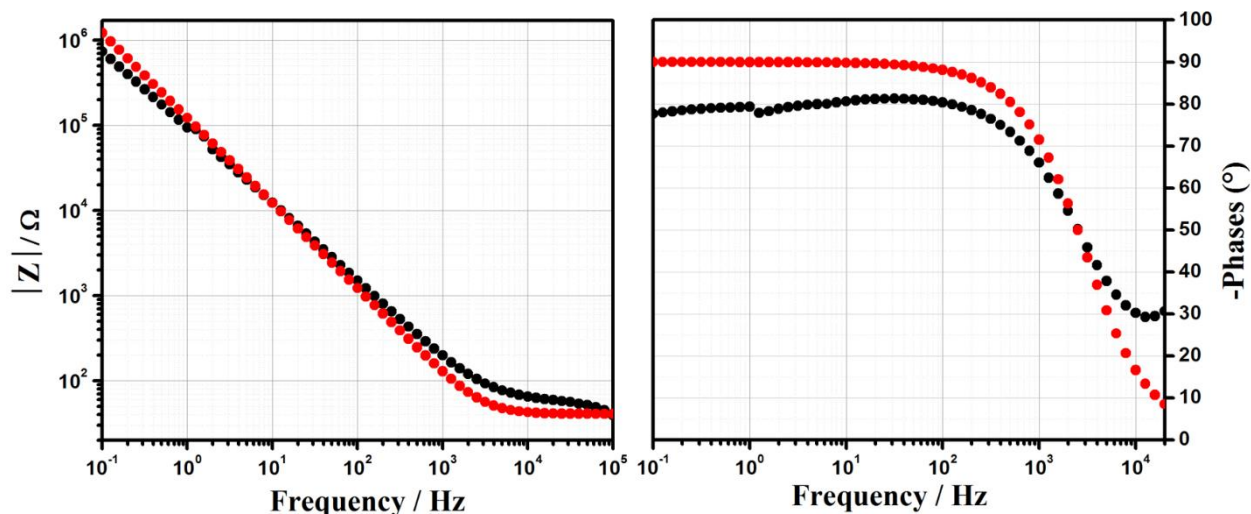


Figure 3.3: Bode modulus (left) and phase angle (right) plots of gold electrode modified by SAM3 obtained in KCl 0.1 M. The experimental data are shown in black and the optimum fit results in red.

According to the equivalent circuit shown in Figure 3.4 The capacitance of the organic layer C_{org} is:

$$\frac{1}{C_{org}} = \frac{1}{C_{dl}} + \frac{1}{C_{SAMI}} \chi \frac{C_{SAMI} + C_{MPA}}{(1-\theta).C_{SAMI} + C_{MPA}} \quad \text{Equation 3.1}$$

C_{dl} and C_{SAMI} were extracted from Table 2.4 and C_{MPA} was calculated from the planer capacitor equation:

$$C_{MPA} = \frac{\epsilon \epsilon_0 A}{d} \quad \text{Equation 3.2}$$

Where: ϵ is the SAM dielectric constant,

ϵ_0 is the permittivity of free space,

A is the electrode area,

d is the thickness of the dielectric layer, ($d = 5 \text{ \AA}$ according to the literature [1]).

Based on the geometry of the SAM1, one can expect the maximum value of esterification efficiency $\theta=0.5$. The calculation of θ was performed using one of the two following assumptions:

(i) **assumption 1:** $C_{dl} \gg C_{org}$. In this case:

$$C_{org} = (1 - \theta) \cdot C_{SAM1} + \frac{\theta \cdot C_{SAM1} \cdot C_{MPA}}{C_{SAM1} + C_{MPA}} \quad \text{Equation 3.3}$$

This gives $\theta = 0.41$.

(ii) **assumption 2:** $C_{dl} = C_{uncoated\ gold}$. In this case:

$$C_{org} = \frac{C_{dl} \cdot C_{SAM1} \cdot (C_{MPA} + C_{SAM1} - \theta C_{SAM1})}{C_{SAM1} (C_{MPA} + C_{SAM1} - \theta C_{SAM1}) + C_{dl} \cdot (C_{MPA} + C_{SAM1})} \quad \text{Equation 3.4}$$

This gives $\theta = 0.43$.

Taking into account both assumptions, the mean value of θ is 0.42. This estimation allows us to suggest that 84% of SAM1 molecules are esterified during the formation of the SAM3.

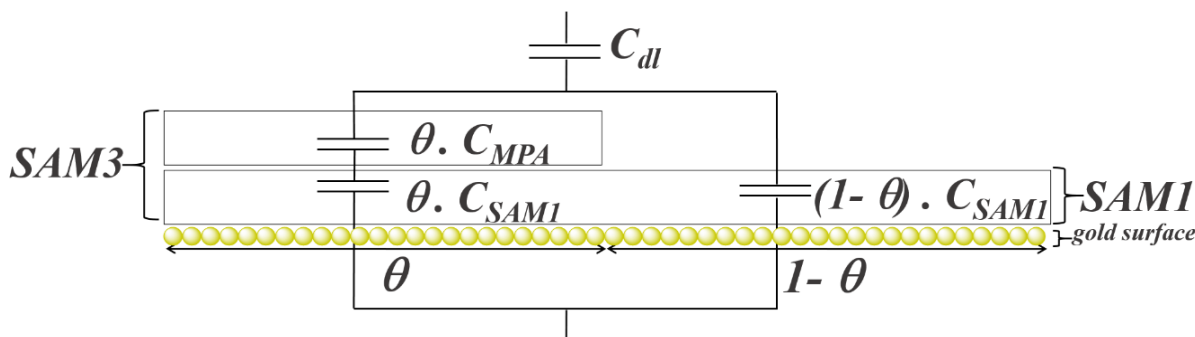


Figure 3.4: Esterification efficiency of SAM1 and its conversion into SAM3 can be estimated quantitatively from capacitive analysis using this model. Here: C_{dl} is the specific capacitance of the electrical double layer, C_{SAM1} and C_{MPA} is the specific capacitance of the esterified organic layer (SAM3) occupying the θ part of the electrode surface while C_{SAM1} is the specific capacitance of the non-esterified organic layer (SAM1) occupying the $(1-\theta)$ part of the electrode surface.

1.20 Addition of redox label

Although the impedance spectra, capacitive analysis and cyclic voltammetry indicate an improvement in the insulating properties of the organic layer on the gold surface, one cannot distinguish if these effects are caused by a formation of a thicker insulating layer or just by filling of possible defects in the SAM1. To answer this question, we immobilized BQ on the surface of SAM3. Free thiol groups on the gold surface will bound to the α,β -unsaturated carbonyl groups of the BQ molecules. One can expect that if SH groups are exposed on the electrode surface (like in the case of SAM2), an interaction of BQ with thiols will lead to its covalent immobilization

through 1,4-Michael conjugated addition. The BQ undergoes a reversible electrochemical redox process at modest potentials, therefore the resulting BQ-modified organic layer (further denoted as SAM4) should be electrochemically active. Alternatively, if no thiol group is present on the electrode surface (like in SAM1), no BQ moieties will be present on the electrode surface after such incubation and washing, and no electrochemical activity will be observed.

The results of this test are shown in Figure 3.5. No electrochemical activity of BQ was observed after such procedure for bare gold (curve i) and for SAM1 (curve ii), therefore, the washing procedure does remove physically adsorbed BQ. However, after incubation of SAM3 in BQ solution and subsequent washing, a clear electrochemical activity, which is typical for immobilized BQ is observed (curve iii).

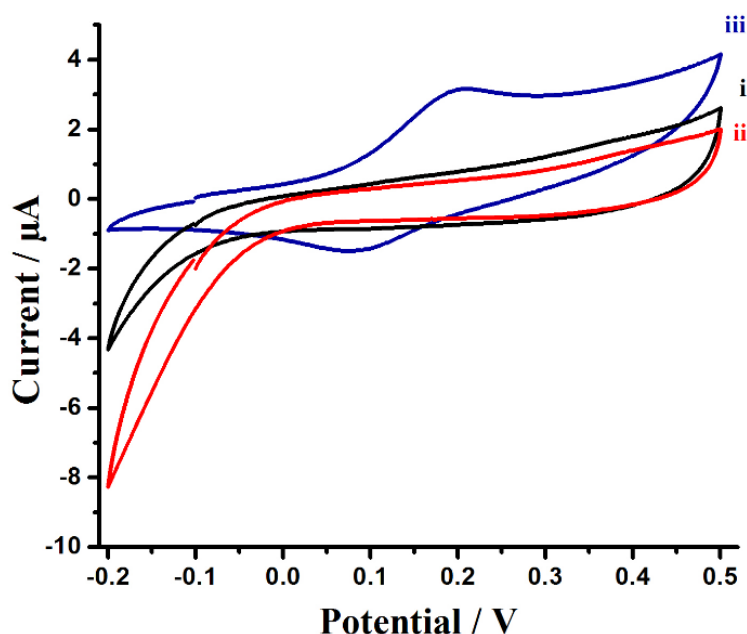


Figure 3.5: Voltamperometric responses of BQ (5mM / EtOH) after 40 min incubation of bare gold electrode (i), SAM1(ii) and SAM3 (iii) in 0.1 M PBS pH=7.4, the scan rate is 25 mV.s⁻¹. After such treatment the electrodes were washed thoroughly with water and methanol.

14. XPS characterization of SAM3

Formation of SAM3 on the gold surface was also studied by means of XPS. Since this latter can be used to confirm the presence of the desired element in the film and to evaluate its atomic composition [2], the technique turns out to be very useful to study the behavior of the added MPA on SAM1 and to determine the presence of each element qualitatively and quantitatively. One can imagine that an interaction of MPA with SAM1 can lead not only to esterification with formation

of SAM3 but also to direct binding of this compound to the gold. To analyze a possible contribution of the latter process, the gold slides modified by SAM3 were studied by XPS in the sulfur 2p as well as oxygen 1s spectral regions. The S2p spectrum relative to SAM3 (Figure 3.6) shows an increase of the intensity ratio of free -SH peaks at 163.7 and 164.9 eV, corresponding to the spin-orbit split doublet of S(2p_{3/2}) and S(2p_{1/2}) respectively, from 0.14 for SAM1 (Figure 2.11, left) to 0.32 (Figure 3.6).

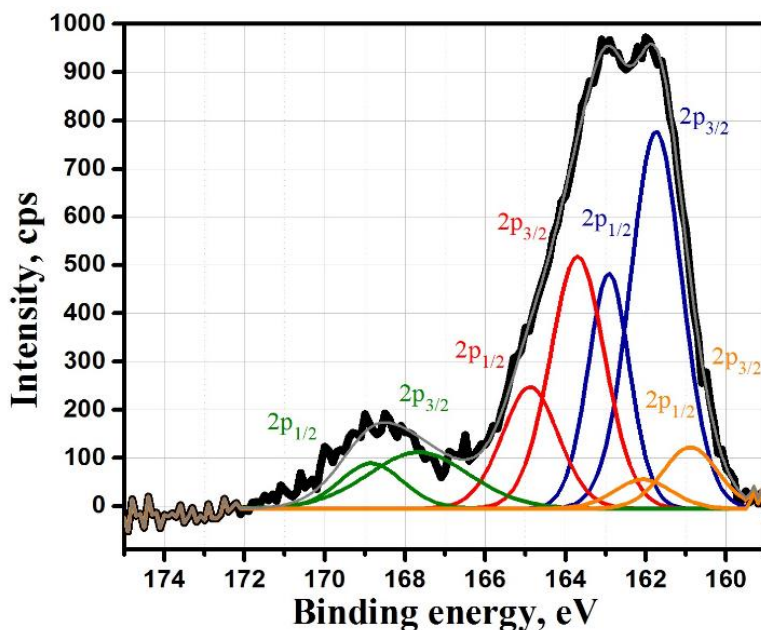


Figure 3.6: S2p spectrum of gold coated slide modified by SAM3. Decomposition into single spectral components of a Gauss-Lorentzian shape is shown, the baseline was subtracted.

In addition, the peaks relating to O1s (Figure 3.7, right) obtained by deconvolution show the presence of two additional peaks in comparison with O1s spectrum of SAM1 (Figure 3.7, left). These peaks relate to C=O bond (532 eV) and C-O-C bond (533.5 eV). The results demonstrate clearly the esterification effect of the MPA on SAM1. The low intensity high energy component (535.2 eV) can be attributed to the chemisorbed oxygen from water molecules. O1s XPS spectrum for gold slide modified SAM1 shows one intensive peak at 532.4 eV relating to C-O-H bond (Figure 3.7, left). The same peak is also shown after addition of MPA but its intensity is weak proving the small amount of MPA molecules bond to gold. S2p XPS spectra corresponding to SAM3 (Figure 3.6) show an additional S2p peaks at 160.9 and 162.0 eV with low intensity attributed probably to the spin-orbit split doublet of S(2p_{3/2}) and S(2p_{1/2}) of S-Au bond from the MPA. The intensity ratio of this peak (0.08) is much less than that from DiSH (0.46). Therefore,

in the frame of the deconvolution uncertainty we can conclude that the total area of defects coated by MPA through formation of thiol bond to the gold is about 15%. If the esterification efficiency is 84%, it means that MPA molecules have about 3 times higher probability to esterify the OH-groups of SAM1 than to fill the defects in the SAM1 forming the bond with gold surface.

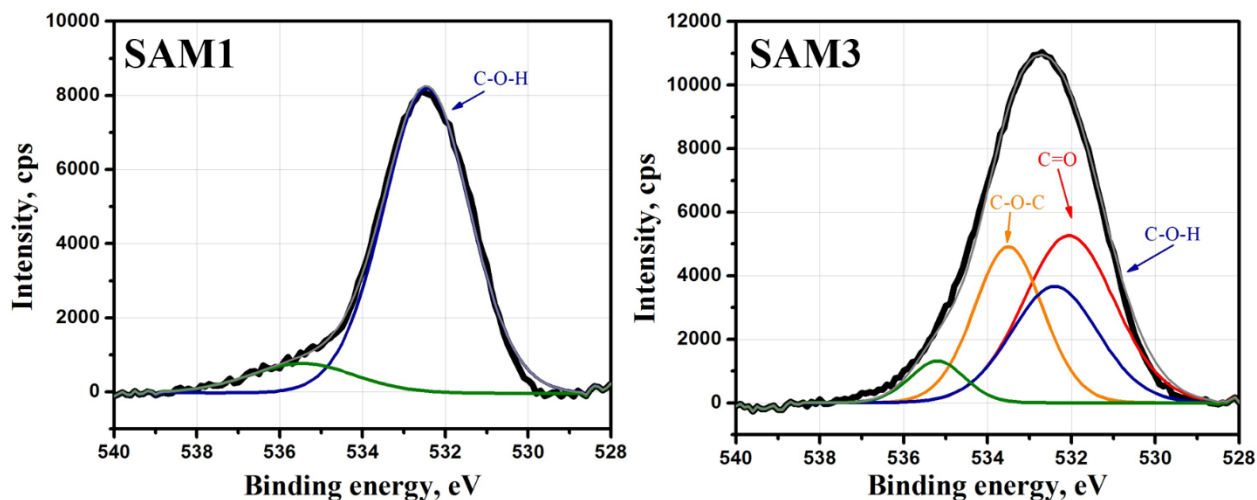


Figure 3.7: Oxygen XPS-spectrum (1s) of gold slide coated by SAM1 (left) and SAM3 (right) after subtraction of baseline. In addition, the result of the decomposition into spectral components of a Gauss-Lorentzian shape is shown.

15. Electrochemical behavior of SAM4

In order to form an electrochemically active film, the gold electrode modified with SAM3 was immersed in an ethanolic solution of BQ as described previously. The electrochemical characterization of the obtained surface was performed using CV. Figure 3.8.a shows cyclic voltammograms measured at different scan rates, in PBS at pH = 7.4, after bubbling the solution with argon. The values of the anodic and cathodic potentials of the peaks are correspondingly +0.22 V and +0.09 V vs. AgCl/Ag. In comparison to our recent work [3] performed with a longer spacer between BQ and gold electrode, the difference between peak potentials for the SAM4 is much smaller, the potential value of the oxidation peak is almost the same, and the potential of the cathodic peak is shifted to anodic direction. Exactly the same effect was observed [4] for immobilization of BQ on SAMs of different thickness. The dependence of the oxidative and reductive peak currents on the sweep rate is linear (Figure 3.8.b), such behavior is typical for electroactive molecules which are immobilized on the electrode surface.

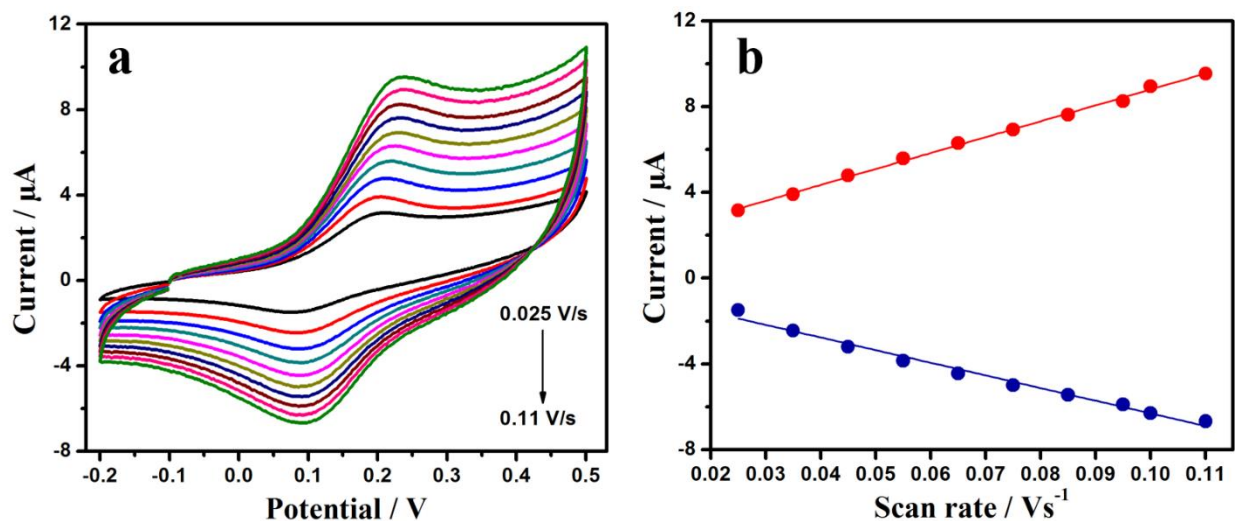


Figure 3.8: a) Cyclic voltammograms of gold electrode modified by SAM4 in 0.1M PBS at pH=7.4. The sweep rates are: 0.025, 0.035, 0.045, 0.055, 0.065, 0.075, 0.085, 0.095, 0.1 and 0.11 Vs⁻¹. b) Dependence of the oxidation (red squares) and reduction (bleu squares) peak currents on the sweep rate.

Furthermore, CV allows us to calculate the surface density of BQ from the integration of the anodic or cathodic peak area considering a bielectronic transfer per molecule. The determination of the peak area after baseline correction gives directly access to the charge using the Nova software version 2.1.2. This correction is necessary since it allows the avoidance of the contribution of residual currents as well as capacitive current. The charge ratio of the oxidation and reduction currents is $Q_{ox}/Q_{red} = 0.89 \pm 0.06$, this indicates an almost reversible electrochemical reaction. The values of the oxidation ($7.2 \pm 0.5 \times 10^{-6}$ C) and reduction ($8.0 \pm 0.3 \times 10^{-6}$ C) peak charges allow us to calculate the surface density of BQ according to the equation 3.5 [5]. This calculation is possible since the peak current is at all points proportional to the scan rate for a reaction occurring at the surface. This contrasts with the oxido-reduction phenomena associated with species diffusion where the current is proportional to the square root of the scan rate.

$$\Gamma = Q/nFA \quad \text{Equation 3.5}$$

$$Q = \text{peak area} / \nu$$

Where: Γ is the surface density, (mol·cm⁻²)

Q is the amount of charge consumed after subtraction of capacitive contribution, (C)

n is the number of electrons involved per one adsorbed molecule,

F is the Faraday constant,

A is the electroactive surface area, (cm^2)

ν is the scan rate, ($\text{V}\cdot\text{s}^{-1}$).

Postulating a two-electron redox process [6,7], this value gives $\Gamma_{\text{BQ}} = 2.5 \pm 0.2 \times 10^{-10} \text{ mol}\cdot\text{cm}^{-2}$.

In order to estimate the efficiency of the whole multistage process of surface modification, we have calculated the surface density of SAM1 molecules from geometrical considerations [8]. According to Love *et al.*, the maximum number of Au atoms in 1 m^2 is 1.4×10^{19} . If we consider that one thiol group is positioned in the 3-fold hollows of the gold lattice the theoretical density of thiol groups bonded to gold is $4.64 \times 10^{18} \text{ molecule}\cdot\text{m}^{-2}$. The surface density of SAM1 molecules calculated according to this estimation is $2.32 \times 10^{14} \text{ molecule}\cdot\text{cm}^{-2}$. This gives $65.0 \pm 4.5\%$ efficiency of the whole multistage process of surface modification.

16. Immobilization of redox-active ligand on SAM4

The quasi-reversible redox signal of the immobilized BQ obtained by CV (Figure 3.8.a) provides a sensitive feature for in-situ and ex-situ monitoring of the BQ reaction with thiolated nucleophiles. The thiolated receptors are considered as Michael donors whereas quinones, containing a polarized double bond, are considered as Michael acceptors [9]. The 6-(ferrocenyl)hexanethiol, further referred as FcSH was used to study the binding to BQ moiety via Michael addition. An advantage of this compound is its intrinsic electrochemical activity. The electrochemical measurements were carried using CV and chronoamperometry (CA).

1.21 In-situ immobilization

The immobilization of FcSH (Figure 3.9) results in the large decrease of the oxidation and reduction peaks relative to BQ adsorbed on the surface (referred to BQ_{SAM} in the figure) and the appearance of two oxidation peaks: the first one at $+0.345 \text{ V}$ attributed to the ferrocene covalently bonded to BQ (referred to FcSH_{BQ} in the figure) and the second one at $+0.486 \text{ V}$ (referred to FcSH_{SAM} in the figure), which we attribute to the FcSH directly adsorbed to the gold surface probably on the defects remaining after formation of SAM3. This estimation can be probably confirmed by the fact that the ferrocene in this layer requires a higher potential to be oxidized.

During the second scan, we notice the decrease of the capacitive current at positive potentials suggesting the formation of an additional molecular structure.

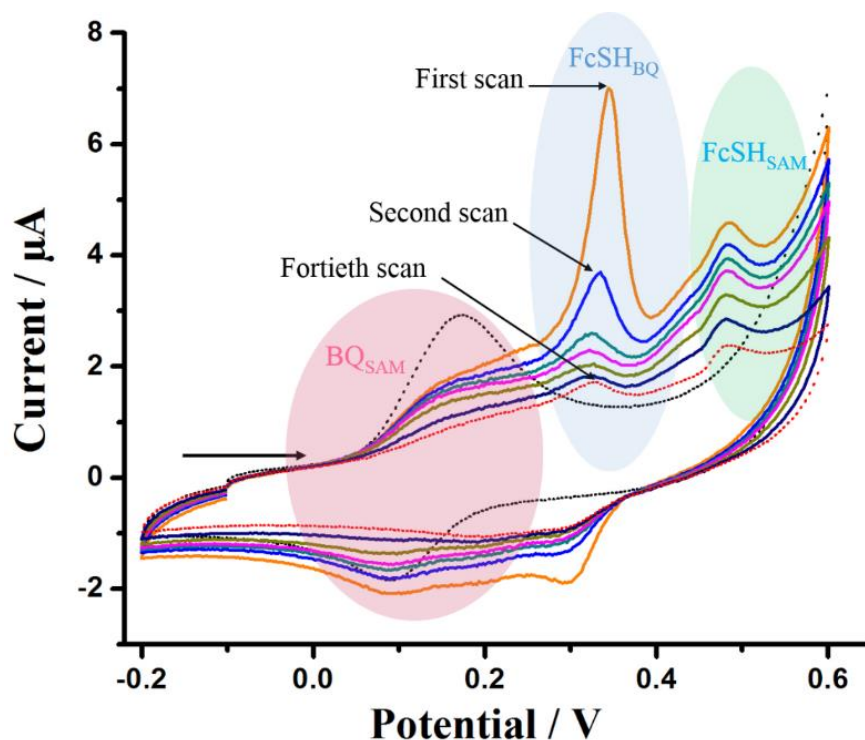
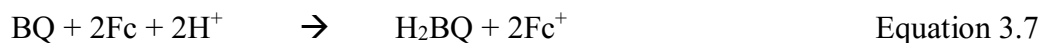
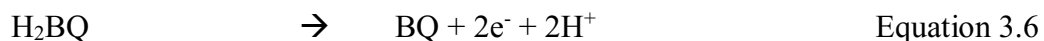


Figure 3.9: Successive CVs of gold electrode coated by SAM4 before (black dotted line) and after addition of Fc-SH ($C = 1\text{mM}$ diluted in acetonitrile) in PBS ($\text{pH} = 7.4$) at scan rate of 25 mV/s . Arrows indicate the direction of the scanning.

Finally, we note that the somewhat particular aspect of the peaks relative to Fc-SH-related quinone can be explained by the catalytic effect exerted by the oxidation of quinones, which oxidizes the ferrocene in turn according to the following mechanism:



At the end of the process and after rearrangement of the grafts at the gold substrate (started from the fortieth scan), we can see the improvement of the reversibility as well as the stability of the signal relative to the ferrocene added to the SAM4.

1.22 Ex-situ immobilization

To prove the principle of electrically addressed covalent immobilization, FcSH was also applied and its immobilization was studied using CA. One can expect that if FcSH is added, it will react with the BQ moiety during the time when the cycled electrode potential is higher than +0.22 V and the BQ moiety is in its oxidized form. The results are shown in Figure 3.10. First, CVs of the electrodes with immobilized BQ were recorded in PBS solution (black curves). Then the electrodes were incubated for 800 s in 1mM FcSH solution in acetonitrile at electrical potentials of either +0.4 V or -0.4 V. The electrodes were rinsed thoroughly with ethanol and water to remove physisorbed FcSH and placed into PBS for cyclic voltammetric measurements at pH = 7.4. The electrodes incubated under anodic potential are shown in Figure 3.10.a: the electrochemical activity of BQ disappeared and a new pair of oxidation/reduction peaks appeared. The potentials of this pair were observed at +0.39 V and ~-0.35 V for the oxidation and reduction processes correspondingly (red curve). The loss of the electrochemical activity of BQ indicates on destroying of its aromatic structure. Therefore, one can suggest that the observed peaks are attributed to the to the ferrocene covalently bonded to BQ (referred to FcSH_{BQ} in the figure) through Michael addition. Similar effect was reported by Li *et al.* [10]. While, the electrode incubated at the cathodic potential (Figure 3.10 b, red curve) displays quite different cyclic voltammetric curve: redox peaks of BQ persist with small shift probably due to the system disturbance and we note also absence of the redox peaks of the monolayer of FcSH contrary to our previous work [3]. Therefore, we can confirm that SAM4 is more stable than BQ-terminated SAM in the ref. [3] (as a comparison between SAMs that differ by the number of anchor site per molecule).

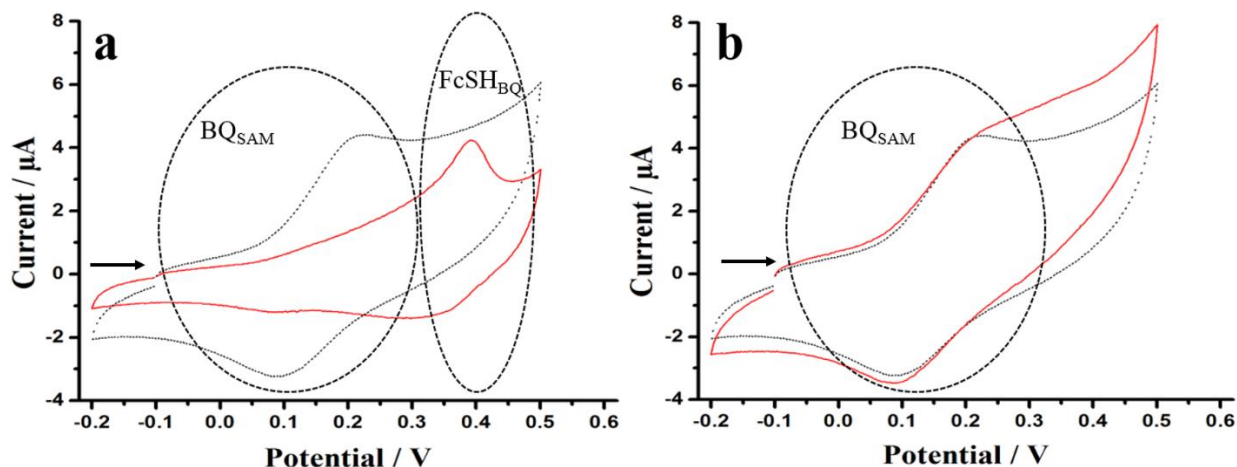


Figure 3.10: CVs of gold electrodes coated by SAM4 before (black curves) and after (red curves) interaction with FcSH from 1mM solution in acetonitrile by subsequent incubation in this solution for 800 s at electrode potential +0.4 V (a) and -0.4 V (b). The measurement was performed in PBS (pH = 7.4) at sweep rate 0.05 Vs^{-1} . Arrows indicate the direction of scanning.

In conclusion, we can confirm that addition of thiolated nucleophiles receptors to the SAM4 can be controlled using electrochemical measurements, therefore, the prepared SAM can be applied for different tasks of chemical sensing and biosensing.

17. Application of SAM4 for electrochemical sensing of NADH

NADH is involved as a cofactor in a large number of enzymatic reactions of NAD^+/NADH -dependent dehydrogenases. The electrochemical oxidation of NADH has thus been the subject of numerous studies related to the development of amperometric biosensors [11]. Problems inherent to such anodic detection are the large overvoltage encountered for NADH oxidation at ordinary electrodes [12] and surface fouling associated with the accumulation of reaction products [13]. Consequently, considerable effort has been devoted toward the goal of identifying new electrode materials that will reduce the overpotential for NADH oxidation and minimize surface passivation effects. The most successful approach involves redox mediators confined to the electrode surface [14]. A number of electrode modification have been reported using, e.g., quinones derivatives [11,15,16].

Figure 3.11 shows the electrocatalytic mechanism proposed for the reaction involving the immobilized BQ moieties and the NADH molecules. One can suggest that the dissolved NADH

diffuses to the electrode surface, where it reduces *p*-benzoquinone to form NAD⁺ and *p*-hydroquinone. Then *p*-hydroquinone is then reoxidized on the electrode surface being available again for the next catalytic cycle.

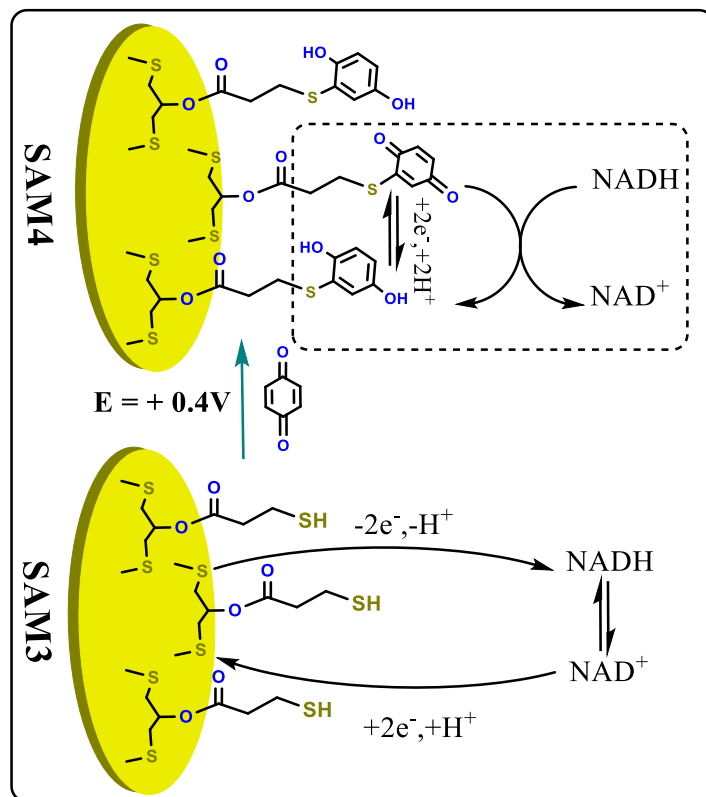


Figure 3.11: Schematic representation of NADH oxydo-reduction mechanism in the presence of SAM3 and SAM4.

To prove this assumption, chronoamperometric measurements (Figure 3.12, left) were performed at +0.4 V when quinone is converted into electrocatalytically active BQ. The same experiment with SAM3 has shown ~6 times lower oxidation current. The evolution of the chronoamperometric response versus NADH concentration produced a calibration curve (Figure 3.12, right) over a linear range till ~2.0 mM with a progressive equation of $I = 5.28 \times 10^{-8}[\text{NADH}] + 3.026 \times 10^{-8}$ ($R^2 = 0.0994$) and a limit of detection (LOD) of ~0.7 mM, as determined from $C_{\text{LOD}} = 3 \times S_b/m$, where S_b is standard deviation of three replicate blank signals and m the slope of calibration curve. The sensitivity of the electrode toward NADH was also obtained from the corresponding calibration plot and was $0.332 \mu\text{A} \cdot \text{mM}^{-1} \text{cm}^{-2}$ (~53 nA/mM).

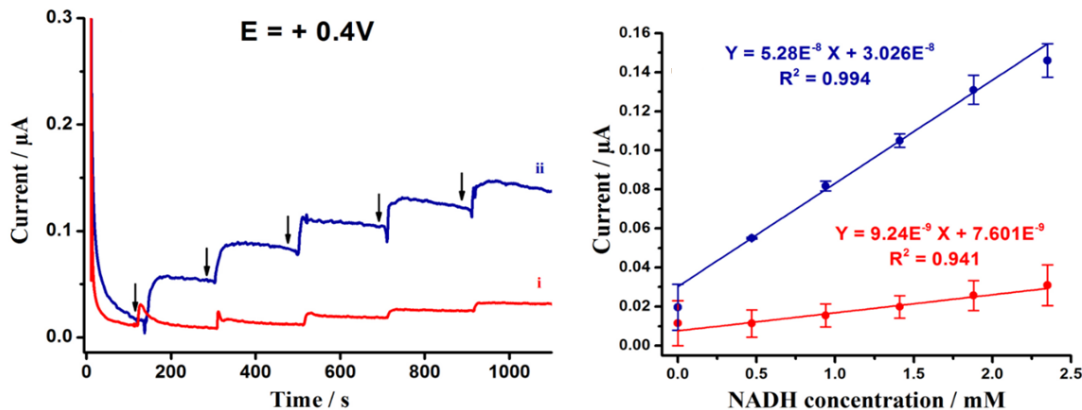


Figure 3.12: Chronoamperometric responses of SAM3 (curve i) and SAM4 (curve ii) to subsequent additions of NADH (left) and concentration dependence of this effect (right). The arrow indicates an injection of 20 μL NADH (0.235 M) (left). At zero-time moment the electrode potential was switched from 0 V to +0.4 V vs. AgCl/Ag. Electrolyte: 0.1 M PBS, pH = 7.4. The measurements were performed under argon stream at continuous stirring.

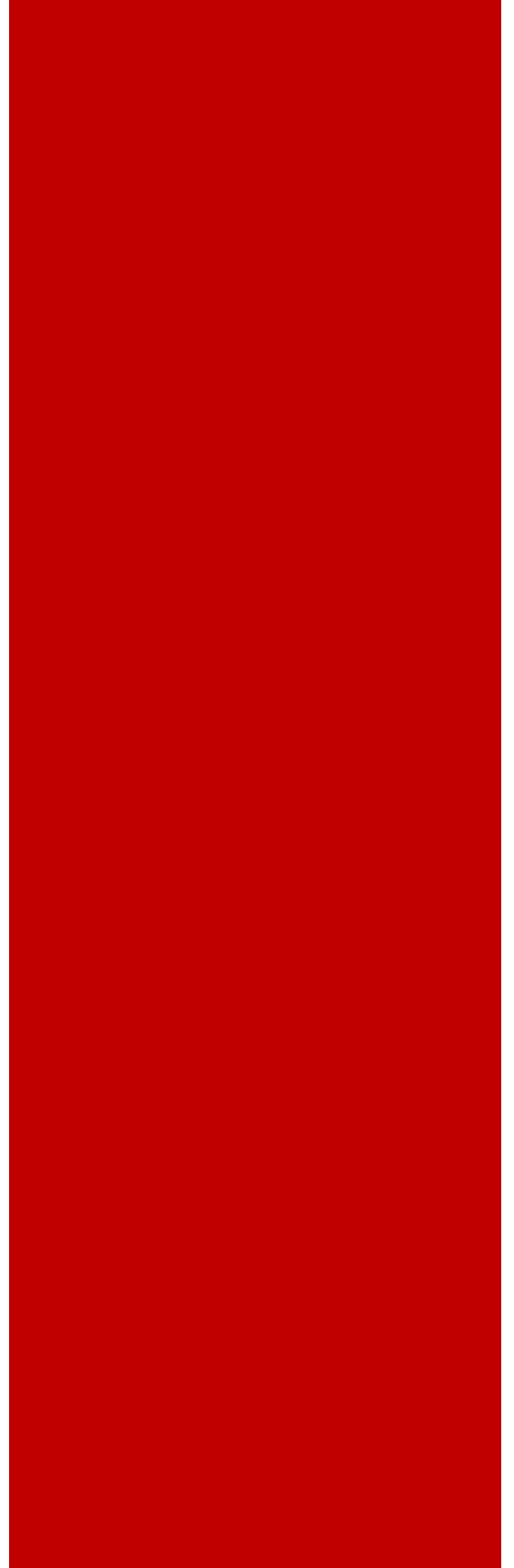
18. Conclusion

In this chapter, we have described the formation of an electrochemically active SAM. The preparation of the SAM was involved in two steps: Steglich esterification followed by Michael addition of BQ moieties. Both steps were characterized using electrochemical measurements. The esterification of SAM1 was proved by CV and EIS. These latter show the formation of an additional layer that forms a barrier against the electron transfer. Capacitive analysis of impedance spectra measured in aqueous medium allows to calculate the value of esterification efficiency $\theta = 0.42$ suggesting that 84% of SAM1 molecules are esterified during the formation of the SAM3. This estimation was proved by XPS studies which gave a detailed analysis on the behavior of MPA in contact with SAM1. The surface density of the immobilized BQ was $\Gamma_{BQ} = 2.5 \pm 0.2 \times 10^{-10}$ mol \cdot cm $^{-2}$. This gives $65.0 \pm 4.5\%$ efficiency of the whole multistage process of surface modification. The electrochemically active SAM provides a sensitive feature for monitoring of the BQ reaction with thiolated nucleophiles. As an example, we have performed the addition of FcSH using passive incubation and by applying electrical potentials. The formed system was used for electrocatalytic oxidation of NADH. Results have shown a great improvement in NADH detection between SAM3 and SAM4 which indicates great promise of BQ-terminated SAMs for the design of amperometric biosensors, in connection to the immobilization of suitable dehydrogenase enzymes. The electrochemically active SAM4 shows its ability to promote electron-transfer reactions of other biologically or environmentally important compounds.

References

- [1] S. Chah, J. Yi, C. M. Pettit, D. Roy, J. H. Fendler, *Langmuir*, **2002**, 18, 314–318.
- [2] A.-S. Duwez, *J. Electron Spectrosc. Relat. Phenom.*, **2004**, 134, 97–138.
- [3] A. Hammami, N. Raouafi, V. M. Mirsky, *Biosens. Bioelectron.*, **2018**, 121, 72–79.
- [4] H.-G. Hong, W. Park, *Langmuir*, **2001**, 17, 2485–2492.
- [5] A. J. Bard, L. R. Faulkner, *Electrochemical Methods*, second ed., Wiley, New York, **2001**.
- [6] K. Hasan, Y. Dilgin, S. C. Emek, M. Tavahodi, H.-E. Åkerlund, P.-Å. Albertsson, L. Gorton, *Chem. Electro. Chem.*, **2014**, 1, 131–139.
- [7] L. A. Shundrin, I. G. Irtegova, N. V. Vasilieva, I. A. Khalfina, *Tetrahedron Lett.*, **2016**, 57, 392–395.
- [8] J. C. Love, L. A. Estroff, J. K. Kriebel, R. G. Nuzzo, G. M. Whitesides, *Chem. Rev.*, **2005**, 105, 1103–1170.
- [9] L. R. De Astudillo, L. Rivera, R. Brito-Gómez, R. J. Tremont, *J. Electroanal. Chem.*, **2010**, 640, 56–60.
- [10] J. Li, C.-L. Sun, L. Tan, Y.-L. Xie, H.-L. Zhang, *Langmuir*, **2013**, 29, 5199–5206.
- [11] A. Maleki, D. Nematollahi, J. Clausmeyer, J. Henig, N. Plumeré, W. Schuhmann, *Electroanalysis*, **2012**, 24, 1932–1936.
- [12] M. Musameh, J. Wang, A. Merkoci, Y. Lin, *Electrochem. Commun.*, **2002**, 4, 743–746.
- [13] J. Wang, L. Angnes, T. Martinez, *Bioelectrochem. Bioenerg.*, **1992**, 29, 215–221.
- [14] W. J. Blaedel, R. A. Jenkins, *Anal. Chem.*, **1975**, 47, 1337–1343.
- [15] L. Gorton, E. Domínguez, *Mol. Biotechnol.*, **2002**, 82, 371–392.
- [16] H. R. Zare, N. Nasirizadeh, S.-M. Golabi, M. Namazian, M. Mazloum-Ardakan, D. Nematollahi, *Sensor. Actuat. B: Chem.*, **2006**, 114, 610–617.

**Chapter 4: Application of
SAM4 in electrocatalytic
hydrogen peroxide sensing**



19. Introduction

Electrocatalytic chemical sensors are applied intensively for direct detection of various chemical species or as transducers in biosensors [1-7]. One of the mostly important chemical sensors in which the electrocatalytic effect is to exploit for the hydrogen peroxide sensing. Such devices are important not only for direct determination of this compound but also for enzymatic biosensors where hydrogen peroxide is the byproduct of the enzymatic oxidation of organic compounds. A number of electrocatalysts for hydrogen peroxide based on chemically modified electrodes with different design strategies involving complexes of the Robson type [8], metal/bimetallic nanomaterials [9], Prussian blue [10-11], carbon nanotubes or graphene [12] were reported. The mostly applied experimental approach for electrode functionalization is based on the technology of SAMs of thiolates forming a stable monomolecular film on the gold surface [13-16] and therefore widely applied in chemical and biological sensors [17,18].

The design of the electrocatalytic sensors for hydrogen peroxide based on SAMs should fulfil two requirements: (i) the sensor structure should be stable to provide well reproducible results in the wide range of environmental conditions and for a long time, (ii) effective electron transfer to the electrode. These requirements are controversy because high stability of immobilized compounds is usually achieved by using of a thick hydrophobic anchor layer [19] which in turn hinders electron tunneling through this layer. To achieve a high stability of thin SAMs, compounds with multiple thiol groups should be used. An exemple the BQ-terminated-SAM based on symmetrical dithiol:1,3-dimercaptopropan-2-ol (SAM4) described in the previous chapters (chapter 2 and 3).

This chapter describes the investment of this SAM for the development of a new electrocatalytic sensor for hydrogen peroxide. Sensor analysis was performed by CV at the potential range from -0.6 V till $+0.9$ V as well as in the anodic or cathodic range only. Analytical evaluation of the sensor performance was done in the voltammetric- as well as in the chronoamperometric mode. All electrochemical experiments were performed in 0.1 M PBS at pH = 7.4 .

20. Cyclic voltammetric analysis

1.23 Case of wide potential range

An addition of hydrogen peroxide leads to dramatic changes in the voltammetric curves (Figure 4.1). Figure 4.1 shows CVs recorded to the Au modified SAM4 in presence of atmospheric oxygen (red) and under Ar (blue) in the supporting electrolyte and in the presence of 2.5 mM hydrogen peroxide. The oxidation and reduction peaks of BQ are not observed in the indicated current scale. No oxidation peak is observed either in air or argon without addition of hydrogen peroxide (Figure 4.1, the curves i). However, when hydrogen peroxide is introduced into the solution, a well pronounced oxidation peak at $\sim +0.4$ V is displayed (Figure 4.1, the curves ii). The reduction peak at cathodic potentials without hydrogen peroxide is observed in the measurements under air atmosphere but disappears after solution bubbling by argon (Figure 4.1, curves i) therefore it can be attributed to the effect of oxygen. In the presence of hydrogen peroxide this peak is observed also under argon atmosphere, but it is higher under air atmosphere (Figure 4.1, curves ii).

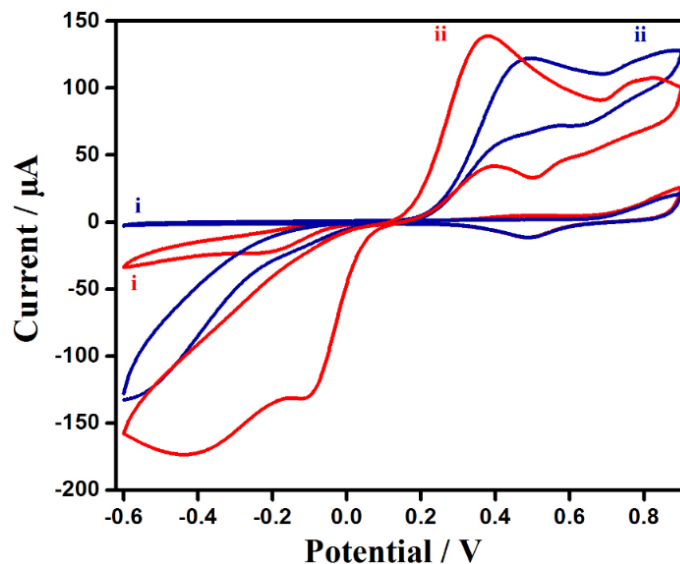
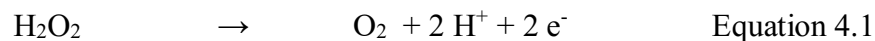


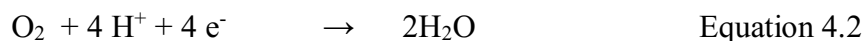
Figure 4.1: CVs recorded with gold electrodes coated by SAM4 under air (red curves) or argon (blue curves) atmosphere in the absence (curves i) and in the presence (curves ii) of 2.5 mM H_2O_2 at scan rate of 50 mV/s.

Anodic oxidation of hydrogen peroxide is a well investigated process [20], it occurs according to the reaction schematized by Equation 4.1:

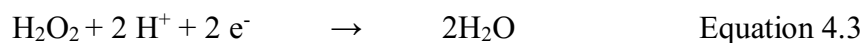


The value of the oxidation potential of hydrogen peroxide on gold electrodes is +490 mV (vs. AgCl/Ag) at pH = 7.4 in [21] or 475 mV in [22]. Gerlache et al. [21] reported a strong dependence of this potential on the electrode surface. Indeed, in the presence of impurities or gold oxides the potential is shifted to 870 mV (vs. AgCl/Ag) at pH = 7.4.

The reaction of oxidative decomposition of hydrogen peroxide releases oxygen, which can be highlighted by the formation of gas bubbles on the gold electrode. During the cathodic scan the formed (and also atmospheric) oxygen is reduced to water according to the reaction governed by the Equation 4.2 [23-24].



In the next step hydrogen peroxide is reduced to water [23-26], according to Equation 4.3.



These processes explain the behavior of the reduction current during the scan into cathodic direction (Figure 4.1, curves ii). No reduction current is observed under argon atmosphere without hydrogen peroxide in the solution (Figure 4.1, blue curve, i). Reduction of atmospheric air leads to a low cathodic current (Figure 4.1, red curve, i) and is displayed like a peak of low current intensity in the voltammogram. Reduction of hydrogen peroxide [27] without atmospheric air leads to the formation of a large wide wave (Figure 4.1, blue curve, ii). This process should also include the reduction of some amount of oxygen [28-31] formed during anodic scan, but this amount is too small to yield a clear peak on the curve. But the same experiment being performed in atmospheric air shows a pronounced peak which can be attributed to the reduction of oxygen (Figure 4.1, red curve, ii). Therefore, in the experiment shown in Figure 4.1 two types of electrochemical decompositions of hydrogen peroxide are observed: oxidation and reduction.

The contribution of oxygen electrochemistry and two types of electrochemical decomposition of hydrogen peroxide complicate quantitative electrochemical detection of this analyte. This problem can be overcome by measurements at the anodic potentials only (when no oxygen consumption and no reduction of hydrogen peroxide occur) or at the cathodic potentials only (when no oxygen generation and no oxidation of hydrogen peroxide occur).

1.24 Case of the cathodic range

CVs measured at cathodic potentials are shown in Figure 4.2. The measurements were performed under air (Figure 4.2.A) or under an argon (Figure 4.2.B) atmosphere at different concentrations of hydrogen peroxide. In both cases the increase of the hydrogen peroxide concentration leads to the increase of the reduction current. In this experiment there is no oxidation of hydrogen peroxide, therefore the effect in (Figure 4.2.B) is caused by the reduction of hydrogen peroxide only. A contribution of atmospheric oxygen leads to the additional wide peak (Figure 4.2.A), similar to the cathodic region of the data shown in Figure 4.1.

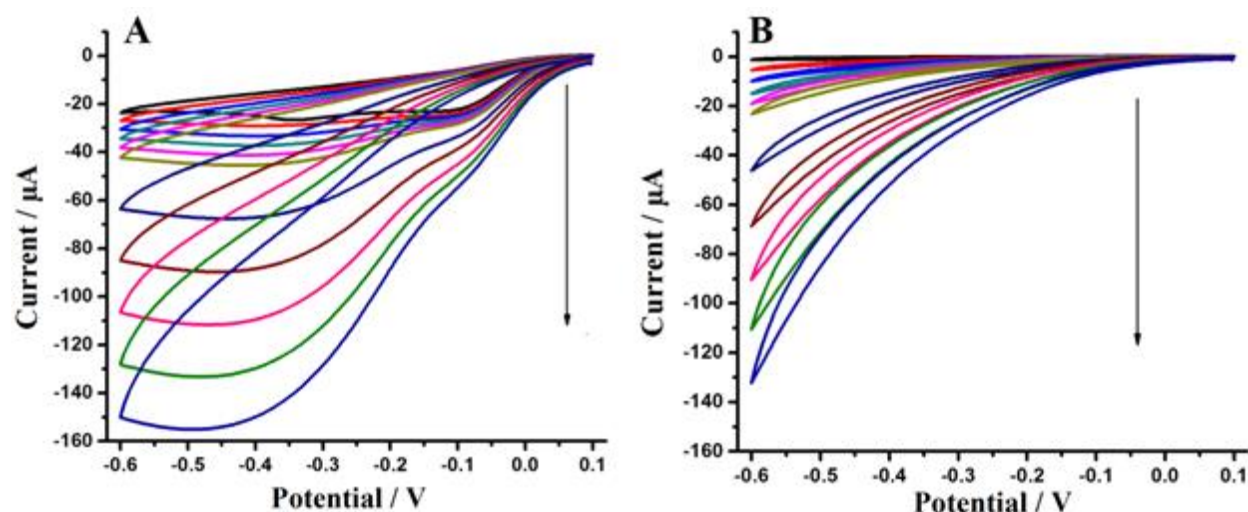


Figure 4.2: CVs recorded with gold electrodes coated by SAM4 under air (A) or argon (B) atmosphere in the solution containing 0, 0.1, 0.2, 0.3, 0.4, 0.5, 1, 1.5, 2, 2.5 or 3 mM of H_2O_2 at 0.05 V/s. The arrows indicate an increase of concentration of hydrogen peroxide.

1.25 Case of the anodic range using different gold surfaces

The CVs at anodic range are more complex (Figure 4.3). CVs recorded with the gold electrode modified by SAM4 (Figure 4.3.C) show two oxidation peaks: the first one appears at 380 mV, the second one is observed at higher anodic potential (~ 800 mV). An increase of the concentration of hydrogen peroxide leads to an increase of the first peak (380 mV) while the second oxidation peak remains unchanged. Gerlache *et al.* have reported a similar effect and attributed the second peak to the gold oxidation [21].

To evaluate a possible electrocatalytic effect of BQ, the same experiment was performed with uncoated gold electrode (Figure 4.3.A) as well as with gold electrode modified by SAM3 (same

structure as SAM4 without terminal BQ moiety) (Figure 4.3.B). The behavior of the uncoated gold electrode is qualitatively similar to that coated by SAM4. Like in [21] the CVs being measured on the uncoated gold electrode show two oxidation peaks (at 350 and 800 mV) while only the first one depends on the presence of hydrogen peroxide (Figure 4.3.A). Although the oxidation of hydrogen peroxide on the gold electrode modified by SAM4 is observed at a little higher potential, the magnitude of this current peak is about twice higher (Figure 4.3.C and D). A deposition of SAM3 shows essential blocking effect: the oxidation of hydrogen peroxide is starting at higher potentials (~ 560 mV), no pronounced oxidation peak observed (Figure 4.3.B). An immobilization of BQ on the surface of this SAM can lead only to further increase of its thickness. Surprisingly, this leads to strong shift of the oxidation potential of hydrogen peroxide to cathodic direction and to the strong increase of the oxidation current (Figure 4.3.B and C). The ratio of the oxidation currents at the electrode potential 0.38 V in the wide concentration range of hydrogen peroxide is ~ 10 (Figure 4.3.D). This demonstrate clearly electrocatalytic effect of the BQ moiety.

Most probably during the potential sweep in the anodic direction the dissolved hydrogen peroxide diffuses to the electrode surface where it reduces *p*-benzoquinone with formation of oxygen and *p*-hydroquinone. Then *p*-hydroquinone is re-oxidized on the electrode surface being available again for the next electrocatalytic cycle. On the cathodic scan (Figure 4.3.C), an oxidation peak is clearly observed at the potential of ~ 380 mV at the reverse potential sweep, suggesting that the generated BQ was formed which is due to further oxidation of hydrogen peroxide. Similar oxidative behavior of hydrogen peroxide was also explored by Muhurasu et al. [32].

The observed electrocatalytical effect can be used for analytical purposes. The measurement can be performed by CV, CA or by other electrochemical techniques. The dependence of the magnitude of the oxidation peak current on the hydrogen peroxide concentration is presented in (Figure 4.3.D). It can be served as the calibration curve. At the concentrations below 2 mM this dependence is linear with a correlation coefficient $r = 1.03$ [33]. For the used experimental conditions this dependence gives analytical sensitivity of $3460 \text{ A}\cdot\text{m}^{-2}\cdot\text{mol}^{-1}\cdot\text{L}$. The LOD determined as the ratio of three values of the signal measured without hydrogen peroxide to the slope is $\sim 4 \mu\text{M}$. The standard deviation of the data obtained in the concentration range from 0.1 till 3 mM with three independently is below 4.2%.

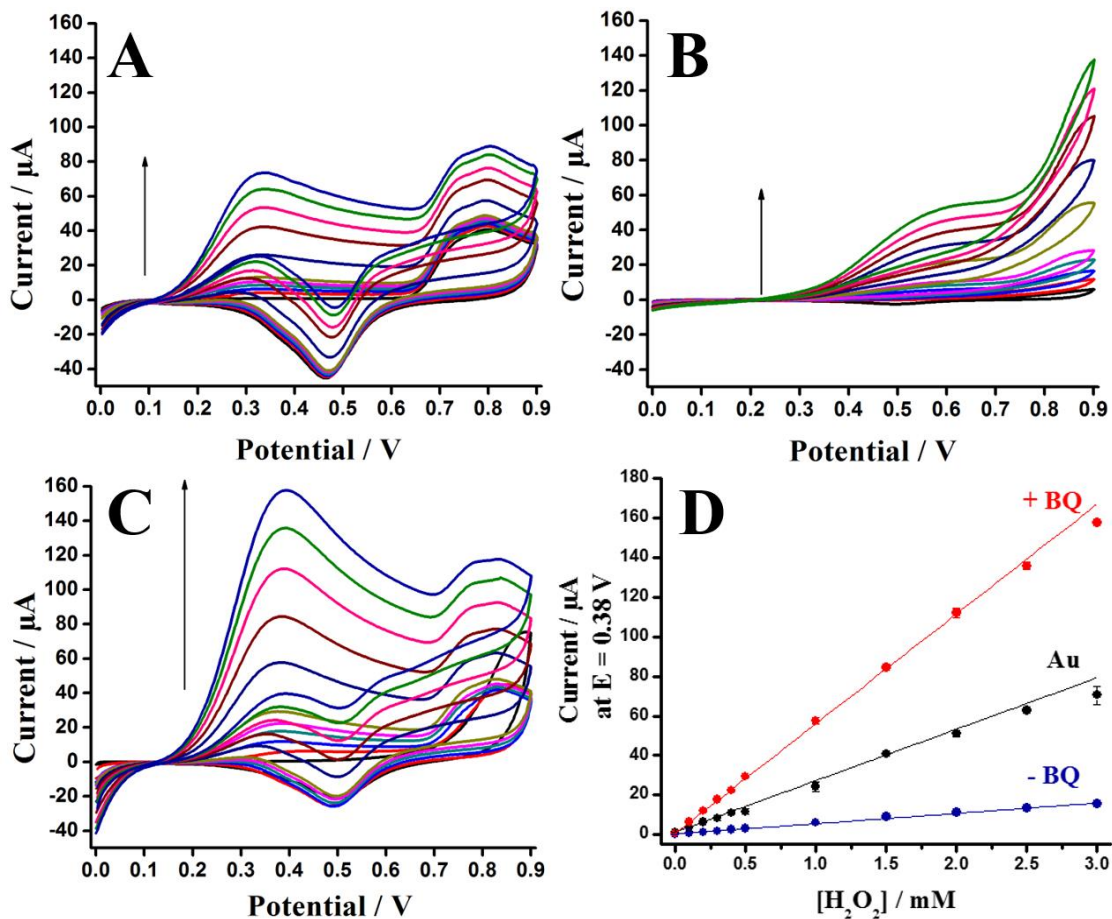


Figure 4.3: CVs recorded from 0 to +0.9 V in the solution containing 0, 0.1, 0.2, 0.3, 0.4, 0.5, 1, 1.5, 2, 2.5 and 3 mM H_2O_2 at scan rate as 50 mV s^{-1} for uncoated gold electrode (A), gold electrode modified SAM3 (B) and SAM4 (C) and the concentration dependence of the oxidative current on the concentration of hydrogen peroxide at the electrode potential +0.38 V measured on the uncoated gold electrode (Au), gold electrode coated by SAM3 (-BQ) and SAM4 (+BQ).

An influence of the scan rate on the current peak of hydrogen peroxide oxidation was studied. The results are shown in Figure 4.4. The observed square root dependence (Figure 4.4 B) indicates that the catalyst is working very fast, and the whole electrochemical process is controlled by diffusion.

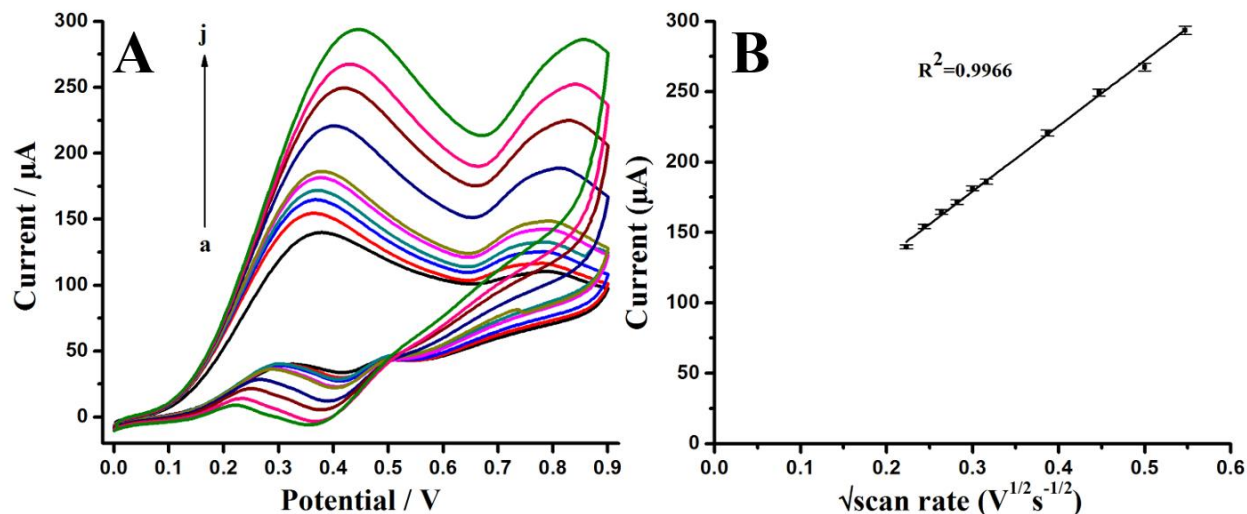


Figure 4.4: Influence of the scan rate on the CV of oxidation of 2.5 mM hydrogen peroxide on the gold electrode coated by SAM4 at (a) 50, (b) 60, (c) 70, (d) 80, (e) 90, (f) 100, (g) 150, (h) 200, (i) 250 and (j) 300 mV/s (A) and dependence of the oxidation current peak on the square root of the scan rate (B).

21. Chronoamperometric analysis

Chronoamperometric measurements of hydrogen peroxide are shown in Figure 4.5. The measurements were performed at the potential +0.4 V which corresponds to the peak of the voltammogram of electrocatalytic oxidation of hydrogen peroxide on BQ (Fig. 4.3.C). An addition of hydrogen peroxide leads to increase of the current (Figure 4.5.A). Linear relationship was obtained in the range of concentrations 0.1-0.5 mM (Figure. 4.5.B). The sensitivity and the LOD calculate from this dependence, are $1760 \text{ A}\cdot\text{m}^{-2}\cdot\text{L}\cdot\text{mol}^{-1}$ and $2.3 \mu\text{M}$, respectively. At higher concentrations a trend for saturation was observed (Figure. 4.5.B). The maximal catalytic current observed at the highest studied concentration of hydrogen peroxide can be recalculated into the catalyst turnover. The value of current at 3 mM is equal to $49 \mu\text{A}$. We can take into account that $I_{\text{max}} = \kappa z e_0 \Gamma A$, where κ is the rate of the catalyst turnover, z is the stoichiometry of the catalyzed reaction, e_0 is the elementary charge, A is the electrode area and Γ is the surface concentration of BQ moieties on the electrode surface. For the oxidation of hydrogen peroxide the value $z = 2$ is expected. The value of Γ is equal to $1.5 \times 10^{18} \text{ molecules/m}^2$ (see paragraph 15 in chapter 3). This gives the value of the catalyst turnover $\kappa \sim 6 \text{ molecules/s}$. This low value is caused by the diffusion limitation of the catalytic process.

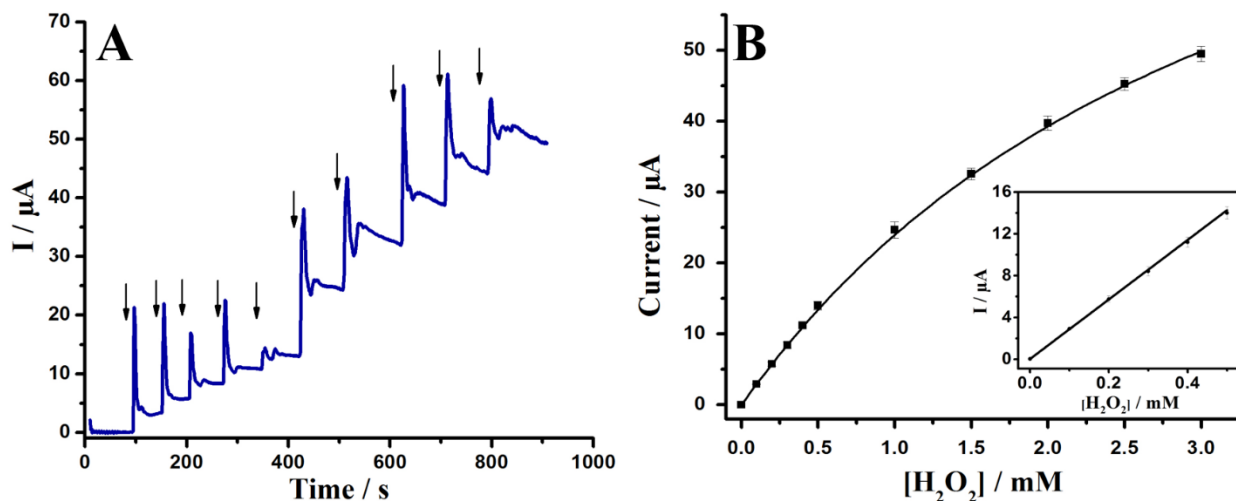


Figure 4.5: Chronoamperometric responses for successive hydrogen peroxide additions recorded using SAM4-modified gold electrode at the electrode potential +0.4 V(A) and corresponding concentration dependence (B).

22. Selectivity and performance

The proposed sensor has been tested against some interferences present in blood such as glucose, uric acid and ascorbic acid. These compounds are usual interferences in applications of electrocatalytic sensors in biological media, and the tested concentrations were two times higher than their physiological concentrations [34]. As shown in Figure 4.6, no response was observed on additions of these substrates proving a good selectivity of the sensor towards hydrogen peroxide.

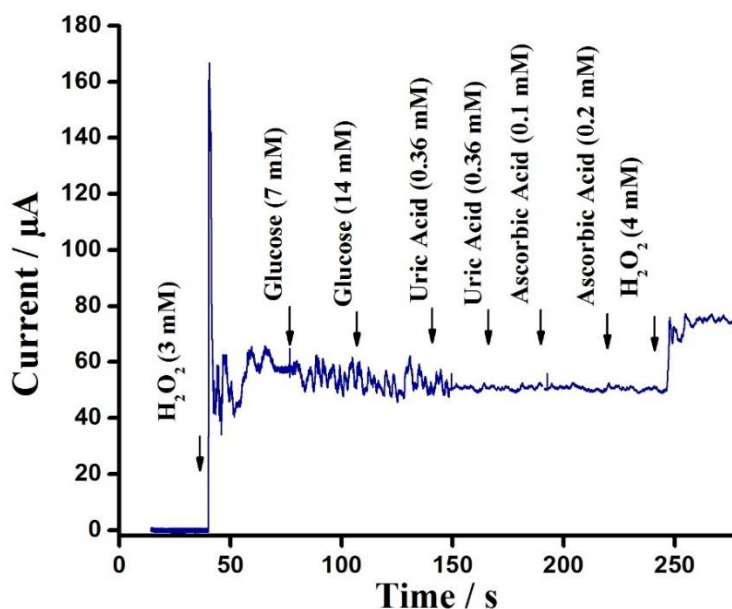


Figure 4.6: Sensor response measured in chronoamperometric mode at +0.4 V: investigation of sensor selectivity.

The literature data on the comparison of different oxidative electrocatalysts suggested for the sensing of hydrogen peroxide are summarized in Table 4.1. This comparison shows that only very few electrocatalytic materials provide effective oxidation of hydrogen peroxide at electrode potential below 0.5 V vs. AgCl/Ag (sat. KCl). BQ belongs to these materials. The catalysts based on inorganic oxides [35-37] provide oxidation of hydrogen peroxide at some lower potential. The results of the selectivity test were not reported, but a catalytic activity of inorganic materials has usually poor selectivity [38]. A comparison of analytical sensitivity required normalization to the effective electrode surface area, it makes difficult a comparison with the electrodes coated by nanomaterials. Among the electrodes with well-defined area, the BQ-based electrocatalytic sensors give the highest value of the normalized analytical sensitivity.

The comparison with literature data has shown that electrocatalytic sensors for hydrogen peroxide based on BQ-terminated SAMs provide well competitive analytical properties in sense of selectivity, operating electrode potential and analytical sensitivity. In the same time, the comparison of CVs in Figures 4.3.A and B shows an essential blocking of the electrochemical activity by the SAM. This allows us to suggest that an immobilization of the BQ moiety closer to the electrode surface will lead to further essential improvement of electrocatalytic activity.

Table 4.1: Comparison of oxidative electrocatalysts for hydrogen peroxide.

Electrode	Method	Sensitivity (A·m ⁻² ·mol ⁻¹ ·L)	Oxidation potential ^a (V)	LOD (μM)	Selectivity test: a response to			References
					Glucose	Uric acid	Ascorbic acid	
AuMFs/ITO	CV/CA	1.3×10 ^{7b}	+0.55	1.1	yes	no	no	[32]
oxoruthenium(III) /Pt	CV/CA	260	+0.605	n. d.	n. d.	n. d.	n. d.	[39]
Co ₃ O ₄ nanowalls/GCE	CA	1.7×10 ^{4b}	+0.8	2.8	n. d.	n. d.	n. d.	[40]
FcAPS ^c /GCE	CA	0.5	+0.645	2.07	no	n. d.	no	[41]
MnO ₂ /Na- montmorillonite/ GCE	CA	310	+0.695	0.15	n. d.	yes	yes	[42]
NP PtNi/GCE	CA	1220	+0.501	1.0	yes	yes	yes	[43]
Co ₃ O ₄ NPs ^d /GCE	CV/CA	5.9×10 ⁴ / 4.9×10 ^{4b}	+0.75	0.05/ 4×10 ⁻⁴	n. d.	n. d.	n. d.	[44]
MnO ₂ /CPE	CA	1.0×10 ^{7e}	+0.795	1.5	n. d.	n. d.	yes	[45]
Pt/TiO ₂ nanocomposite	CA	8.5 ^b	+0.3	4.0	n. d.	n. d.	n. d.	[35]
Cobalt oxide/CoTRP ^f / GCE	CV	n. d.	+0.3	0.2	n. d.	n. d.	n. d.	[36]
Nano- MnO ₂ /carbon paste	CA	n. d.	+0.3	2.0	n. d.	n. d.	n. d.	[37]
Pt-BDD	CA	3100	+0.55	0.03	n. d.	n. d.	n. d.	[46]
Poly(DA- Fc)/GCE	CA	0.7 ^g	+0.55	5.0	no	n. d.	no	[47]
SPCE ^h -Co ₃ O ₄	CA	3476	+0.8	0.145	n. d.	n. d.	n. d.	[48]
Fc-rGO electrode	CA	1.2×10 ⁴	+0.6	0.44	n. d.	n. d.	n. d.	[49]
BQ/Au	CV/CA	3500/1800	+0.4 V	4/2.3	no	no	no	this work

Comments:

AuMFs/ITO = gold microflower/indium tin oxide.

oxoruthenium(III) = oxo-bridged ruthenium(III) complex platinum.

MnO₂/Na-montmorillonite = MnO₂ nanoparticles–colloidal Na-montmorillonite.

NP PtNi = nanoporous platine nickel alloy.

MnO₂/CPE = MnO₂ graphite composite modified carbon powder electrode.

Pt-BDD = Pt-implanted boron-doped diamond.

Poly(DA-Fc) = polydopamine-ferrocene film.

Fc-rGO electrode = ferrocene-functionalized reduced graphene oxide electrode.

GCE: glassy carbon electrode.

^a potential of the oxidation peak (vs sat AgCl/Ag (KCl)).

^b macroscopic electrode area was considered.

^c ferrocene entrapped into a cross-linked aminopolyethersulfone film.

^d nanoparticles.

^e the electrode area is not indicated; the sensitivity was calculated for the electrode area 1 cm².

^f tetraruthenated cobalt-porphyrin.

^g $\mu\text{A } \mu\text{M}^{-1}$ (no indication on the electrode surface).

^h screen-printed carbon electrode.

n. d. means no data.

23. Conclusion

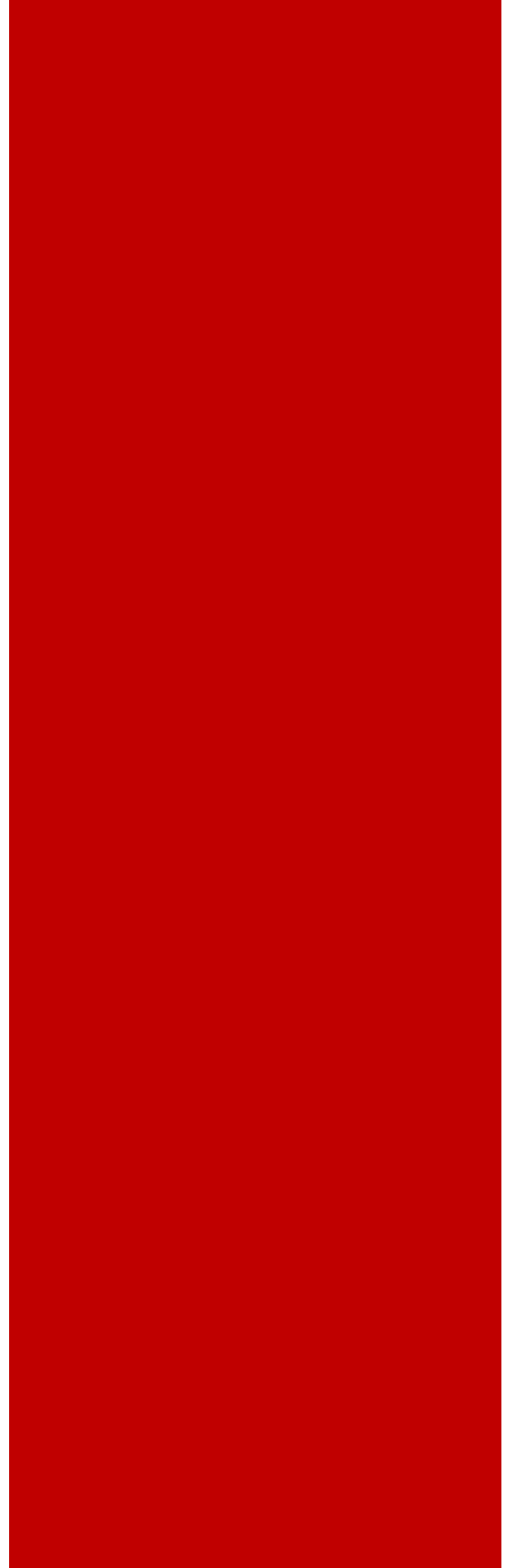
In this chapter, we have demonstrated that BQ is a perspective material for the development of electrocatalytic sensors for hydrogen peroxide. In comparison with other catalytic materials, it provides high selectivity against typical interferences at a relatively low oxidation potential and high analytical sensitivity. The high sensitivity allows us to consider applications of this system in the analysis of hydrogen peroxide in different technological processes or as a transducer in enzymatic biosensors based on oxidoreductases, for example a biosensor for glucose based on glucoseoxidase.

References

- [1] J. E. Mueller, D. Fantauzzi, T. Jacob, Multiscale Modeling of Electrochemical Systems, *Electrocatalysis*, **2013**.
- [2] J. Janata, M. Josowicz, *Anal. Chem.*, **1998**, 70, 179–208.
- [3] E. A. H. Hall, J. J. Gooding, C. E. Hall, *Mikrochim. Acta*, **1995**, 121, 119–145.
- [4] E. Bakker, M. Telting-Diaz, *Anal. Chem.*, **2002**, 74, 2781–2800.
- [5] U. Wollenberger, *Biotechnol. Genet. Eng.*, **1996**, 13, 237–266.
- [6] A. Lambrianou, S. Demin, E. A. H. Hall, *Protein Engineering and Electrochemical Biosensors, Adv. Biochem. Engin. / Biotechnol.*, **2008**, 109, 65–96.
- [7] M. S. Akram, J. U. Rehman, E. A. H. Hall, *Annu. Rev. Anal. Chem.*, **2014**, 7, 257–274.
- [8] N. V. Roznyatovskaya, V. K. Laurinavichute, G. A. Tsirlina, V. M. Mirsky, *J. Solid State Electrochem.*, **2007**, 11, 981–992.
- [9] S. Chen, R. Yuan, Y. Chai, F. Hu, *Microchim. Acta*, **2013**, 180, 15–32.
- [10] F. Ricci, A. Amine, C. S. Tuta, A. A. Ciucu, F. Lucarelli, G. Palleschi, D. Moscone, *Anal. Chim. Acta*, **2003**, 485, 111–120.
- [11] Y. Li, X. Liu, X. Zeng, Y. Liu, X. Liu, W. Wei, S. Luo, *Microchim. Acta*, **2009**, 165, 393–398.
- [12] A. Rabti, N. Raouafi, A. Merkoçi, *Carbon*, **2016**, 108, 481–514.
- [13] J. C. Love, L. A. Estroff, J. K. Kriebel, R. G. Nuzzo, G. M. Whitesides, *Chem. Rev.*, **2005**, 105, 1103–1169.
- [14] A. Ulman, *Chem. Rev.*, **1996**, 96, 1533–1554.
- [15] V. M. Mirsky, *Trends Anal. chem.*, **2002**, 21, 439–450.
- [16] P. E. Laibinis, G. M. Whitesides, D. L. Allara, Y. T. Tao, A. N. Parikh, R. G. Nuzzo, *J. Am. Chem. Soc.*, **1991**, 113, 7152–7167.
- [17] S. Flink, F. C. J. M. van Veggel, D. N. Reinhoudt, *Adv. Mater.*, **2000**, 12, 1315–1328.
- [18] T. Wink, S. J. van Zuilen, A. Bult, W. P. van Bennekom, *Analyst*, **1997**, 122, 43–50.
- [19] M. Riepl, V. M. Mirsky, I. Novotny, V. Tvarozek, V. Rehacek, O. S. Wolfbeis, *Anal. Chim. Acta*, **1999**, 392, 77–84.
- [20] A. Hickling, W. H. Wilson, *J. Electrochem. Soc.*, **1951**, 98, 425–433.
- [21] M. Gerlache, Z. Senturk, G. Quarin, J.-M. Kauffmann, *Electroanalysis*, **1997**, 9, 1088–1092.
- [22] D. Knittel, Q. Wei, E. Schollmeyer, *Fresenius J. Anal. Chem.*, **1994**, 348, 820–824.
- [23] E. Yeager, *Electrochim. Acta*, **1984**, 29, 1527–1537.
- [24] E. Yeager, *J. Mol. Catal.*, **1986**, 38, 5–25.
- [25] I. Sirés, E. Brillas, M. A. Oturan, M. A. Rodrigo, M. Panizza, *Environ. Sci. Pollut. Res.*, **2014**, 21, 8336–8367.
- [26] W. Zhou, X. Meng, J. Gao, A. N. Alshwabkeh, *Chemosphere*, **2019**, 225, 588–607.
- [27] C. M. Sánchez-Sánchez, A. J. Bard, *Anal. Chem.*, **2009**, 81, 8094–8100.
- [28] M. S. El-Deab, T. Okajima, T. Ohsaka, *J. Electrochem. Soc.*, **2003**, 150, 851–857.
- [29] C. R. Raj, A. I. Abdelrahman, T. Ohsaka, *Electrochem. Commun.*, 2005, 7, 888–893.
- [30] J. H. Shim, J. Kim, C. Lee, Y. Lee, *J. Phys. Chem. C*, **2011**, 115, 305–309.
- [31] G. Gotti, D. Evrard, K. Fajerweg, P. Gros, *J. Solid State Electrochem.*, **2016**, 20, 1539–1550.
- [32] A. Muthurasu, H. Y. Kim, *Electrochim. Acta*, **2018**, 283, 1425–1431.
- [33] J. Benesty, J. Chen, Y. Huang, I. Cohen, *Pearson Correlation Coefficient, Springer Topics in Signal Processing*, **2009**, 1–4.

- [34] Clinical Guide to Laboratory Tests, 3rd Ed (Ed.: N. W. Tietz) Philadelphia W.B. Saunders, **1995**.
- [35] X. Cui, Z. Li, Y. Yang, W. Zhang, Q. Wang, *Electroanalysis*, **2008**, 20, 970–975.
- [36] M. S. M. Quintino, H. Winnischofer, K. Araki, H. E. Toma, L. Angnes, *Analyst*, **2005**, 130, 221–226.
- [37] Y. Lin, X. Cui, L. Li, *Electrochem. Commun.*, **2005**, 7, 166–172.
- [38] S. Wang, Y. Kang, L. Wang, H. Zhang, Y. Wang, Y. Wang, *Sensor. Actuat. B-Chem.*, **2013**, 182, 467–481.
- [39] M. F. S. Teixeira, F. H. Cincotto, P. A. Raymundo-Pereira, *Electrochim. Acta*, **2011**, 56, 6804–6811.
- [40] W. Jia, M. Guo, Z. Zheng, T. Yu, E. G. Rodriguez, Y. Wang, Y. Lei, *J. Electroanal. Chem.*, **2009**, 625, 27–32.
- [41] M. Mattoussi, F. Matoussi, N. Raouafi, *Sensor. Actuat. B-Chem.*, **2018**, 274, 412–418.
- [42] S. Yao, S. Yuan, J. Xu, Y. wang, J. Luo, S. Hu, *Appl. Clay Sci.*, **2006**, 33, 35–42.
- [43] C. Xu, J. Wang, J. Zhou, *Sensor. Actuat. B-Chem.*, **2013**, 182, 408–415.
- [44] A. Salimi, R. Hallaj, S. Soltanian, H. Mamkhezri, *Anal. Chim. Acta*, **2007**, 594, 24–31.
- [45] B. Šljukić, R. G. Compton, *Electroanalysis*, **2007**, 19, 1275–1280.
- [46] T. A. Ivandini, R. Sato, Y. Makide, A. Fujishima, Y. Einaga, *Diam. Relat. Mater.*, **2005**, 14, 2133–2138.
- [47] T. N. Kumar, S. Sivabalan, N. Chandrasekaran, K. L. N. Phani, *J. Mater. Chem. B*, **2014**, 2, 6081–6088.
- [48] S. Barkaoui, M. Haddaoui, H. Dhaouadi, N. Raouafi, F. Touati, *J. Solid State Chem.*, **2015**, 228, 226–231.
- [49] A. Rabti, C. C. Mayorga-Martinez, L. Baptista-Pires, N. Raouafi, A. Merkoçi, *Anal. Chim. Acta*, **2016**, 926, 28–35.

General Conclusion



The aim that we set ourselves in this work was to study and improve the conditions for the formation of self-assembled monolayers on a solid surface in order to design more developed electrochemical chemosensors. Therefore, we opted for an adsorbate with an anchor site, having two thiol groups located symmetrically, covalently bonded to an electroactive end group and a polycrystalline gold substrate. This choice was guided by considerations of stability (good gold-sulfur affinity) and performance of electrochemical analysis techniques (redox center) in order to follow the evolution of the SAM in real time.

First of all, we proceeded to the synthesis of a new anchor site, 1,3-dimercapto-propan-2-ol, which has not been previously used in the development of SAMs. Fundamentally, the symmetrical structure of the compound as well as the possession of two thiol groups should provide well-oriented SAMs onto the gold surface. We have demonstrated that the operating conditions for the preparation of the SAM strongly contribute in the immobilization structure of the layer. It was concluded that immobilization of DiSH occurs not through immobilization of only one thiol or only two thiol groups but from the contribution of both structures. Many approaches were performed using other anchor sites in order to compare the stability of the SAM made from DiSH with those obtained from other thiolated compounds. It was proved that the pre-synthesized anchor site provides the formation of a thin and stable SAM.

To modulate electroactive properties to the SAM we proceeded to immobilize 3-mercaptopropionic acid on the formed layer, followed by addition of benzoquinone. The choice of the MPA is based on the fact that it can provide covalent bonds with the anchor site of the SAM (through Steglich esterification) and with the redox site (through Michael addition).

The synergy of effects linked to the high conductivity of gold and the redox property of quinone and its stability in aqueous medium made it possible to detect analytes at low concentrations of the order of a few mmol/L. A new amperometric sensor based on BQ-terminated SAM for the detection of NADH was performed. This sensor is simple to manufacture, inexpensive and sensitive. Experimental results show that the amperometric response of the sensor has been shown to be an increasing function of the amount of the NADH added. The NADH response induces an increase in the current at the potential + 0.4 V (vs AgCl/Ag, sat. KCl) corresponding to the

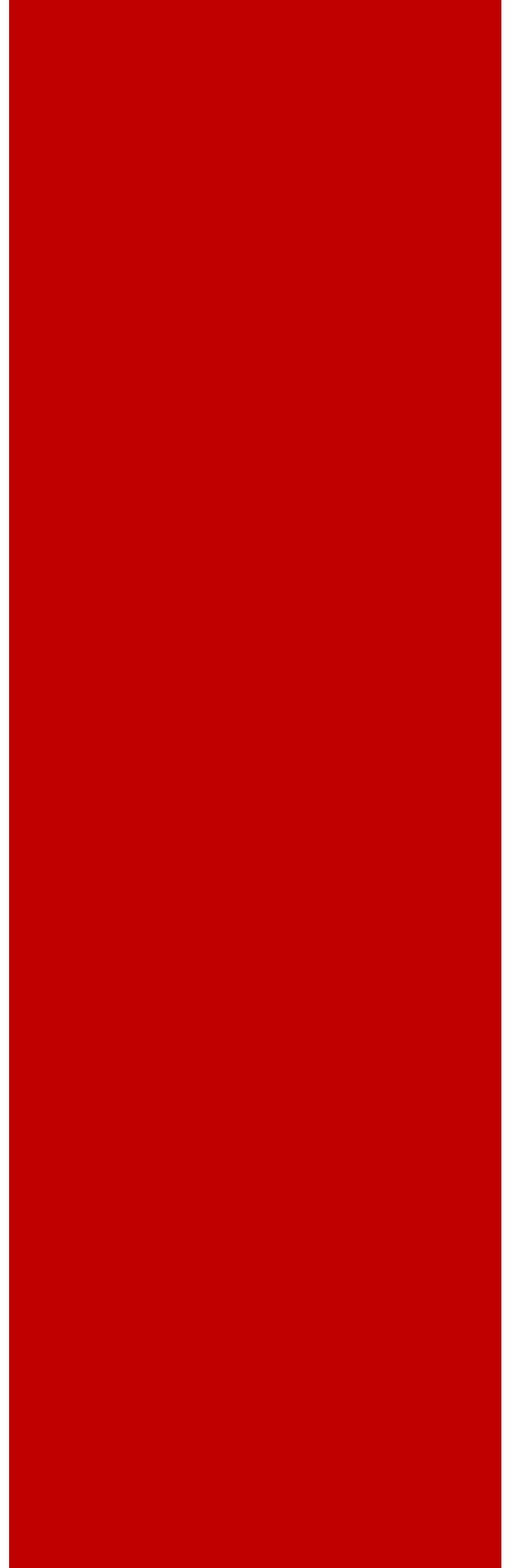
General Conclusion

oxidation of hydroquinone to benzoquinone. A mechanism to explain the increase in current associated with the recognition phenomenon has been proposed.

Moreover, we used the same SAM for the electrocatalytic degradation of hydrogen peroxide. Voltammetric analysis was performed at the potential range from -0.6 V till +0.9 V as well as in the anodic range when only oxidation of hydrogen peroxide occurs or in the cathodic range when only reduction of hydrogen peroxide occurs. The results indicate oxidative electrochemical decomposition of hydrogen peroxide at the potential of +0.4 V. The sensor exhibited linear response over the concentration range from 0.1 mM to 2.5 mM with a limit of detection $\sim 4 \mu\text{M}$. In addition, analytical evaluation of the sensor performance was done in the chronoamperometric mode. Results show that in comparison to other oxidative electrocatalysts, BQ-based electrocatalytic sensor provide well competitive analytical properties in sense of selectivity, operating electrode potential and analytical sensitivity.

According to the experimental work described in this manuscript, the new electrochemical sensor showed its ability to promote electron-transfer reactions and therefore can be applied in other reactions involving other biological or environmental important compounds.

Annexes



Annex A: Lists of abbreviations

A.1. Fundamental physical constants

β	Transfert coefficient	$\beta = 0.5$
F	Faraday constant	$96485.309 \text{ C}\cdot\text{mol}^{-1}$
R	Molar gas constant	$8.314510 \text{ J}\cdot\text{mol}^{-1}\cdot\text{K}^{-1}$
k	Boltzmann constant	$1.38066\times 10^{-23} \text{ J}\cdot\text{K}^{-1}$
T	Temperature	$25 \text{ }^\circ\text{C} = 298 \text{ K}$
η	Viscosity of water	$10^{-3} \text{ Kg}\cdot\text{m}^{-1}\cdot\text{s}^{-1}$
ε	Dielectric constant	$\varepsilon = 2.3$
ε_0	Pemitivity of free space	$5.85\times 10^{-12} \text{ F}\cdot\text{m}^{-1}$

Non-SI units:

e_0	Elementary charge	$1.160217733\times 10^{-19} \text{ J}$
-------	-------------------	--

A.2. Symbols

T	Temperature
R	Resistance
C	Capacitance

Annexes

Z	Impedance
I	Current
i	Current
E	Potential
V	Scan rate
v	Scan rate
Q	Charge
q	Charge
t	Time
τ	Time
w	Radial frequency
r	Correlation coefficient
r	Radius
Φ	Diameter
L	Length
d	Thickness
A	Area of the electrode
A	Electrochemically effective electrode area
c	Concentration
n	Electron number

Annexes

Γ	Surface density
k^0	Effective constant rate
θ	Esterification efficiency
D	Diffusion coefficient

A.3. Abbreviations

DiSH	1,3-dimercaptopropan-2-ol
MPA	3-mercaptopropionic acid
DCC	N-N'-dicyclohexylcarbodiimide
DMAP	4-(dimethylamino)pyridine
BQ	1,4-benzoquinone
FcSH	6-(ferrocenyl)hexanethiol
NADH	β -nicotinamide adenine dinucleotide
PBS	Phosphate buffered saline
SAM	Self-assembled monolayer
SAM1	DiSH-based SAM (1 mM, 12h)
SAM2	DiSH-based SAM (0.1 M, 3h)
SAM3	SH-terminated SAM
SAM4	BQ-terminated SAM
NMR	Nuclear magnetic resonance

Annexes

IR	Infrared
WCA	Water contact angle
XPS	X-ray photoelectron spectroscopy
CV	Cyclic voltammetry
CV	Cyclic voltammogram
EIS	Electrochemical impedance spectroscopy
QMC	Quantum mechanical calculation
CA	Chromoamerometry
CA	Chronoamperogram
RT	Room temperature
LOD	Limit of detection
S_b	Standard deviation
m	Slope

Annex B: Experimental section

B.1. Organic synthesis

B.1.1. Reagents and solvents

1,3-dichloro-2-propanol (98%), potassium thioacetate (98%), sodium borohydride ($\geq 96\%$), 3-mercaptopropionic acid ($\geq 99\%$), 4-(dimethylamino)pyridine ($\geq 99\%$), 1,4-benzoquinone ($\geq 98\%$), 2-mercaptoethanol ($\geq 99\%$), 1-hexanthiol (95%), 6-(ferrocenyl)hexanethiol, potassium hexacyanoferrate III (99%), potassium hexacyanoferrate II trihydrate ($\geq 99\%$), L-ascorbic acid 2-phosphate sesquimagnesium salt hydrate ($\geq 95\%$), uric acid sodium salt and dextrose were purchased from Sigma-Aldrich (Germany) (www.sigmaaldrich.com), potassium chloride ($\geq 99\%$), potassium dihydrogen phosphate ($\geq 99\%$), di-potassium hydrogen phosphate trihydrate ($\geq 99\%$) and hydrogen peroxide (H_2O_2) 30% were purchased from Carlroth (Germany), β -nicotinamide adenine dinucleotide reduced disodium salt hydrate (NADH-Na_2) was from Merck (Darmstadt, Germany) and N,N'-dicyclohexylcarbodiimide ($\sim 99\%$) was from Fluka. Potassium salts were used to prepare the buffer solution.

Phosphate buffered saline solution was prepared in demineralized water and the pH was adjusted by the addition of hydrochloric acid aqueous solution. All solvents: ethanol absolute ($\geq 99.8\%$), 2-propanol ($\geq 99.8\%$) and acetone ($\geq 99.8\%$) were from VWR chemicals. Acetonitrile ($\geq 99.9\%$) was from Honeywell.

B.1.2. Characterization of 1,3-dimercaptopropan-2-ol before and after deprotection

^1H and ^{13}C NMR spectra were recorded in a Bruker Advance 300 MHz apparatus. The chemical shifts are given in ppm according to tetramethylsilane (TMS) as an internal reference. The following symbols have been adopted to indicate the multiplicity of signals: s (singlet), dd (doublet of doublet) and quin (quintuplet). The vertical displacement of the integral gives the relative number of protons. FTIR spectra were collected by Nicolet iS10 device using Smart iTR unit and analyzed using OMNIC software, version 8.0.342 (Thermo Fisher Scientific).

Spectral characterizations of 1,3-dithioacetatepropan-2-ol: ^1H NMR (CDCl_3 , 300 MHz): δ (ppm): 2.08 (s, 6 H, CH_3), 2.77 (dd, 2 H, CH_2), 2.99 (dd, 2 H, CH_2), 4.74 (quin, 1 H, CH); ^{13}C NMR (CDCl_3 , 75.5 MHz): δ (ppm): 30.4 (CH_3), 30.6 (C-S), 70.6 (C-OH), 193.9 (C=O);

IR (cm^{-1}): $\nu_{\text{O-H}}$: 3336, $\nu_{\text{C-H}}$: 2922, $\nu_{\text{C-H}}$: 2968, $\nu_{\text{C=O}}$: 1685, $\delta_{\text{O-H}}$: 1209, $\nu_{\text{C-O}}$: 1128, $\nu_{\text{C-S}}$: 720 before and IR (cm^{-1}): $\nu_{\text{O-H}}$: 3328, $\nu_{\text{C-H}}$: 2932, $\nu_{\text{C-H}}$: 2872, $\nu_{\text{S-H}}$: 2554, $\delta_{\text{C-H}}$: 1416, $\delta_{\text{O-H}}$: 1291, $\nu_{\text{C-O}}$: 1168, $\nu_{\text{C-C}}$: 1044, $\delta_{\text{C-H}}$: 757 after removing of the acetate group.

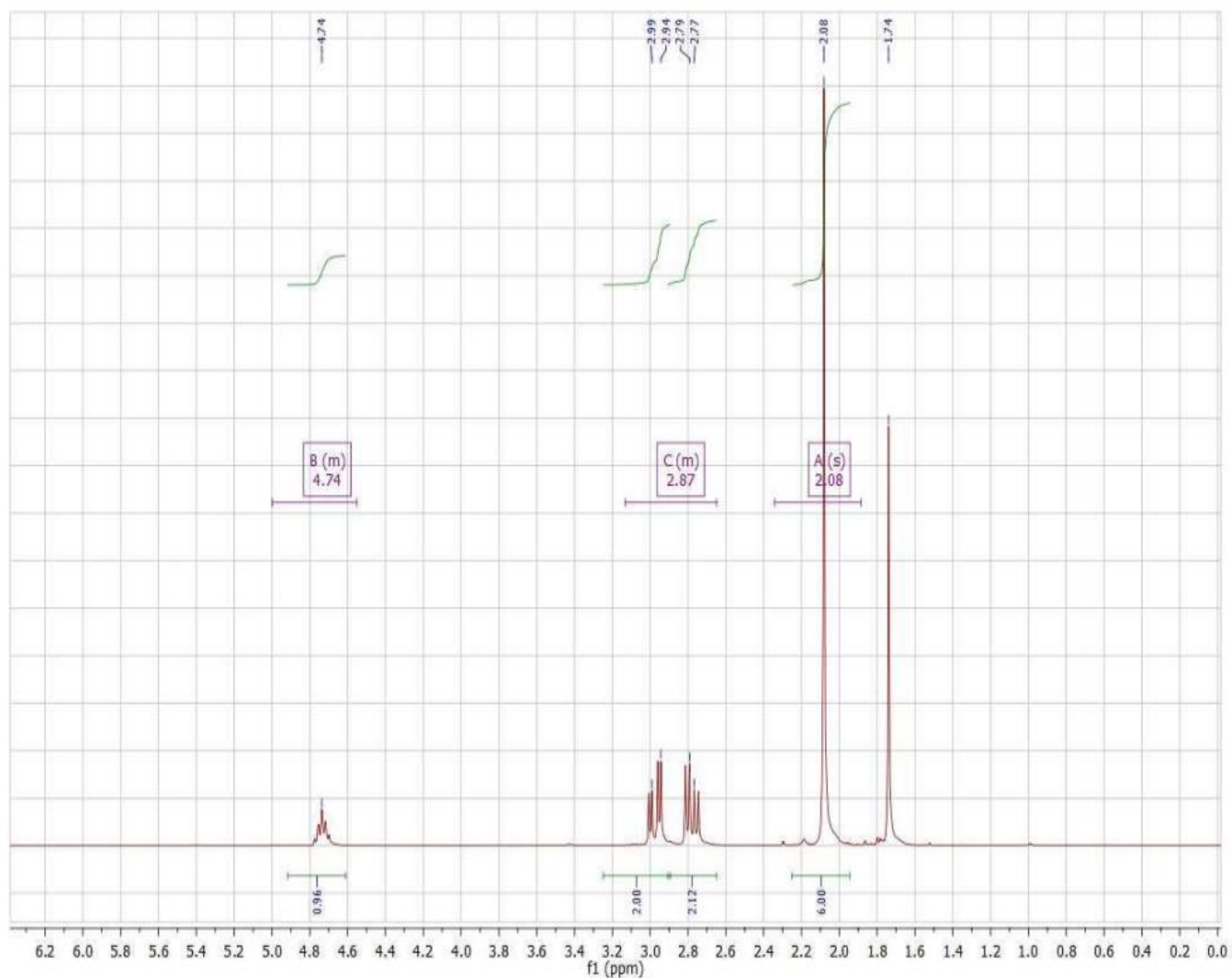


Figure 1: ^1H NMR spectra of 1,3-dithioacetatepropan-2-ol.

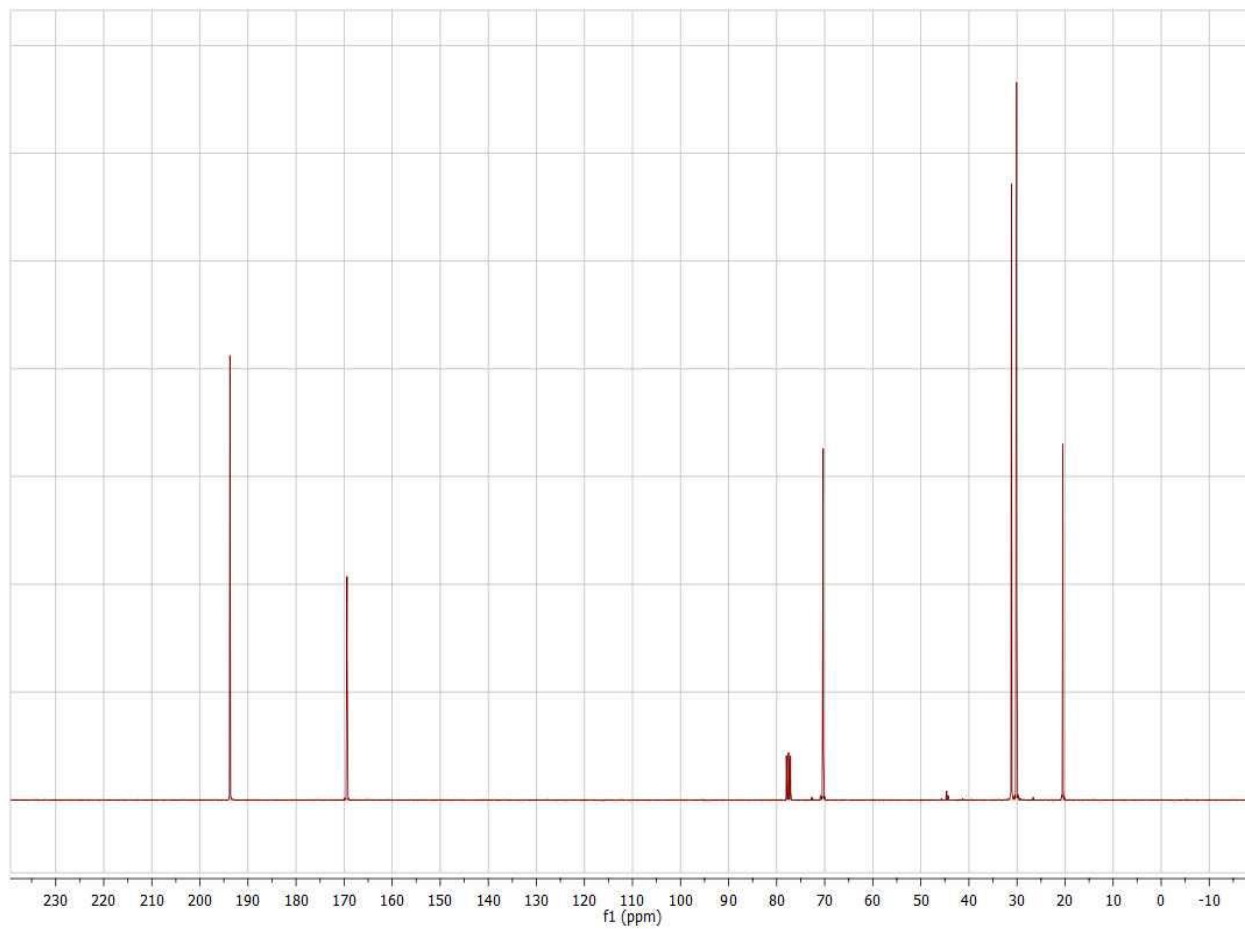


Figure 2: ^{13}C NMR spectra of 1,3-dithioacetatepropan-2-ol.

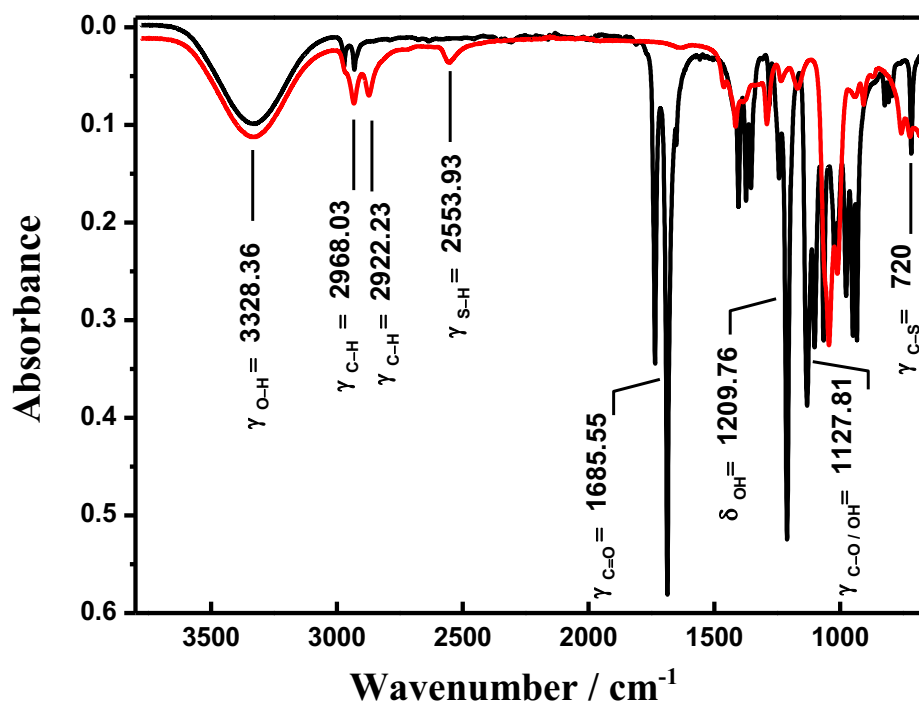


Figure 3: FT-IR spectra of 1,3-dithioacetatepropan-2-ol before (black curve) and after (red curve) deprotection.

B.2. Quantum mechanical calculations

QMCs were performed using the density functional theory (DFT) as implemented in the Gaussian 09 software packet. The geometries were optimized at the B3LYP level of theory and the 6-311+G (d,p) basis set.

B.3. Gold surface characterization using WCA and XPS

WCA was measured by KSV instrument CAM 101 (www.biolinescientific.com) with KSV CAM 200 software.

XPS measurements were carried out in the laboratory-based tool using magnesium anode (excitation energy 1253.6 eV) provided by Specs GmbH. The excited photoelectrons were collected at a take-off angle of 50° by the hemispherical electron analyzer made by Omicron. The sampling depth (ID) of the photoelectron originating from the S2p level for these experimental conditions is equal to ~ 2.8 nm. ($ID = 3 \times \sin 50^\circ \times IMFP_{S2p} = 3 \times 0.7 \times 1.312 \text{ nm} = 2.8 \text{ nm}$;

<http://electronsoftware.altervista.org/lab/IMFP.html>). The spectra were fitted by Gaussian–Lorentzian curves with subtraction of the Shirley-type background using CasaXPS software.

B.4. Electrochemistry

Electrochemical measurements: cyclic voltammetry, impedance spectroscopy, kinetic capacitance, step-potential chronoamperometry and chronoamperometry were performed using PC-controlled Autolab PGstat12 equipped with a FRA32 impedance module and controlled by NOVA 2.1.2 software (Metrohm, www.metrohm.com). A conventional three electrodes glass cell was used for electrochemical experiments. Platinum wire of 0.25 mm in diameter was served as the auxiliary electrode, Ag/AgCl (sat. KCl) electrode with a double salt bridge (Metrohm) as the reference electrode, and a bare or a modified polycrystalline gold wire (diameter 0.5 mm, length 1.0 cm) as the working electrode. The gold wire was coated by melted glass to get a constant value of the electrode surface area. All the experiments were performed at room temperature (RT), after degasing by nitrogen bubbling.

Annex C: List of publications

A. Laroussi, M. Kot, J. I. Flege, N. Raouafi, V. M. Mirsky, Self-assembled monolayers from symmetrical di-thiols: preparation, characterization and application for the assembly of electrochemically active films, *Appl. Surf. Sci.*, **2020**, 513, 145827.

A. Laroussi, N. Raouafi, V. M. Mirsky, Electrocatalytic sensor for hydrogen peroxide based on immobilized benzoquinone, **2021**, (submitted).

B. Snopok, **A. Laroussi**, C. Cafolla, K. Voïtchovsky, T. Snopok, V. Mirsky, Gold surface cleaning by etching polishing: Optimization of polycrystalline film topography and surface functionality for biosensing, *Surf. Interfaces*, **2021**, 22, 100818.